COPPER DITHIOCARBAMATE COMPLEXES AND COPPER SULFIDE NANOPARTICLES: SYNTHESIS, CHARACTERIZATION AND ANTIFUNGAL STUDIES

BOTHA Nandipha Loveness

Department of Chemistry

Faculty of Science and Agriculture

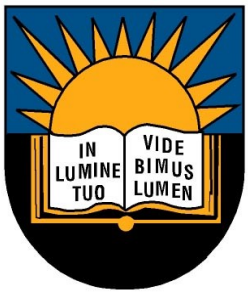

University of Fort Hare
Together in Excellence

January 2015

COPPER DITHIOCARBAMATE COMPLEXES AND COPPER SULFIDE NANOPARTICLES: SYNTHESIS, CHARACTERIZATION AND ANTIFUNGAL STUDIES

By

BOTHA Nandipha Loveness (200904696)
B. Sc., B. Sc. (Honours) Chemistry (UFH)

Being a dissertation submitted to the Faculty of Science and Agriculture in fulfilment of the requirements for the award of the degree of

Master of Science in Chemistry

of the

University of Fort Hare,

Supervisor: Professor P. A. Ajibade

January 2015

DECLARATION BY CANDIDATE

"I hereby declare that this dissertation submitted for MSc degree in Chemistry, at the University of Fort Hare, is my own original work and has not previously been submitted to any other institution of higher learning. I further declare that all sources cited or quoted are indicated and acknowledged by means of a comprehensive list of references".

_____ _____

Date **Botha L. Nandipha**

CERTIFICATION

This is to certify that this research is a record of original work carried out by Botha L. Nandipha under my supervision in the Inorganic Materials Research laboratory of the Department of Chemistry, University of Fort Hare in fulfilments of the requirements for the award of Master of Science degree in Chemistry.

_____ _____

Date **Supervisor**

P. A. Ajibade
Professor of Inorganic Materials Chemistry
B. Sc (Hons), MSc (Ibadan);
PhD (UniZul); MRSC (London)

DEDICATION

I lovingly dedicate this work to my mother, Nombulelo Mgijima, who supported me each step of the way, who stood by me when life had bitter taste and continuously gave me love and support.

ACKNOWLEDGEMENT

It is with immense gratitude that I acknowledge the Almighty God for His love, protection, support and help during the time of this study. Without Him, this research would not have been successful. I would also like to express the deepest appreciation to my supervisor, Professor P. A. Ajibade for his guidance. Without his guidance and persistent help, this work would not have been possible.

I also extend my appreciation to:

- The department of chemistry at the University of Fort Hare for the opportunity to carry out this research project and the technical staff members who assisted in various ways.
- The *Inorganic Materials Research* group for assistance and advice.
- Govan Mbeki Research and Development Centre, University of Fort Hare for supervisor-linked bursary.
- My family for their love and support.

TABLE OF CONTENT

LIST OF FIGURES

LIST OF SCHEMES

LIST OF TABLES

ABBREVIATIONS

AIDS – Acquired immune deficiency syndrome

DTCs – Dithiocarbamates

DMF – Dimethyl formamide

DMSO – Dimethyl sulfoxide

EDX – Energy dispersive X-ray

eq. – Equation

et al. – Et alia

Fig. – Figure

FTIR – Fourier Transform Infrared spectroscopy

HDA – Hexadecylamine

JCPDS – Joint Committee on Powder Diffraction Standards

LMCT - Ligand to Metal Charge Transfer

mg – Milligrams

MIC – Minimal inhibitory concentration

NPs – Nanoparticles

nm – Nanometer

NMR – Nuclear magnetic resonance

SEM – Scanning electron microscopy

TEM – Transmission electron microscope

TOP – Trioctylphosphine

UV-Vis – Ultraviolet-visible spectroscopy

XRD – X-Ray diffraction

SYMBOLS

θ – Theta

β – Beta

α – Alpha

λ – Sigma

^{o}C – Degrees Celsius

K – Kelvin

% - Percent

g – Grams

mol – Moles

h – Hour

RESEARCH OUTPUTS/SUBMITTED MANUSCRIPTS

1. **Nandipha L. Botha and Peter A. Ajibade**

   Synthesis, optical and structural studies of hexadecylamine capped copper sulfide nanoparticles. (*Submitted to Materials Letters*- MLBLVE–D–15– 00030)

2. **Nandipha L. Botha and Peter A. Ajibade**

   Effects of temperature on the structural properties of copper sulfide nanoparticles prepared from dithiocarbamato single source precursors. (*Submitted to Materials Research Bulletin*- MRB – 14 – 1849)

3. **Nandipha L. Botha and Peter A. Ajibade**

   Preparation of copper sulfide nanoparticles bis(piperidine dithiocarbamato) Cu(II) and the effects of thermolysis temperature on optical and structural properties. (To be submitted)

4. **Nandipha L. Botha, Peter A. Ajibade and Anofi O. T. Ashafa**

   Synthesis, characterization, antibacterial and antifungal studies of some Copper(II) dithiocarbamate complexes. (*To be submitted*)

ABSTRACT

Six dithiocarbamate ligands were synthesized from anisidine, aniline, ethyl aniline, butyl amine, morpholine and piperidine and used to synthesize homoleptic copper(II) dithiocarbamate complexes. The ligands and their corresponding complexes were characterized by conductivity measurement, FTIR and UV-Vis spectroscopy. The ligands were further characterized using NMR spectroscopy. The electronic spectra of the complexes showed that the coordination geometries around the Cu^{2+} ion is four coordinate square planar. FTIR spectroscopic studies indicated that the dithiocarbamate ligands are bidentately coordinated to the copper ion through the sulfur atoms with the C-S stretching frequencies changing from two peaks in the ligands to single sharp peaks in the corresponding metal complexes.

The complexes were used as single source precursors to synthesize copper sulfide nanoparticles. All the six complexes were thermolysed at 180 ^{o}C to prepare copper sulfide nanoparticles and three of them were further thermolysed at 120 ^{o}C to study the effects of temperature on size and shape of the nanoparticles. All the nanoparticles were characterized with UV-Vis, PL, XRD, TEM, SEM and EDX. The optical properties of the as-prepared CuS nanoparticles showed that they are quantum confined with absorption band edges that are blue shifted compared to bulk CuS and all the as-prepared CuS nanoparticles showed narrow emission curves. The XRD diffraction patterns were indexed to the hexagonal covellite CuS crystalline phase with estimated particle sizes of 15.8-23.24 nm. These sizes are significantly different from the values, 3.02-98.94 nm obtained from TEM studies. The TEM images also showed nanoparticles with varied shapes with some agglomerations. SEM micrographs

showed that the morphologies of the nanoparticles are mostly smooth surfaces and EDX spectra analyses confirmed the formation of the nanoparticles. Thermolysis of three of the complexes at 120 ^{o}C confirmed that temperature do affect the optical and structural properties of the CuS nanoparticles.

Only three complexes soluble in DMSO were screened for their antimicrobial activity. Three complexes C1, C4 and C5 were screened against four fungi organisms, namely: *Candida rugosa*, *Candida neoformans*, *Candida albicans* and *Trychophyton mucoides.* All the compounds were promising as shown by the minimum inhibitory concentrations determined. C5 was the most active compound against all the organisms. They were also screened against four bacteria organisms and they were all active but not as they were against fungi organisms.

CHAPTER ONE

1.0 INTRODUCTION AND LITERATURE REVIEW

1.1. Introduction

The importance of fungi as agents of plant and human diseases, producers of industrial and pharmacological products, and as decomposers has spurred scientists worldwide to study their biology. The impact that fungi have with regards to plant health, food loss, and human nutrition is staggering. Pathogenic fungi have caused some of the world's great famines and human suffering [1]. It has been estimated that the fungi kingdom contains more than 1.5 million species, but about 250,000 species have been fully identified and described taxonomically [2,3]. Many fungi, are important plant and lower animal parasites and can cause damage to crops, fruit, forest, ornamental trees and other plants [3].

Plants are constantly exposed and threatened by a variety of pathogenic microorganisms and diseases caused by plant pathogenic fungi significantly contribute to the overall loss in crop yield worldwide [4]. In agriculture, annual crop losses due to pre- and post-harvest fungal diseases exceed 2.8 trillion rand, and, in the United States of America alone, over 2.2 billion rand are yearly spent on fungicides [2]. The pathogen attacks nearly all kinds of succulent plants including flowers, shrub weeds and almost all vegetables [5]. Fungi attack all parts of a plant and under suitable conditions, fungi can damage plant translocation tissues, killing a plant in a relatively short period of time. Thus, fungal diseases like 'blights', 'rusts', 'smuts', 'mildews', 'scabs' are very common in plants [6].

The top ten fungal plant pathogen list includes, in rank order:

(1*) Magnaporthe oryzae*.

(2*) Botrytis cinerea*.

(3) *Puccinia spp*.

(4) *Fusarium graminearum*.

(5) *Fusarium oxysporum*.

(6) *Blumeria graminis*.

(7) *Mycosphaerella graminicola*.

(8) *Colletotrichum spp*.

(9) *Ustilago maydis*.

(10) *Melampsora lini* [7].

The outbreak of meningitis associated with contaminated methylprednisolone acetate from the New England compounding centre highlights the ability for a subset of fungal pathogens to cause infection in members of plant and animal kingdoms [8]. Without the use of fungicides for managing bloom and foliar diseases, these diseases would limit crop production in the world where many people at present are facing food shortages and hunger. Fungicides are currently used in the management of flower, foliar, and fruit diseases of many crops worldwide, especially when cultivars with natural host resistance are not available [9].

Different fungicides have been used to control fungal crop diseases and there is a growing interest in research on the possible use of natural products such as plant based essential oils and extracts, which may be less damaging for pest and disease control [4], but still the existence of crop pathogenic fungi has not stopped. However, at present, the search for new fungicide is of paramount importance due to increase of resistant and new strains of fungi. Fungicides are chemical compounds or biological organism use to kill or inhibit mycelial growth or fungal spore. The carbamet (organic sulfur) fungicides form a very important group among fungicides. Most of these are foliage fungicides [10]. Among common synthetic chemicals used as antifungal agents, dithiocarbamates compounds are most prominent and some dithiocarbamate compounds are commercially available as fungicides [3].

1.1.1 Dithiocarbamates

Dithiocarbamates (DTCs) are bidentate chelating ligands which have received a great deal of attention due to their wide use as agrochemicals, pharmaceuticals, intermediates in organic synthesis, as protecting group in peptide synthesis or as chelators in materials chemistry [11]. From an inorganic chemistry stand point, dithiocarbamates are highly versatile ligands toward main group metals [12]. Dithiocarbamates are a class of metal-chelating, antioxidant compounds with various applications in medicine for the treatment of bacterial and fungal infections, and possible treatment of Acquired immune deficiency syndrome (AIDS) [13].

Among the various sulfur bearing ligands, the DTCs, [$S_2CNR^1R^2$], a class of Lewis bases capable of coordinating to a wide number of metal ions, are unique due to its S–C–S delocalized electronic system [14]. They can stabilize a variety of oxidation states and coordination geometries, and seemingly small modifications to the ligand can lead to significant changes in the structure–behaviour of the complexes formed. Dithiocarbamate ligands exist in different resonance form of the dithiocarbamic moiety (Scheme 1.1) and can act as monodentate, bidentate chelating or bidentate bridging ligands due to their binding character [15]. The structural organization of the resulting metal complexes is determined by these binding properties [16].

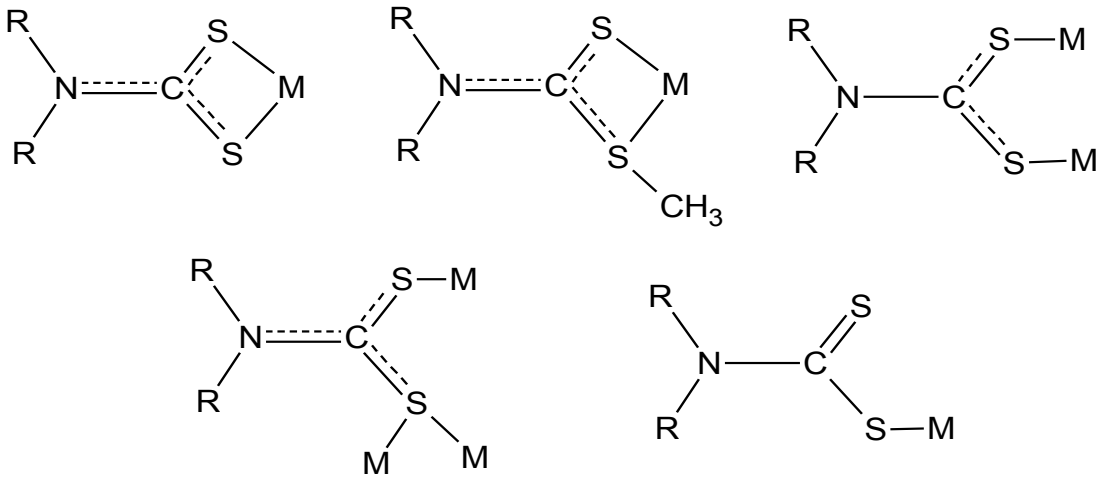

Scheme 1.1: Binding forms of dithiocarbamate ligands to metal complexes [17].

Main group dithiocarbamate complexes have wide-ranging applications in materials and separation science, and have potential use as chemotherapeutics, pesticides, and fungicides [12]. DTCs have been studied extensively over recent decades in response to their growing applications in many new areas of analytical chemistry (as fungicides, pesticides, vulcanization accelerations), industry (flotation agents and high pressure lubricants) and biology (in antibacterial, cytostatic, antifungal, immune regulatory

activities) [18,19], as antiwear, extreme pressure and antioxidant additives in lubricating oils and greases.

1.1.2 Nanoparticles

In recent years, nanomaterial have received considerable attention due to their unique physical and chemical properties which differ significantly from those of bulk materials [20]. Nanoparticles (NP) are of great concern to the environment because of their small size and serious attention must be given to the potential of the particles to interact with organisms and ecosystems in unexpected ways [21]. A spinnable coating capable of releasing metal species to a broth of living organisms in a controlled manner is an extremely interesting material for a number of biotechnological applications. Polymer/metal nanocomposites are a viable choice but very little is known about their biological properties [22].

Exploitation of the toxic properties of nanoparticles against bacteria, fungi and viruses, in particular metals and metal oxides, as well as their incorporation into polymeric materials have increased markedly over the past decade [23]. CuS is an important semiconductor that have metallic conductivity, can transform into a superconductor at 1.6 K and exhibits fast-ion conduction at high temperatures. It also has potential applications as a thermoelectric cooling material, an optical filter, a solar cell, an optical recording material and a super ionic material [24]. In the last 20 years, nanoparticle-based agents have been developed for treating a variety of diseases such as cancer, diabetes, asthma, allergy, and infections [25]. Recent studies have demonstrated

antimicrobial activities of various nanoparticle materials, including silver, copper, titanium dioxide and zinc oxide [20], and results showed that specially formulated metal oxide nanoparticles have good antibacterial activity [26]. Therefore, antimicrobial formulations made from a variety of NPs have high bactericidal activities [27].

1.2. Literature review

The control of plant diseases using chemicals started during the 1850s when Bordeaux mixture was introduced to control downy mildew. Thus, protection of many crops became possible using organic fungicides [28]. From 1940 to 1970 there were a number of new chemicals introduced as fungicides. The dithiocarbamates represented a major improvement over the previously used inorganic fungicides in that they were more active, less phytotoxic and easier to prepare by the user. Dithiocarbamate were then introduced as the most widely used group of organic fungicides [29].

1.2.1. Dithiocarbamate complexes

Transition metal dithiocarbamate complexes are known to have large scale biological effects with various applications as antifungals, herbicides and insecticides in the agricultural practice, in the materials science, and medicine [30], agrochemicals, pharmaceuticals, intermediates in organic synthesis, as protecting group in peptide synthesis or as chelators in material chemistry [31]. Metal complexes of dithiocarbamate ligands have been synthesised [32] and investigated in order to gain

insight into the nature of the metal sulfur bond in many biomolecules and also because of their potential application as anticancer agents [33].

Dithiocarbamates are a class of fungicides extensively used in many crops worldwide because they are highly efficient in controlling plant pathogenic fungi with relatively low mammalian acute toxicity [34]. Most dithiocarbamate applications are based on the properties of the metal complexes of dithiocarbamate, especially with transition metal ions [13]. Among inorganic antimicrobial agents, copper compounds have been used widely in agriculture practices as fungicide.

The dithiocarbamate ligands reported in the dithiocarboxy group as the ligator group, so they behave like bidentate ligands in complexes, dithiocarbamates have been found to act almost as uninegative bidentate ligands, coordinating through both sulfur atoms, and both tetra and hexa-coordinated complexes of many transition metal ions have been isolated [34]. Despite some obvious similarities, dithiocarbamate ligands differ significantly in coordinating ability and properties from those of similar monoanionic 1,1-dithio ligands, such as xanthates and dithiophosphates because of the dominant contribution of the $R_2N^+=CS_2^{2-}$ canonical form which they exhibit in their complexes [35]. Dithiocarbamate ligands have extensive coordination chemistry and wide range of applications [36, 37]. The interest in the dithiocarbamate ligand resulted in a large number of mono- and bimetallic coordination compounds that exhibited interesting structural motifs and properties [38]. The chemistry and properties of metal dithiocarbamate and xanthate complexes have been reported [39].

The fungicidal activity of alkyl-bis-dithiocarbamic acid salts of alkali, alkaline earth and transition metals has been known for a long time [40]. Thus for an example the US Patent No. 2,317,765 contained fungicidally active mixtures in which the active ingredients are the di-sodium, copper or iron salt of ethylene-bis-dithiocarbamic acid [40]. Furthermore in Austrian patent specification No. 193, 891, disodium, copper and zinc propylene-bis-dithiocarbamates are described as substances active against plant pathogenic fungi [40]. However, the chemistry of 1, 1,-dithio chelates of main group elements is less widely explored unlike those of transition metals [41].

Macias *et al*. [33] reported that several studies on the preparation of dithiocarbamates derived from α-amino acids and their coordination compounds with several metal cations have been made. In the study several amino acids were used to prepare dithiocarbamates and their copper complexes. The effect of the hydrocarbon chain on the ability of the dithiocarbamate to coordinate to copper cations and their single crystals x-ray structures were determined [33]. Dithiocarbamates and their metal complexes have received much attention due to their diverse applications and interesting biological, structural, magnetic, electrochemical and thermal properties [42]. Main group dithiocarbamate complexes find wide-ranging applications in materials and separation science, and have potential use as chemotherapeutics, pesticides, and fungicides [30]. The literature on main group dithiocarbamates as a whole has not been reviewed extensively since the 1970s despite the large number of publications that have appeared subsequently [12].

The iron(II) and iron(III) dithiocarbamates have been studied for their spin crossover phenomenon, radical traps for NO, and as antioxidants and pro-oxidants in biological systems. Well known are the following dithiocarbamate complexes: Ru(IV), Au(III), Cu(III), Ni(IV), and Fe(IV) [43]. The antibacterial studies reveal that the metal complexes exhibit broad spectrum antibacterial activity against *Escherichia coli*, *Staphylococcus aureus*, *Klebsiella oxytoca* and *Pseudomonas aureginosa* [44]. The work reported by Tiekink showed that, while all organotin dithiocarbamates studied were fungicidal, it was the triphenyltin dithiocarbamate, $Ph_3Sn(S_2CNEt_2)$, and its pyrrolidine derivative that had the lowest minimal inhibitory concentrations [45].

Khan *et al*. [46] after synthesized, characterized and carried out anticancer studies of mixed ligand dithiocarbamate palladium(II) complexes, reported that mixed ligand dithiocarbamate amine complexes of palladium(II) have antitumour activity comparable to the *cis*platin and circumvented the cross resistance to *cis*platin. Sulfur containing ligands are currently under trials as chemoprotectants in platinum based chemotherapy, in particular thiocarbonyl, thiol and dithiocarbamate ligands have the ability to modulate the nephrotoxicity of the *cis*platin. Dithiocarbamates reduce the cytotoxicity of platinum based drugs by selective removal of platinum from enzyme thiol complex by nucleophilic attack of sulfur atoms on platinum moiety [46].

McCubbin *et al*. [47] reported dithiocarbamate-functionalized dendrimers as ligands for metal complexes. In the study, zeroth and first-generation poly(amido)amine dendrimers were functionalized with dithiocarbamate end groups and reacted with ruthenium complexes, to form metallodendrimers. Monomeric ruthenium

dithiocarbamate complexes were also prepared as model compounds and their spectroscopic data compared with those of the metallodendrimers [47]. The dithiocarbamate complexes, $[Cu(AMPDTC)_2)Cl_2]$ and $[Mn(AMPDTC)_2Cl_2]$ exhibits magnetic property and has electronic spectra which can be assigned to low spin Cu(II) and Mn(II) in octahedral environment and these complexes show selective activity towards some of the test microorganisms [48].

De lima *et al.* [36], reported the biological studies of some copper(II) dithiocarbamate complexes in which complexes with dithiocarbamate ligands contained substituted organic functional groups, where R^1 and or R^2 equal to CH_2CH_2OH. Crystal structures were reported for a number of metal complexes including those of alkali metals, copper, nickel, zinc, mercury and antimony. The *in vitro* activities of all the complexes were investigated against colonies of *C. albicans, S. aureus* and *P. aeruginosa.* Their biocidal results against *C. albicans*, in terms of Minimal Inhibitory Concentration (MIC), were quite promising. All complexes were inactive against *P. aeruginosa* [36].

Ferreira *et al*. [14] reported the synthesis, characterization and antimicrobial properties of new copper(II) DTC complexes. This study was interested in attaching less simple DTC ligands to Cu(II) cations in order to evaluate the biocide responses. Three synthesized and characterized dithiocarbamate complexes were $[Cu\{S_2CN(Me)(R^1)\}_2]$, $[Cu\{S_2CN(Me)(R^2)\}_2]$ and $[Cu\{S_2CN(R^3)(R^4)\}_2]$. Despite the poor activity towards the tested bacteria, complexes were quite effective against the fungi species [14]. One advantage of copper-based antimicrobial materials is its multitoxicity, which renders copper effective also against multiresistant germs like the

"superbug" methicillin resistant *Staphylococcus aureus* or *carbapenemase*-resistant bacteria. Copper and many of its alloys have been registered as antimicrobial materials at the United State Environmental Protection Agency (EPA) in 2008 [49]. While dithiocarbamate complexes have been known for over a century, with many thousands having been prepared, the vast majority of these contain only simple alkyl substituents such as methyl and ethyl. A developing interest in the area of dithiocarbamate chemistry is the functionalization of the backbone such that new applications and interactions can be developed [50].

1.2.2. Dithiocarbamates as fungicides

Dithiocarbamate compounds are widely used in agriculture and some are commercially available. Dithiocarbamates such as *Metam*, *Maneb*, *Mancozeb*, *Ferbam*, methylene-bis(dithiocarbamate) (Figure 1.1) are widely used as standard fungicides against variety of plant diseases [51, 52]. Although they were introduced 40–70 years ago, dithiocarbamate fungicides still represent an important class of plant protection product that are still widely used today [53]. They act as multisite contact fungicides that work by protecting the plant surface to prevent infection. They are converted to various salts to improve their solubility and biological potentials [54]. In general, dithiocarbamates are considered chemicals of low toxicity for humans. However, some of these fungicides are found to be toxic and poisonous to humans, some on fishes and animals.

The effects of *maneb* in humans are diverse with some causing problems in humans via absorption through the skin and respiratory system [55]. *Ziram* and *Zineb* are

effective dithiocarbamate fungicides [56], but *Ziram* has been proven to be more toxic than *Ferbam* in adult fowl, while *Ferbam* is known to be toxic to the liver, kidney and lungs. *Muncozeb* has low toxicity to animals and is not toxic to fish but also has low toxicity to animals. In thylene bisdithiocarbamates, *Nabam* should be mixed with water before use because its toxic doses may result in nerve damage. *Zineb* unlike the others has low toxicity but causes yellow watery diarrhoea to animals such as sheep [57].

These are some of the most widely used dithiocarbamates in Agriculture:

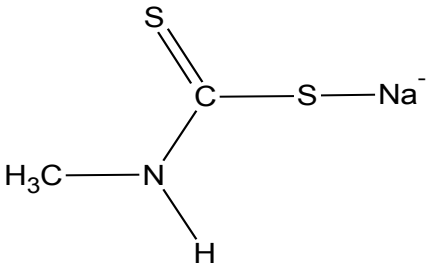

Methyldithiocarbamate

Metam sodium (nemotocide)

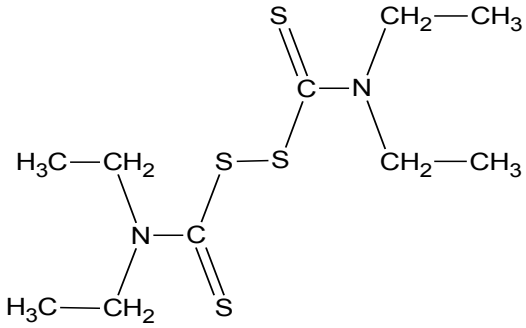

Tetraethyl thiuram disulphide

Disulfram (drug)

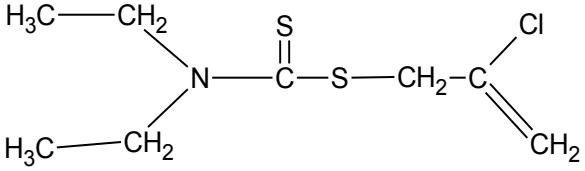

Diethyldithiocarbamate

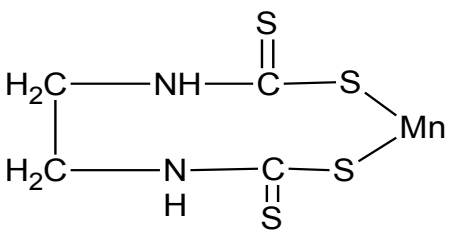

Ethylenebisdithiocarbamate

sulfallate (herbicide) *Maneb* (fungicide)

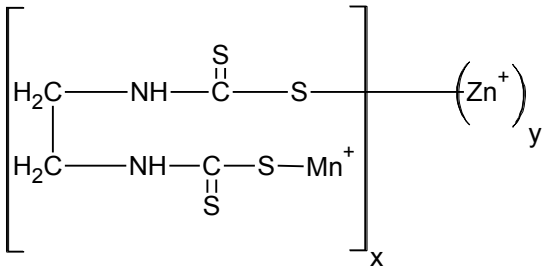

Ethylenebisdithiocarbamate *Mancozeb* (fungicide)

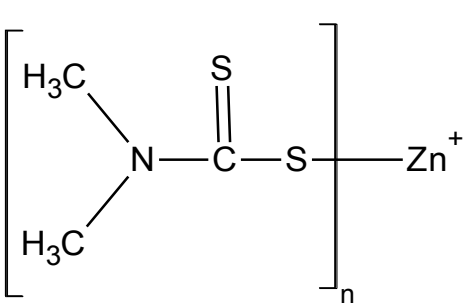

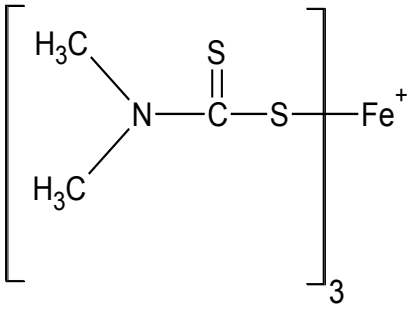

Zinc dimethyldithiocarbamates Iron dimethyldithiocarbamates

Ziram (fungicide) *Ferbam* (fungicide)

Figure 1.1: Structure of some of the widely used dithiocarbamate metal complexes and their trade names [58].

1.2.3. Nanomaterials

Prior to the extensive use of chemotherapeutics in modern health care system, inorganic antimicrobials such as silver and copper were used since ancient times to treat microbial infections. In recent times, the advances in the field of nanoscience's and nanotechnology has brought to fore the nanosized inorganic and organic particles which are finding increasing applications as amendments in industrial, medicine and

therapeutics, synthetic textiles and food packaging products. Nanoparticles (NPs) usually ranging in dimension from 1-100 nanometers (nm) have properties different from their bulk equivalent [59].

Nanostructure materials have attracted a great deal of attention in the last few years for their different characteristics that cannot be obtained from conventional macroscopic materials. Owing to quantum confinement effects, nanoparticles show novel optical, electrical, magnetic, chemical and structural properties that might find important technological applications [60]. Research in nanomaterials has received considerable attention because of their different properties and numerous applications in different areas. Applications of such materials in different fields depend on the type and nature of the NPs [61]. Semiconductor nanoparticles are of great interest because they exhibit significantly improved physical, chemical and biological properties [62]. Among metallic nanoparticles, copper nanocrystals have received considerable interest, due to their good optical, electrical and thermal properties [61]. Copper sulfide nanocrystals has fairly complex crystal chemistry owing to its ability to form sub-stoichiometric compounds Cu_xS ($2 \geq x \geq 1$). CuS exist in two common crystalline phases, the amorphous brown chalcocite Cu_2S and green crystalline covellite CuS [60].

For the application of nanoparticles in biology, biocompatibility is a highly desired trait. Biocompatibility is the materials ability to perform medically without exertion of undesired local or systemic effects [59]. Different metal nanoparticles have been used for different antimicrobial activities. The antimicrobial activity of the nanoparticles is known to be a function of the surface area in contact with the microorganisms.

Nanoparticles are commonly used in cosmetics and medicine coatings [62]. Recently, zinc oxide (ZnO) nanoparticles have been explored as an antimicrobial agent, and feasible to incorporate in the food active packaging system [63].

Purposeful use of CuO NPs due to their antimicrobial properties calls for extra attention from the environmental protection viewpoint. Unlike antibiotics that have specific targets in bacterial cells for their toxic action, copper containing NPs are also toxic to other organisms that may be exposed to these NPs via co-exposure or various waste streams [64]. In the study of biological effects of different nanoparticles, Yu and Li [65] mentioned that the effects of zinc oxide nanoparticles on neural stem cell apoptosis suggested that nano-sized zinc oxide would cause cell death when present in concentrations of 12 ppm or higher in a dose-dependent but not size-dependent manner. This suggests that all nanosized zinc is potentially dangerous, not only the super fine variety [65].

With the development of nanotechnology, copper has been increasingly used in the form of nanoparticles and applied in antimicrobial textiles [64]. The CuNPs synthesized in the study reported by Kanhed *et al.* showed the promising antifungal activity against plant pathogenic fungi *F. oxysporum, C. lunata, A. alternata,* and *P. destructiva.* The improved antifungal activity of CuNPs was due to their large surface area to volume ratio. The activity of CuNPs was found to be better than that of the commercially available fungicide against all the four plant pathogenic fungi [62]. CuS nanoparticles have been used for different purposes. Advantage of copper sulfide nanoparticles

synthesis is that, initial materials and chemicals for synthesis are cheaper and readily available [66].

Guo *et al.* [67], reported the syntheses of amorphous and crystalline copper sulfide nanoparticles and study their specific activities on different cells. As one of the most important transition metal chalcogenides semiconductor materials, copper sulfide, have varied applications in photo catalysis, solar cell devices, optical limiting, as biosensors and Li-ion batteries. As a mimic peroxidase, CuS NPs exhibited good catalytic properties, stability, and dispersibility compared to other peroxidase nanomimetics [67]. The CuS NPs were also successfully used for amperometric sensing of H_2O_2 and as peroxidase mimetic for colorimetric detection of glucose [68].

1.2.4. Biological studies of CuS nanoparticles

The fact that nanoparticles exist in the same size domain as proteins makes nanomaterials suitable for bio-tagging or labelling [69, 70]. Applications for copper nanocrystals includes their use as an anti-microbial, anti-biotic and anti-fungal (fungicide) agent when incorporated in coatings, plastics, textiles, in copper diet supplements, in the interconnect for micro, integrated circuits, for its ability to absorb radioactive caesium, in super strong metals, alloys, in nanowire, nanofiber, in certain alloy and catalyst applications. Although only few studies have been reported on the antifungal properties of copper nanoparticles, they show copper nanoparticles to have a significant promise as bactericidal agent. However, other nanoparticles, such as platinum, gold, iron oxide, silica and its oxides, and nickel have not shown bactericidal effects in studies with *Escherichia coli* [71].

Antimicrobial activity of CuS NPs was first studied on *B. anthracis* spores and cells in addition to its photothermal therapy effect. It was found that CuS NPs were highly efficient in inactivating *B. anthracis* cells, but not effective to the spores. The CuS NPs showed strong antimicrobial effects to *B. anthracis* cells, and thus a great potential to be an effective antimicrobial agent to bacterial cells [72]. There is very few research reported on the biological studies of copper sulfide nanoparticles. Researchers have been concentrating on the biological studies of silver nanoparticles and metal oxide nanoparticles.

Even though among metallic nanoparticles, copper nanoparticles have drawn attention owing to their versatile applications but there is no much research work done on CuS NPs. Copper sulfide nanoparticles has been biologically synthesized from mine wastewaters [73]. Other studies have shown that AgNPs with low toxicity and a broad spectrum of antimicrobial activity is also very effective against plant phytopathogenic fungi [74, 75]. Also Gavanji *et al.* [76] studied the effect of silver nanoparticles as biocontrol agent fungi *Trichoderma viride* and *T. harzianum*. But since silver is expensive compared to other metals like copper, there is an urgent need to develop cheap and environmental friendly antifungal agents [76].

The biocidal properties of copper are widely acknowledged and various copper compounds have been used as antifoul agents for centuries. With the development of nanotechnology, copper has been increasingly used in the form of nanoparticles [64]. When different formulations of copper are dissolved in water, copper ions are released into solution. These copper ions are toxic to fungi and bacteria because of their ability

to destroy proteins in plant tissues. On the other hand, studies into the effects of sulfur and sulfide compounds on plants are still few [77]. Truong *et al.* [78] reported on differential stability of lead sulfide nanoparticles influences biological responses in embryonic zebra fish [78]. Recently, Schneider *et al*. [79] reported the selective antimicrobial activity associated with sulfur nanoparticles.

1.2.5. Problem statement

Pathogenic and toxinogenic fungi are one of the major economic problems of crop and food production as the presence of their microorganisms threatens the plants. Although losses caused by plant pathogens may be minimized using disease-tolerant cultivars, sanitation practices, crop rotation, fungicides are often essential to maximize crop yields [28]. Chemical control has been critical in preventing losses that are due to plant diseases, especially with the development of numerous specific action fungicides since the 1960s [80].

But still the number of resistant fungal pathogenic and toxinogenic species is rising and the need for a new antifungal substances and alternative treatments is becoming increasingly obvious [81]. As the world population increases, we also need to increase food production. Despite the choice of effective fungicides available, new anti-fungal chemicals are still needed to improve the yield. For many years, a variety of different synthetic chemicals has been used as antifungal agents to inhibit the growth of plant pathogenic fungi. However, there are series of problems for the effective use of these chemicals in areas where the fungi have developed resistance [4].

The emerging infectious diseases and the development of drug resistance in the pathogenic bacteria and fungi at an alarming rate is a matter of serious concern. Despite the increased knowledge of microbial pathogenesis and application of modern therapeutics, the morbidity and mortality associated with the microbial infections still remains high. Therefore, there is a pressing demand to discover novel strategies and identify new antimicrobial agents from natural and inorganic substances to develop the next generation of drugs or agents to control microbial infections [41].

1.2.6. Rationale for the current study

In view of the growing cases of drug resistance microorganisms, there is an urgent need to search for new promising antimicrobial agents, more bio-specific and less toxic to the host and the environment. Therefore, the understanding of the interaction of metal-based drugs with biological systems still justify the study of the chemistry and physical properties of newly synthesized metal containing dithiocarbamate complexes.

Dithiocarbamate fungicides are used worldwide on a range of crops, mainly due to their high efficiency in controlling plant fungal diseases and relatively low mammalian acute toxicity [59]. However, more and more studies showed that this kind of fungicides were not easily eliminated and may represent a threat to human health and environment. Therefore, how to make better use of the advantages of dithiocarbamate-based fungicides and avoid their weakness is a problem to be solved [82]. Dithiocarbamates are preferred fungicides for fruits and vegetables due to their strong efficiency and their relatively low human toxicity while being produced quite cheaply [83].

Copper is one of the most important trace elements, present in living organisms in several enzymatic and protein functions. It is important in some enzymatic redox processes: Cytochrome oxidase, tyrosinase or Cu, Zn-superoxide dismutase, resulting from its ability to switch between Cu(II) and Cu(I) oxidation states [14]. The fungicidal activity of dithiocarbamates based metal complexes are well documented [40-49] and many dithiocarbamates are commercially available as fungicides [51, 52]. Nanomaterials such as CuS nanoparticles offer novel applications because of their size-dependent properties and in recent years, various biological application of CuS nanoparticles have been explored [83]. The motivation for the current study therefore is to contribute to the current effort to search for novel antimicrobial agents from dithiocarbamates copper complexes and copper sulfide nanoparticles.

1.2.7. Aim and objectives

The aim of this study is to synthesize and characterize copper dithiocarbamate complexes and use the complexes as single source precursors to synthesize CuS nanoparticles and study the antibacterial and antifungal activity of the compounds.

The objectives of the study are:

- To synthesize six dithiocarbamate ligands.
- To synthesize copper dithiocarbamate complexes.
- To characterize dithiocarbamate ligands and complexes using elemental analysis, conductivity measurements, ^{1}H FTIR, NMR and ^{13}C NMR spectroscopy.
- To use the dithiocarbamate complexes as single source precursors to synthesize CuS nanoparticles.

- To study the optical and structural properties of the CuS nanoparticles.
- To study the effect of temperature on the properties of the CuS nanoparticles.
- To determine the antifungal and antibacterial efficacy of the metal complexes and CuS nanoparticles.

References

[1] Ellis, S. D.; Boehm, M. J.; Mitchell, T. K. Fungal and fungal-like diseases of plants. The Ohio State University Extension. Fact Sheet: Agriculture and Natural Resources, **2008**, PP401.07.

[2] Gonzalez-Fernandez R.; Prats E.; Jorrin-Novo J. V. Proteomics of plant pathogenic fungi. *J. Biomed. Biotech.* **2010**, 932527, 1-36.

[3] Espinel-Ingroff, A. Antifungal agents. *Encyclopaedia of Microbiology* (Third Edition), **2009,** pages 205-222.

[4] Bajpai, V. K.; Kang, S. C. *In vitro* and *in vivo* inhibition of plant pathogenic fungi by essential oil and extracts of *Magnolia liliflora Desr*. *J. Agr. Sci. Tech*. **2012**, 14, 845-856.

[5] Dooley, F. D.; Nair, S. P.; Ward P. D. Increased growth and germination success in plants following hydrogen sulfide administration. *PLoS ONE*. **2013**, 8(4), 62048-62055.

[6] Sarkar, S.; Antimicrobial activity of sulphur nanoparticles on dandruff causing malassezia yeasts. M. Tech Thesis, National Institute of Technology, Rourkela, Department of Chemical Engineering, May 2012.

[7] Dean, R.; Van kan, J. A. L.; Pretorius, Z. A.; Hammond-Kosack, K. E.; Di pietro, A.; Spanu, P. D.; Rudd, J. J.; Dickman, M.; Kahmann, R.; Ellis, J.; Foster G. D. The top ten fungal pathogens in molecular plant pathology. *Mol.* Plant *Path*. **2012**, 13(4), 414–430.

[8] Gauthier, G. M.; Keller, N. P. Crossover fungal pathogens: The biology and pathogenesis of fungi capable of crossing kingdoms to infect plants and humans. *Fungal Gen. Biol*. **2013**, 61,146–157.

[9] Adaskaveg, J.; Gubler, D.; Michailides, T. Fungicides, bactericides, and biologicals for deciduous tree fruit, nut, strawberry, and vine crops. University of California, *Dept. Plant Path.* **2012**, 1-54.

[10] Jamil, S.; Kumar, M. Evaluation of fungicides against phyllosphere mycoflora of foliage plants. *Biol. Int. J*. **2010**, 2(1), 56-59.

[11] Singh, N.; Bhattacharya, S. Synthesis and characterization of some triorgano, diorgano, monoorganotin and a triorganolead heteroaromatic dithiocarbamate complexes. *J. Organomet. Chem*. **2012**, 700, 69-77.

[12] Heard, P. J.; Main group dithiocarbamate complexes. *Progress Inorg. Chem*. **2005**, 53-69.

[13] Vijayanthimala, R.; Krishnan, B.; Vijaya, M. Synthesis, characterisation and study of biological application of simple mixed ligand complexes of nickel(II) with morpholine dithiocarbamate and amines such as ethylene diamine, diethylenetriamine and triethylenetetramine. *J. Pharm. Biol. Chem*. *Sci.* **2014**, 5(3), 0975-8585.

[14] Ferreira, I. P.; de Lima G. M.; Paniago, E. B.; Takahashi, J. A.; Krambrock, K.;, Pinheiro, C. B.; Wardell, J. L.; Visentin, L.C.; Synthesis, characterization, structural and biological aspects of copper(II) dithiocarbamate complexes – Part II, $[Cu\{S_2CN(Me)(R1)\}_2]$, $[Cu\{S_2CN(Me)(R_2)\}_2]$ and $[Cu\{S_2CN(R_3)(R_4)\}_2]$ {R_1 = $ACH_2CH(OMe)_2$, R_2 = 2-methyl-1,3-dioxolane, R_3 = $ACH_2(CH_2)_2N_2CHPhOCH_2Ph$ and R_4 = ACH_2CH_2OH}. *J. Mol. Struct.* **2013**, 1048, 357–366.

[15] Mbese, J. Z.; Ajibade P. A. Synthesis, structural and optical properties of ZnS, CdS and HgS nanoparticles from dithicarbamato single molecule precursors. *J. Sulfur Chem.* **2014**, 35(4), 438-449.

[16] Onwudiwe, D. C.; Ajibade, P. A. Synthesis and characterization of metal complexes of *N*-alkyl-*N*-phenyl dithiocarbamates. *Polyhedron*, **2009**. 1431-1436.

[17] Ajibade, P. A; Onwudiwe, D. C. Synthesis and characterization of group 12 complexes of *N,N*-methyl phenyl-*N,N*-butyl phenyl dithiocarbamate. *J. Coord. Chem*. **2011**, 10, 2963-2973.

[18] Golcu, A. Transition metal complexes of propranolol dithiocarbamate: Synthesis, characterization, analytical properties and biological activity. *Trans. Met. Chem.* **2006**, 31, 405–412.

[19] Pandey, A.; Mathew A. J.; Kamle, M.; Mishra, R. K.; Kumar, P. Efficacy of fungicides for control of white mold (*Sclerotinia sclerotiorum* Lib.) de Bary in lima bean. *J. Hortl. Sci.* **2012,** 7(1), 114-117.

[20] He, L.; Liu, Y; Mustapha, A.; Lin, M. Antifungal activity of zinc oxide nanoparticles against *Botrytis cinerea* and *Penicillium expansum*. *Microbiol. Res*. **2011**,166, 207—215.

[21] Roya, R.; Kumara, S.; Tripathia, A.; Dasa, M.; Dwivedia P. D.; Interactive threats of nanoparticles to the biological system. *Immunol. Lett*. **2014**, 158, 79– 87.

[22] Cioffi, N.; Torsi, L.; Ditaranto, N.; Tantillo, G.; Ghibelli, L.; Sabbatini, L.; Bleve-Zacheo, T.; D'Alessio, M.; Zambonin, P. G.; Traversa, E. Copper nanoparticle/polymer composites with antifungal and bacteriostatic properties. *Chem. Mater.* **2005**, 17, 5255-5262.

[23] Allaker, R. P.; Memarzadeh, K. Nanoparticles and the control of oral infections. *Int. J. Antimicr. Agents*, **2014**, 43, 95– 104.

[24] Wang, C.; Yuan, J.; Niu, H.; Yan, E.; Zhao, H. Investigation of fundamental parameters affecting electrospun PVA/CuS composite nanofibres. *Pigment. Resin Tech*. **2009**, 38, 1, 25–32.

[25] Elena, C. R. Nanoparticles: Opportunities and threats. *Rada, J Bioremed Biodeg.* **2014**, 1-5.

[26] Hamouda, I. M. Current perspectives of nanoparticles in medical and dental biomaterials. *J. Biomed. Res*. **2012**, 26(3), 143-151.

[27] Elsaka S. E.; Hamouda I. M.; Swain M. V. Titanium dioxide nanoparticles addition to a conventional glass-ionomer restorative: Influence on physical and antibacterial properties. *J. Dent*. **2011**, 8, 589–598.

[28] Wilmot, M. Inhibition of phytopathogenic fungi on selected vegetable crops by catechins, caffeine, theanine and extracts of *Camella sinensis* (L.) O. Kuntze. M. Sc. Dissertation, University of Pretoria, Faculty of Natural and Agricultural Science, **2007.**

[29] Morton, V.; Staub, T. A short history of fungicides. *APSnet*. DOI: 10.1094/APSnetFeature-2008-0308.2008.
https://www.apsnet.org/publications/apsnetfeatures/Pages/Fungicides.aspx
(accessed 14 September 2014).

[30] Ivanova, B.; Spiteller, M. Solid-state UV–MALDI–MS assay of transition metal dithiocarbamate fungicides. *Environ. Sci. Pollut Res*. **2014**, 21, 1163–1177.

[31] Goubert-Renaudin, S.; Schneiderb, R.; Walcarius, A. Synthesis of new dithiocarbamate-based organosilanes for grafting on silica. *Tetrahedron Lett***. 2007**, 48, 2113–2116.

[32] Cao, S.; Feng, Y.; Jiang, Y.; Liu, S.; Ding, G.; Li, R. Synthesis and *in vitro* antitumor activity of 4(3H)-quinazolinone derivatives with dithiocarbamate side chains*. Bioorg. Med. Chem. Lett*. **2005**, 15, 1915–1917.

[33] Macias, B.; Villa, M.V.; Chicote, E.; Martin-Velasco, S.; Eiras, A. C.; Borras, J. Copper complexes with dithiocarbamates derived from natural occurring amino acids. Crystal and molecular structure of $[Cu(en)(EtOH)(H_2O)_3][Cu(dtc\text{-}pro)_2]$. *Polyhedron*, **2002**, 21, 1899-1904.

[34] Ahamad, R. M.; Rao, M. M.; Rafi, G.; Mohiddin, J.; Sreeramulu, J. Synthesis, spectral analysis and antimicrobial activity of novel dithiocarbamate Schiff base metal complexes. *Archives Appl. Sci. Res*. **2012**, 4 (2), 858-862.

[35] Gupta, A. N.; Singh, V.; Kumar, V.; Rajput, A.; Singh, L.; Drew, M. G. B.; Singh, N. Syntheses, crystal structures and conducting properties of new homoleptic copper(II) dithiocarbamate complexes. *Inorg. Chim. Acta*, **2013**, 408,145–151.

[36] de Lima, G. M.; Menezes, D. C.; Cavalcanti, C. A.; Jaqueline A. F.; Ferreira, I. P.; Paniago, E. B.; Wardell, J. L.; Wardell, S. M. S. V.; Krambrock, K.; Mendes, I. C.; Beraldo, H. Synthesis, characterisation and biological aspects of copper(II) dithiocarbamate complexes, $[Cu\{S_2CNR(CH_2CH_2OH)\}_2]$, (R = Me, Et, Pr and CH_2CH_2OH*). J. Mol. Struc*. **2011**, 988, 1–8.

[37] Sarma, R.; Kaushik, N. K. Studies on organomercury(II) complexes with piperidine and 2-aminopyridine dithiocarbamates. *Indian J. Chem*. **2004**, 43A(4), 769-772.

[38] Tan. Y.; Jin. S.; Hamers. R. J.; Photostability of CdSe quantum dots functionalized with aromatic dithiocarbamate ligands. *Mater. Interfaces*, **2013**, 5, 12975−12983.

[39] Rajput, K.; Singh, V.; Singh, S. K.; Prasad, L. B.; Drew, M. G. B.; Singh, N. Cooperative metal–ligand-induced properties of heteroleptic copper(I) xanthate/dithiocarbamate PPh_3 complexes. *Eur. J. Inorg. Chem*. **2012**, 24, 3885–3891.

[40] Lehmann, H.; Elberfeld, W.; Burscheid, F. G.; Lautenschlager, W. propylene-(1, 2)-bls-dithiocarbamates. U. S. Patent 3.326.951, **1967**, 36,152.

[41] Han-Dong Y.; Zhai, Y.; Yu-Ying S, Da-Qi, W. Synthesis, characterizations and crystal structures of new antimony(III) complexes with dithiocarbamate ligands. *Polyhedron*. **2008,** 27,663–670.

[42] Baikernova, G. G.; Addulina, G. A.; Gazaliev, A. M.; Fazylov, S. D.; Kudaibergenova, S. Z. Synthesis and antimicrobial activity of anabasine, piperidie and morpholine dithiocarbamates. *Pharmcent. Chem. J*. **2004**, 38(1), 19-20.

[43] Plyusnin, V. F.; Kolomeets, A. V.; Grivin, V. P.; Larionov, S. V.; Lemmetyinen, H. Photochemistry of dithiocarbamate Cu(II) complex in tetrachloromethane. *J. Phys. Chem. A*, **2011**, 115, 1763–1773.

[44] Ekennia, A. C. Antibacterial application of novel mixed-ligand dithiocarbamate complexes of nickel(II). *J. Appl. Chem*. **2013**, 5(2), 36-39.

[45] Tiekink, E. R. T. Tin dithiocarbamates: Applications and structures. *Appl. Organomet. Chem*. **2008**, 22, 533–550.

[46] Khan, H.; Badshah, A.; Murtaz, G.; Said, M.; Rehman, Z.; Neuhausen, C.; Todorova, M.; Jean-Claude, B. J.; Butle, I. S. Synthesis, characterization and anticancer studies of mixed ligand dithiocarbamate palladium(II) complexes. *Eur. J. Med. Chem*. **2011**, 46, 4071-4077.

[47] McCubbin, Q. J.; Stoddart, F. J.; Welton, T.; White, A. J. P.; Williams, D. J. Dithiocarbamate-functionalized dendrimers as ligands for metal complexes*. Inorg. Chem***. 1998**, 37, 3753-3758.

[48] Jayaraju, A.; Ahamad, M. M.; Rao, R. M.; Sreeramulu, J. Synthesis, characterization and biological evaluation of novel dithiocarbamate metal complexes. *Der. Pharm. Chemic.* **2012,** 4(3), 1191-1194.

[49] Michael H.; Andreas E.; Salima M.; Ying C.; Marc S.; Frank M. Role of copper oxides in contact killing of bacteria*. Langmuir*, **2013,** 29, 16160−16166.

[50] Nabipour, H.; Ghammamy, S.; Ashuri, S.; Aghbolagh, Z. S. Synthesis of a new dithiocarbamate compound and study of its biological properties. *Org. Chem. J*. **2010**, 2, 75-80.

[51] Tomas. C.; Katerina. R.; Paul. Z.; Hans. M.; Jana H. Direct analysis of dithiocarbamate fungicides in fruit by ambient mass spectrometry. *Food Addit. Contamin*. **2011**, 28(10), 1372–1382.

[52] Goranka. C.; Wolfgang. S. Residue analysis of dithiocarbamate fungicides. *Anal. Chem*. **2009**, 28(1), 40-50.

[53] Dasgupta, S.; Mujawar, S.; Banerjee, K.; Huebschmann, H. Analysis of Dithiocarbamate Pesticides by GC-MS. *Thermo Fisher Sci. Inc*. **2012**, 1-5.

[54] Singh, M.; Garg, A.; Sidhu, A.; Kumar, V. Synthesis of quaternary ammonium salts with dithiocarbamate moiety and their antifungal activities against Helminthosporium oryzae. *J. Chem. Sci*. **2013**, 125, 3-567.

[55] Deveci, E.; Yorgancilar, E.; Ekinci, C. Effects of manganese ethylene-bis-dithiocarbamate (maneb) on rat nasal respiratory mucosa. *Acta Med. Mediterranea*. **2013**, 29, 875-878.

[56] Malik, K. A.; Faubel, W. Capillary electrophoretic determination of zinc dimethyldithiocarbamate (Ziram) and zinc ethylenebisdithiocarbamate (Zineb). *Talanta*, **2000,** 52, 341–346.

[57] Hasan H. O. Fungicides and their effects on animals, fungicides, Odile Carisse (Ed.) ISBN: 978-953-307-266-1, In Tech. **2010**, 266-307.

[58] Mulkey, M. E. The determination of whether dithiocarbamate pesticides share a common mechanism of toxicity. U.S. Environmental Protection Agency, Washington D.C. 20460. **2001,** 2-46

[59] Ravishankar R. V.; Jamuna B. A. Nanoparticles and their potential application as antimicrobials. *Formatex*. **2011,** 197-203.

[60] Nath, S. K.; Kalita, P. K. Chemical synthesis of copper sulphide nanoparticles embedded in PVA matrix. *Nanosci. Nanotechnol. Int. J*. **2012**, 2(1), 8-12.

[61] Soomro, R. A.; Sherazi, S. T. H.; Memon, S. N.; Shah, M. R.; Kalwar, N. H.; Hallam, K. R.; Shah, A. Synthesis of air stable copper nanoparticles and their use in catalysis. *Adv. Mater. Lett.* **2014**, 5(4), 191-198.

[62] Kanhed, P.; Birla, S.; Gaikwad, S.; Gade, A.; Seabra, A. B.; Rubilar, O.; Duran, N.; Rai, M. *In vitro* antifungal efficacy of copper nanoparticles against selected crop pathogenic fungi. *Mater. Lett*. **2014**, 115, 13–17.

[63] Akbar, A.; Anal, A. K. Zinc oxide nanoparticles loaded active packaging, a challenge study against Salmonella typhimurium and *Staphylococcus aureus* in ready-to-eat poultry meat. *Food Control*, **2014**, 38, 88-95.

[64] Bondarenko, O.; Ivask, A.; Kakinen, A.; Kahru, A. Sub-toxic effects of CuO nanoparticles on bacteria: Kinetics, role of Cu ions and possible mechanisms of action. *Environ. Pollut*. **2012**, 169, 81-89.

[65] Yu, J. X.; Li, T. H. Distinct biological effects of different nanoparticles commonly used in cosmetics and medicine coatings. Cell. *Biosci*. **2011,** 1, 19-27.

[66] Abdullaeva, Z.; Omurzak, E.; Mashimo, T. Synthesis of copper sulfide nanoparticles by pulsed plasma in liquid method. *World Acad. Sci. Eng. Tech.* **2013***,* 66-78.

[67] Guo, L.; Panderi, I.; Yan, D. D.; Szulak, K.; Li, Y.; Chen, Y.; Ma, H.; Niesen, D. B.; Seeram, N.; Ahmed, A.; Yan, B.; Pantazatos, D.; Lu, W. A comparative study of hollow copper sulfide nanoparticles and hollow gold nanospheres on degradability and toxicity. *J. Amer. Chem. Soc*. **2013**, 7(10), 8780–8793.

[68] Dutta, A. K.; Samanta, S.; Partha, K. S.; Adhikary, B.; Biswas, P. CuS nanoparticles as a mimic peroxidase for colorimetric estimation of human blood glucose level. *Talanta*. **2013**, 107, 361-367.

[69] Salata, O. V. Applications of nanoparticles in biology and medicine. J. Nanobiotech. **2004**, 2-3.

[70] Gunalana, S.; Sivaraja, R.; Rajendran, V. Green synthesized ZnO nanoparticles against bacterial and fungal pathogens. *Mater. Int*. **2012**, 22(6), 693–700.

[71] Theivasanthi, T.; Alagar, M. Studies of Copper Nanoparticles Effects on Micro-organisms. Ayya Nadar Janaki Ammal College. **2011**, 1-6.

[72] Addae, E.; Dong, X.; McCoy, E.; Yang, C.; Chen, W.; Yang, L. Investigation of antimicrobial activity of photothermal therapeutic gold/copper sulfide core/shell nanoparticles to bacterial spores and cells. *J. Biol. Eng*. **2014**, 8, 11-22.

[73] Schaffie, M.; Hosseini, M. R. Biological process for synthesis of semiconductor copper sulphide nanoparticle from mine wastewaters. *J. Environ. Chem. Eng*. **2014**, 2, 386–391.

[74] Kim, S. W.; Jung, J. H.; Lamsal, K.; Kim, Y. S.; Min, J. S.; Lee, Y. S. Antifungal effects of silver nanoparticles (Agnps) against various plant pathogenic fungi. *Mycobiology,* **2012**, 40(1), 53-58.

[75] Ingle, A.; Rai, M.; Gade, A.; Bawaskar, M. Fusarium solani: A novel biological agent for the extracellular synthesis of silver nanoparticles. *J. Nanopart. Res*. **2009,** 11, 2079–2085.

[76] Gavanji, S.; Shams, M.; Shafagh, N.; Zand, A. J.; Larki, B.; Mohammadi, M. D.; Taraghian, A. H.; Niknezhad, S. V. Destructive effects of silver nanoparticles on biocontrol agent fungi *Trichoderma viride* and *T. harzianum*. *Caspian J. Appl. Sci. Res.* **2012**, 1(12), 83-90.

[77] Saad, B.; Strimari, M. C.; Saleh, M. I. Flow-injection spectrophotometric method for the determination of Ziram (dithiocarbamate fungicide). *Malaysian J. Anal. Sc*. **2001**, 7(1), 103-107.

[78] Truong, L.; Moody, I. S.; Stankus, D. P.; Nason, J. A.; Lonergan, M.; Tanguay, R. L. Differential stability of lead sulfide nanoparticles influences biological responses in embryonic zebrafish. *Arch Toxicol*. **2011**, 85(7), 787-98.

[79] Schneider, T.; Baldauf, A.; Ba, L. A.; Jamier, V.; Khairan, K.; Sarakbi,M.; Reum, N.; Schneider, M.; Roseler, A.; Becker, K.; Burkholz, T.; Winyard, P. G.; Kelkel, M.; Diederich, M.; Jacob, C. Selective antimicrobial activity associated with sulfur nanoparticles. *J. Biomed. Nanotech*. **2011**, 1-11.

[80] Hirooka, T.; Ishii, H. Chemical control of plant diseases*. J Gen Plant Pathol*. **2013,** 79, 390–401.

[81] Zabka, M.; Pavela, R.; Slezakova, L. Antifungal effect of *Pimenta dioica* essential oil against dangerous pathogenic and toxinogenic fungi. *Indust. Crops Products,* **2009**, 30, 250–253.

[82] Qina, Y.; Liua, S.; Xinga, R.; Yua, H.; Li, K.; Menga, X.; Li R.; Li, P. Synthesis and characterization of dithiocarbamate chitosan derivatives with enhanced antifungal activity. *Carbohydr. Polym*. **2012**, 89, 388– 393.

[83] Goel S.; Chen F.; Cai W. Synthesis and biomedical applications of CuS nanoparticles: From sensors to theranostics. Small. **2014**, 10(4), 631-645.

CHAPTER TWO

2.0. Experimental

2.1. Materials

2.1.1. Chemicals

Aniline, N-ethylaniline, morpholine, piperidine, 2-pyrrolidone, anisidine, butyl amine, carbon disulfide, sodium hydroxide and copper(II) chloride,

2.1.2. Solvents

Diethyl ether, ethanol, DMSO, DMF,

2.2. Physical measurements

2.2.1 FTIR spectroscopy

FT-IR study was carried out using Perkin Elmer FTIR-2000; FTIR spectra were recorded in the range of 400–4000 cm^{-1} at a resolution of 4 cm^{-1} with KBr pellets technique. The KBr pellets were prepared by mixing the sample with KBr powder in ratio 1:100. All the spectra were collected at room temperature.

2.2.2. UV-Vis spectroscopy

The electronic spectra of the complexes in solution were recorded using Perkin-Elmer Lambda 25 UV-Vis spectrometer. The samples were placed in quartz cuvettes of 1 cm path length. The solvents used were different depending on the solubility of the complexes in a particular solvent and its stability.

2.2.3. NMR spectroscopy

The NMR spectra of both ligands and complexes were recorded using Bruker ultrashield 400 NMR spectrometer at frequencies 400.1 MHz for ^{1}H and 100.6 MHz for ^{13}C nuclei. They were recorded under 303 K temperature. The samples were dissolved in DMSO and placed in magnetic field. A radiofrequency generator then irradiated the sample with a short pulse of radiation, causing resonance.

2.3 Synthesis of ligands

2.3.1 Synthesis of sodium salt of anisidine dithiocarbamate, L_1

Sodium hydroxide (2 g, 0.05 mol) dissolved in minimum amount of distilled water was allowed to attain an ice temperature, to this, cold carbon disulfide (3 mL, 0.05 mol) was added. This was then followed by the addition of anisidine (6.1575 g, 0.05 mol). The mixture was stirred for 2-3 h while keeping the temperature below 4 ^{o}C. A white product was then filtered and washed with ether and dried in a desiccator. The reaction is shown in Scheme 2.1. Yield = 7.19 g, 65%.

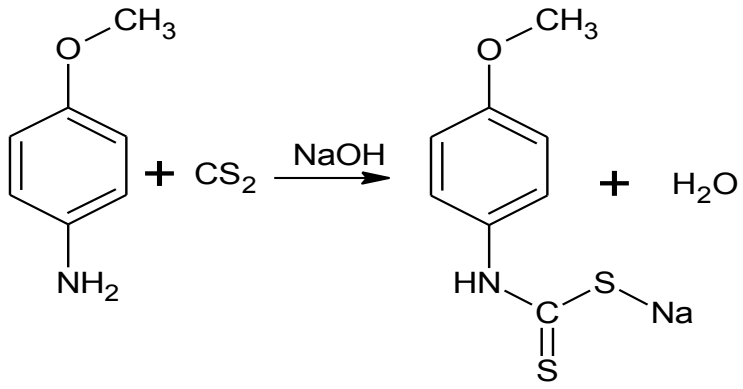

Scheme 2.1: Preparation of sodium salt of anisidine dithiocarbamate

2.3.2 Synthesis of sodium salt of aniline dithiocarbamate, L_2

Sodium hydroxide (2 g, 0.05 mol) dissolved in minimum amount of distilled water was allowed to attain an ice temperature, cold carbon disulfide (3 mL, 0.05 mol) was added to the solution. This was then followed by the addition of aniline (4.6 mL, 0.05 mol). The mixture was stirred for 2-3 h while keeping the temperature below 4 ^{o}C as shown in Scheme 2.2. A yellowish product was then filtered and washed with ether and dried in a desiccator. Yield = 4.97 g, 52%.

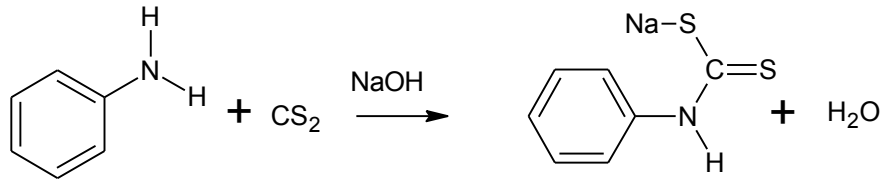

Scheme 2.2: Preparation of sodium salt of aniline dithiocarbamate

2.3.3 Synthesis of sodium salt of ethyl aniline dithiocarbamate, L_3

Sodium ethyl aniline was prepared using the procedure in the literature [1]. Sodium hydroxide (2 g, 0.05 mol) dissolved in minimum amount of distilled water was allowed to attain an ice temperature, followed by the addition of cold carbon disulfide (3 mL, 0.05 mol). This was then followed by the addition of N-ethyl aniline (5.44 mL, 0.05 mol) as shown in Scheme 2.3. The mixture was stirred for 2-3 h while keeping the temperature below 4^{o} C. A yellowish-white product was then filtered and washed with ether and dried in a desiccator. Yield = 5.15 g, 47%.

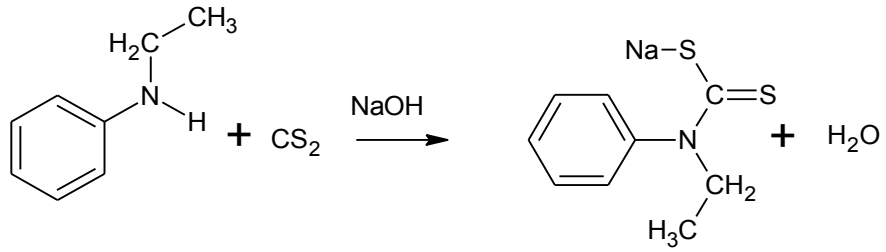

Scheme 2.3: Preparation of sodium salt of ethyl aniline dithiocarbamate.

2.3.4 Synthesis of sodium salt of butylamine dithiocarbamate, L_4

Sodium hydroxide (2 g, 0.05 mol) dissolved in minimum amount of distilled water was allowed to attain an ice temperature, cold carbon disulfide (3 mL, 0.05 mol) was added to the solution. This was then followed by the addition of butyl amine (4.99 mL, 0.05 mol). The mixture was stirred for 2-3 h while keeping the temperature below 4 ^{o}C. A white needle like product was then filtered and washed with ether and dried in a desiccator. Scheme 2.4 shows the reaction. Yield = 4.88 g, 57%.

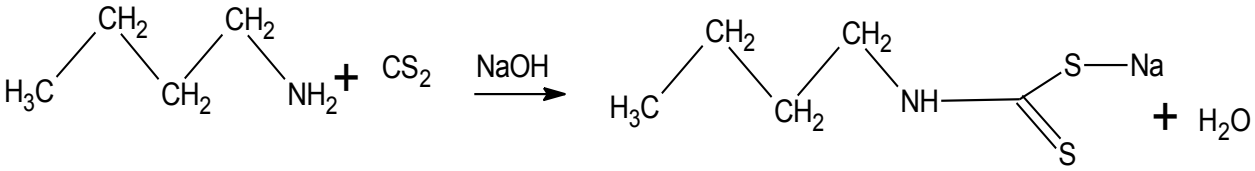

Scheme 2.4: Preparation of sodium salt of butyl amine dithiocarbamate

2.3.5 Synthesis of sodium salt of piperidine dithiocarbamate, L_5

Sodium hydroxide (2 g, 0.05 mol) dissolved in minimum amount of distilled water was allowed to attain an ice temperature, to this cold carbon disulfide (3 mL, 0.05 mol) was added. This was then followed by the addition of piperidine (5.00 mL, 0.05 mol). The mixture was stirred for 2-3 hours while keeping the temperature below 4 ^{0}C as shown

in Scheme 2.5. A white product was then filtered and washed with ether and dried in a desiccator. Yield = 8.25 g, 90%.

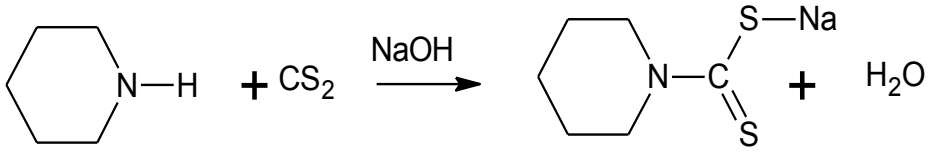

Scheme 2.5: Preparation of sodium salt of piperidine dithiocarbamate

2.3.6 Synthesis of sodium salt of morpholine dithiocarbamate, L_6

Sodium hydroxide (2 g, 0.05 mol) dissolved in minimum amount of distilled water was allowed to attain an ice temperature, to this cold carbon disulfide (3 mL, 0.05 mol) was added. This was then followed by the addition of morpholine (4.8 mL, 0.05 mol). The mixture was stirred for 2-3 h while keeping the temperature below 4 ^{o}C as shown in Scheme 2.6. A white product was then filtered and washed with ether and dried in a desiccator. Yield = 6.29 g, 68%.

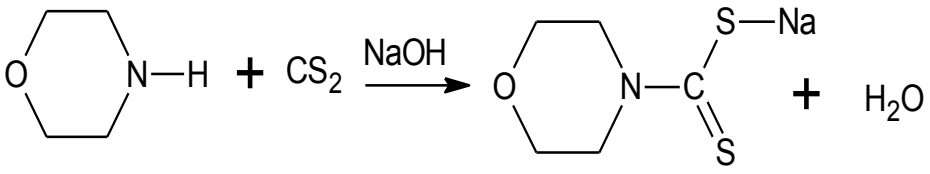

Scheme 2.6: Preparation of sodium salt of morpholine dithiocarbamate

2.4. Synthesis of copper(II) complexes

2.4.1 Synthesis of copper(II) anisidine dithiocarbamate complex

The preparation of the complex was carried out at room temperature. About 15 mL aqueous solution of the $CuCl_2$ (0.107 g, 0.625 mmol), was added to 15 mL aqueous

solution of anisidine (1.250 mmol), the brown precipitate which immediately forms was stirred for about 45 minutes to ensure complete reaction (Scheme 2.7). The solid precipitate was filtered off, rinsed with distilled water and dried at ambient temperature

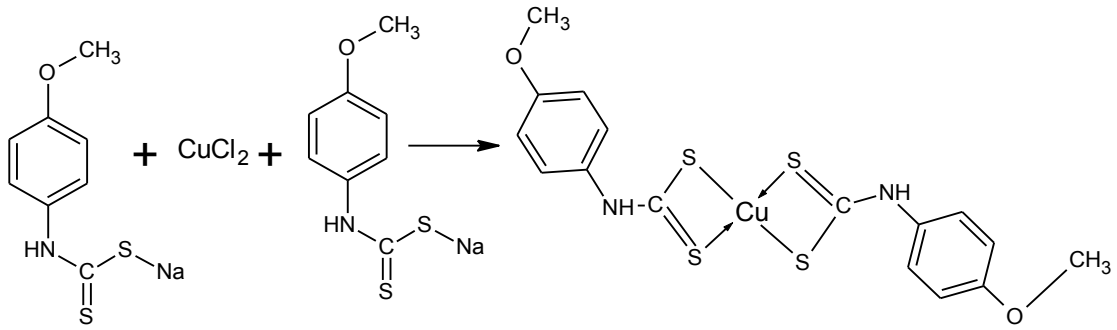

Scheme 2.7: Synthesis of copper(II) anisidine dithiocarbamate complex

2.4.2 Synthesis of copper(II) aniline and ethyl aniline dithiocarbamate complexes

The preparation of complexes was carried out at room temperature. About 15 mL aqueous solution of the $CuCl_2$ (0.107 g, 0.625 mmol), was added to 15 mL aqueous solution of the respective ligand (1.250 mmol), the brown precipitate which immediately forms was stirred for about 45 minutes to ensure complete reaction. The solid precipitate was filtered off, rinsed with distilled water and dried at ambient temperature [2]. The reaction is shown in Scheme 2.8.

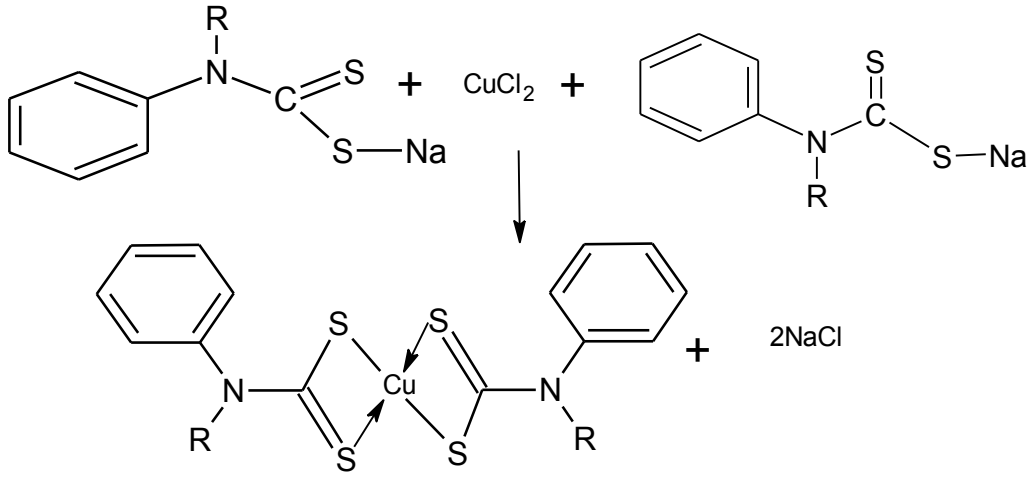

Scheme 2.8: Synthesis of copper(II) aniline dithiocarbamate complex and copper ethyl aniline dithiocarbamate complexes (R = H or C_2H_5).

2.4.3 Synthesis of copper(II) butyl amine dithiocarbamate complex

The preparation of the complex was carried out at room temperature. About 15 mL aqueous solution of the $CuCl_2$ (0.107 g, 0.625 mmol), was added to 15 mL aqueous solution of butyl amine (1.250 mmol), the light brown precipitate which immediately forms was stirred for about 45 minutes to ensure complete reaction. The solid precipitate was filtered off, rinsed with distilled water and dried at ambient temperature. The reaction is shown in Scheme 2.9.

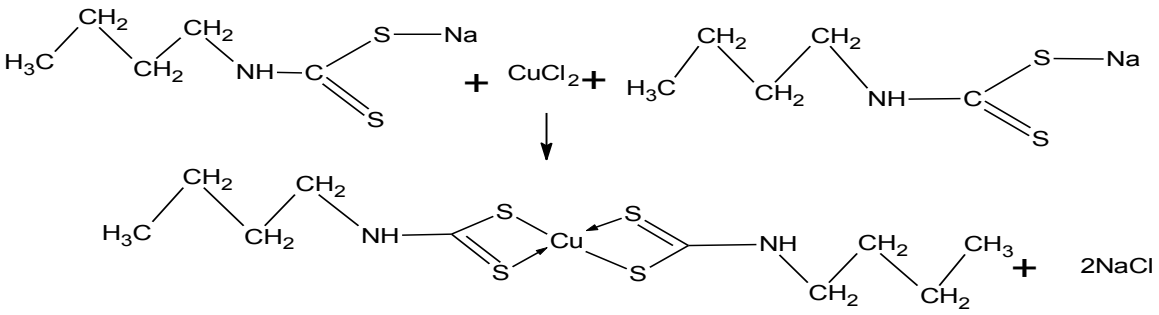

Scheme 2.9: Synthesis of copper(II) butyl amine dithiocarbamate complex.

2.4.4 Synthesis of copper(II) piperidine dithiocarbamate complex

The preparation of the complex was carried out at room temperature. About 15 mL aqueous solution of the $CuCl_2$ (0.107 g, 0.625 mmol), was added to 15 mL aqueous solution of piperidine (1.250 mmol), the yellow precipitate which immediately forms was stirred for about 45 minutes to ensure complete reaction. The solid precipitate was filtered off, rinsed with distilled water and dried at ambient temperature.

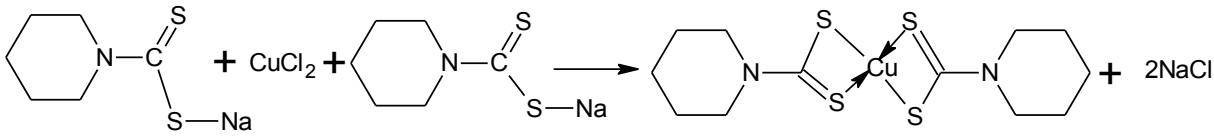

Scheme 2.10: Synthesis of copper piperidine dithiocarbamate complex.

2.4.5 Synthesis of copper morpholine dithiocarbamate complex

The preparation of the complex was carried out at room temperature. About 15 mL aqueous solution of the $CuCl_2$ (0.107 g, 0.625 mmol), was added to 15 mL aqueous solution of morpholine (1.250 mmol), as shown in Scheme 2.11, the dark brown precipitate which immediately forms was stirred for about 45 minutes to ensure complete reaction. The solid precipitate was filtered off, rinsed with distilled water and dried at ambient temperature.

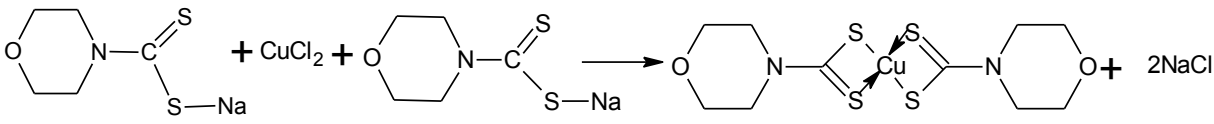

Scheme 2.11: Synthesis of copper(II) morpholine dithiocarbamate complex.

References

[1] Onwudiwe, D. C.; Ajibade, P. A. Synthesis and crystal structure of bis(N-alkyl-N-phenyl dithiocarbamato)mercury(II). *J. Chem. Crystallogr*. **2011,** 41, 980-985.

[2] Onwudiwe, D. C.; Ajibade, P. A. Synthesis and characterization of metal complexes of N-alkyl-N-phenyl dithiocarbamates. *Polyhedron*, **2010**, 29, 1431-1436.

CHAPTER THREE

3.0. Spectroscopic characterization of the dithiocarbamate ligands and copper(II) complexes

3.1. Introduction

Dithiocarbamates are formed by the exothermic reaction between carbon disulfide and appropriate amine in the presence of a strong base such as sodium hydroxide, potassium hydroxide or ammonia solution, as shown in Scheme 3.1 [1].

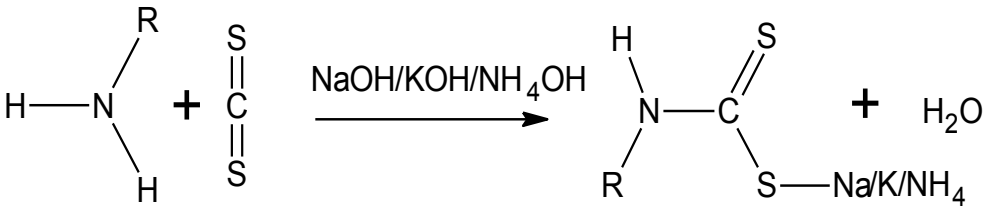

Scheme 3.1: General synthesis of dithiocarbamate ligands [1] (R = alkyl or aryl group)

Most dithiocarbamates are known to be stable under basic and neutral conditions except those synthesized from primary amine that decomposes under basic conditions. However, most dithiocarbamates decompose under acidic conditions to the respective amine and CS_2 [2] as shown in equation 1.

$$R_2NCS^-_2 \longleftrightarrow R_2NH + CS_2 \quad \ldots\ldots 1$$

Dithiocarbamates are often used for the synthesis of transition metal complexes due to their ability to stabilize transition metals in high oxidation state [3]. Dithiocarbamates can form multiple π-bonds and addition π-electrons can move from nitrogen to sulfur through a planar delocalized π-orbital system of the S-C-S moiety of the

dithiocarbamate ligand. Thus, the dithiocarbamic moiety exist in different resonant form (Scheme 3.2). This makes dithiocarbamate ligands to act as strong electron donors [4].

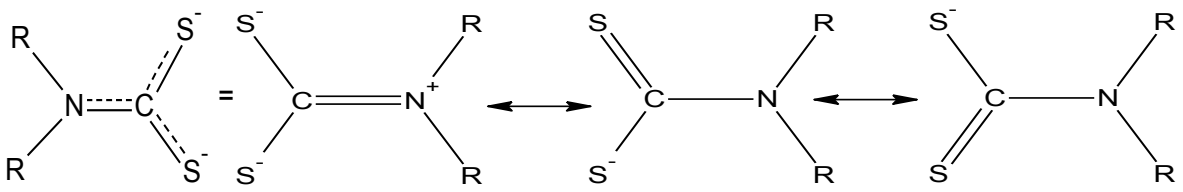

Scheme 3.2: Different resonant forms of dithiocarbamic moiety

As a result of the different resonance forms, dithiocarbamate ligands can coordinate the metal ions as bidentate chelating, monodentate or bidentate bridging ligands [4]. These coordination modes leads to the structural organisation of the resulted metal complexes [5]. Thus, dithiocarbamate complexes are known to give striking structural features [6, 7]. In this chapter, the mechanism of the formation of the dithiocarbamate ligands and their corresponding copper(II) complexes, physical measurements and their spectroscopic characterization are presented.

3.2 Synthesis of ligands and complexes

Since dithiocarbamate salts most often decomposes at high temperature they are usually prepared at very low temperatures and this method can give high yield [7]. This method was adopted in this study. The synthesis of the dithiocarbamate ligands were carried out at a temperature below 4 ^{o}C. The mechanisms of formation of the different ligands are shown in Scheme 3.3.

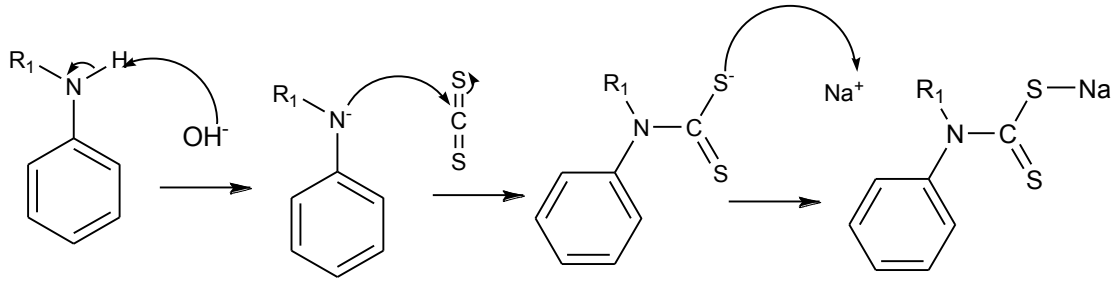

a. Mechanism of formation for the alkyl phenyl dithiocarbamates, aniline and ethyl aniline dithiocarbamates. R^1 = H or CH_3CH_2

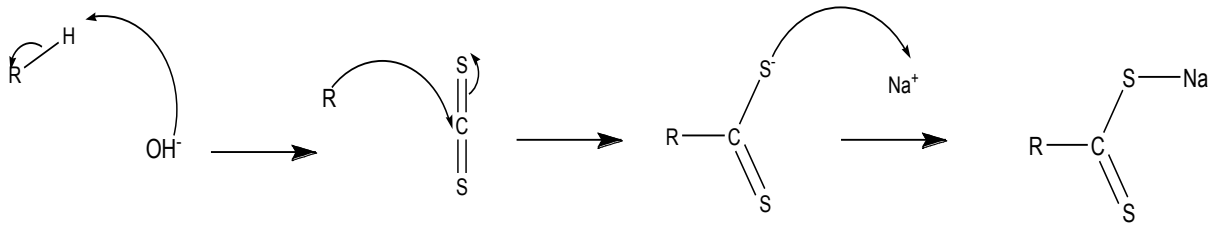

b. Mechanism of formation for anisidine, morpholine and piperidine dithiocarbamates.

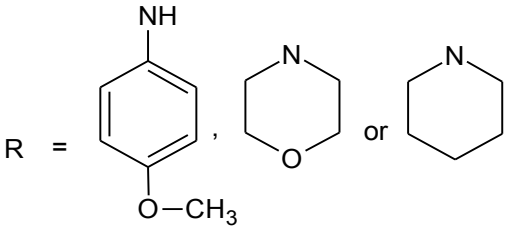

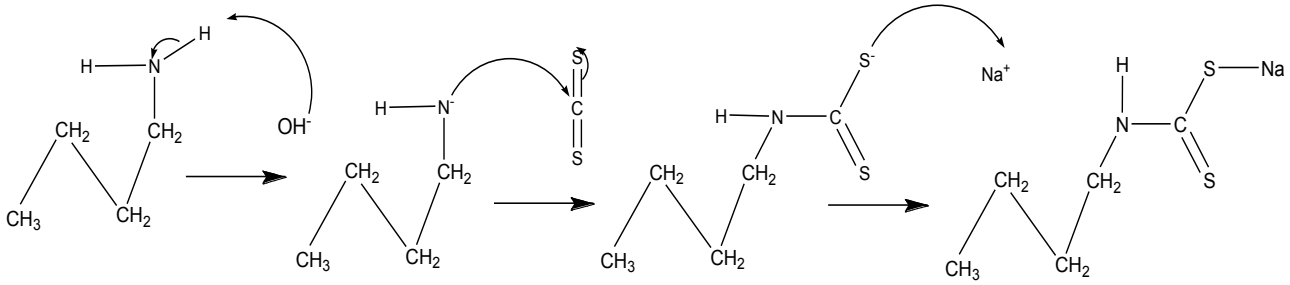

c. Mechanism of formation for butyl amine dithiocarbamate.

Scheme 3.3: Mechanism of formation of dithiocarbamate ligands

The reaction of the respective amines with carbon disulfide and sodium hydroxide gives the dithiocarbamate sodium salts. All the ligands are stable at room temperature. The complexes were obtained after reacting each ligand with copper(II) chloride in a 2:1 mole ratio at room temperature as shown in Scheme 3.4. The complexes are formulated as a four coordinate species in which the dithiocarbamate ligand acts as a bidentate chelating ligands.

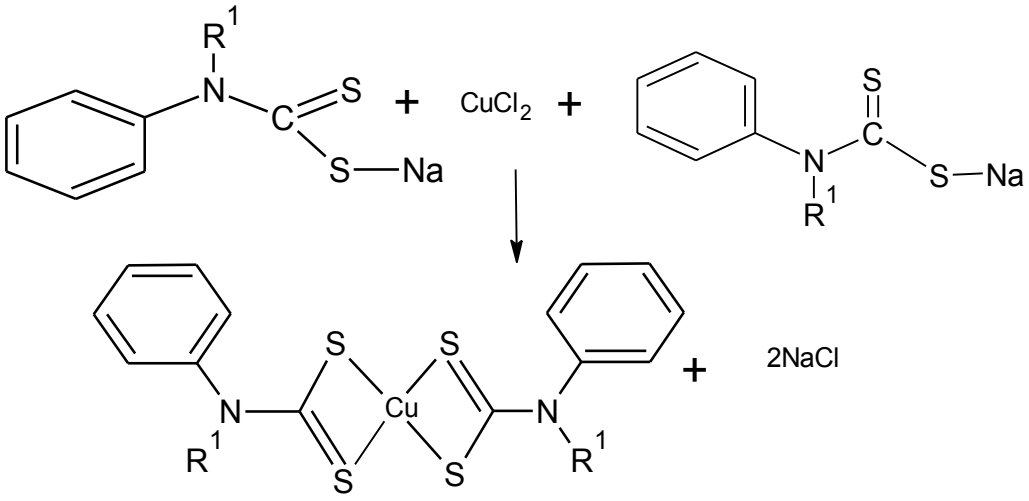

a. Formation of aniline and ethyl aniline copper(II) complexes

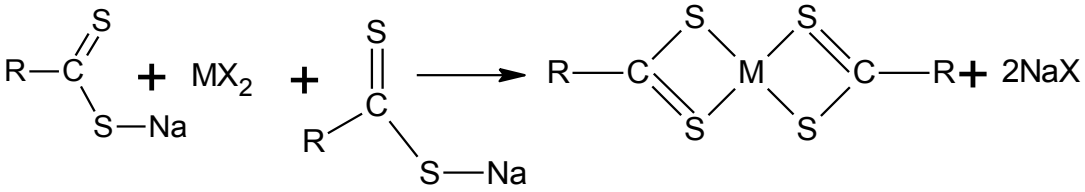

b. Formation of anisidine, morpholine and piperidine copper(II) complexes

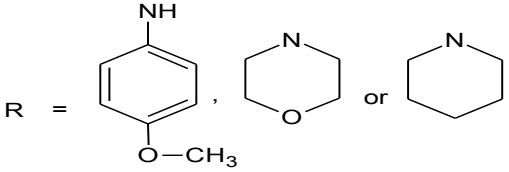

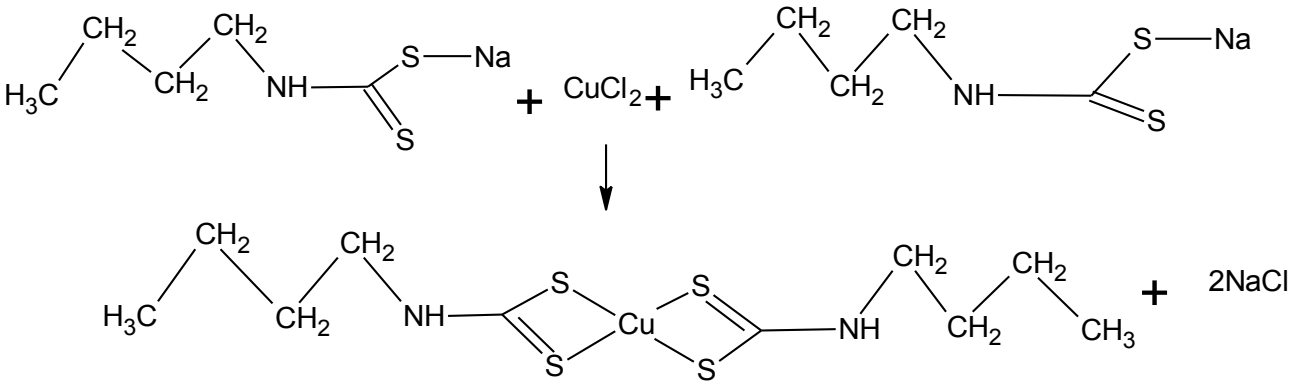

c. Formation of butyl amine copper(II) complexes.

Scheme 3.4: Formation of the Cu(II) dithiocarbamate complexes.

3.3 Physical measurements of ligands and complexes

3.3.1 Solubility tests

Different solvents were used to test the solubility of ligands and complexes. All ligands were soluble in water, therefore, water was used to synthesize the complexes. The complexes were all not soluble in water but soluble in some polar coordinating solvents such as DMF and some in DMSO. The poor solubility of the complexes in common laboratory solvents makes attempts to grow single crystals for x-ray crystallography difficult.

3.3.2 Conductivity measurements of ligands and copper(II) complexes

Conductivity measurements provide a method of testing the degree of ionization of metal complexes in solution, the molecular ions that a compound liberates in solution. The higher the number of ions a compound gives in solution, the higher will be its molar conductivity [8, 9]. The conductivity measurements were carried out at 25 ^{o}C for

all the compounds and presented in Table 3.1. Water was used for all the ligands and for complexes DMSO and DMF was used as solvents. The observed molar conductance for all the complexes shows that they are non-electrolytes in solution and thus confirm the proposed formation of the complexes.

Table 3.1: Molar conductance of the copper(II) complexes

Complexes	**Colours**	**Molar conductance μS/cm**
$[Cu(L1)_2]$	Brown	57,1
$[Cu(L2)_2]$	Brown	24,7
$[Cu(L3)_2]$	Light brown	4,26
$[Cu(L4)_2]$	Yellow	28,7
$[Cu(L5)_2]$	Dark brown	10,01
$[Cu(L6)_2]$	Brown	35,7

3.4. Infrared spectra studies of the ligand and copper(II) complexes

Three important bands are expected in the IR spectra of dithiocarbamate compounds. The first one is the band in the range 1550-1450 cm^{-1} corresponding to ν(C-N) stretching vibrations [10]. The second one is the vibration in the finger print region in the range 1060–940 cm^{-1}, associated with ν(C-S) bands [11]. The third important band occurs at far infrared region and is associated with the ν(M-S) vibration in the range 400–300 cm^{-1} [2]. The infrared spectra of the ligands and their corresponding complexes were compared and carefully assigned. Relevant FTIR data is presented in Table 3.2.

Table 3.2 Summarized FTIR results for ligands and complexes

Compounds	N-H (cm^{-1})	C-N (cm^{-1})	^{sym}C-S (cm^{-1})	^{asym}C-S (cm^{-1})	M-S (cm^{-1})
L1	3414.34	1548.59	1101.59	1029.00	
$[Cu(L1)_2]$	3414.34	1506.47	1039.40		327.28
L2	3416.47	1476.03	1137.95	994.69	
$[Cu(L2)_2]$	3451.01	1450.33	1109.00		328.46
L3	3407.85	1448.04	1055.29	990.12	
$[Cu(L3)_2]$	3417.38	1472.78	1067.15		329.70
L4	3431.04	1506.69	1038.66	920.14	
$[Cu(L4)_2]$	3415.04	1507.21	916.61		327.69
L5	3371.81	1468.39	1006.67	965.84	
$[Cu(L5)_2]$	3414.95	1506.32	994.07		327.60
L6	3409.69	1461.18	1021.41	980.31	
$Cu(L6)_2$	3416.51	1484.02	1016.09		327.82

3.4.1. FTIR spectra of anisidine dithiocarbamate (L1) and copper(II) complex, $[Cu(L1)_2]$.

The infrared spectra of anisidine dithiocarbamate was compared with the copper(II) complex (Figure 3.1). For the free ligand, the ν(N-H) which is due to the N-H bond of the amine was observed at 3414 cm^{-1} and there was no shift of this peak in the complex, this indicates that the N-H was not bonded to the metal ion. The peaks at 3223 cm^{-1} and 1618 cm^{-1} were assigned to ν(=C-H) and ν(C=C) of the ring. The ligand also showed two bands around 2800 cm^{-1} corresponding to C-H stretching vibrations

from the OCH_3 group. In the ligand, the ν(C-N) stretching vibration is observed at 1548 cm^{-1}, a small shift of this peak was observed in the complex which might be due to the formation of the partial double bond confirming the formation of the complex [12]. The C-S symmetrical and asymmetrical stretching vibrations were observed at 1039 and 1101 cm^{-1} respectively in the ligand. In the complex, only one peak corresponding to the ν(C-S) vibration was observed at 1029 cm^{-1} and confirmed bidentate coordination of the dithiocarbamate ligands to the Cu(II) metal ion [13]. The M-S stretching vibration was assigned to the bands that appeared at 327 cm^{-1}.

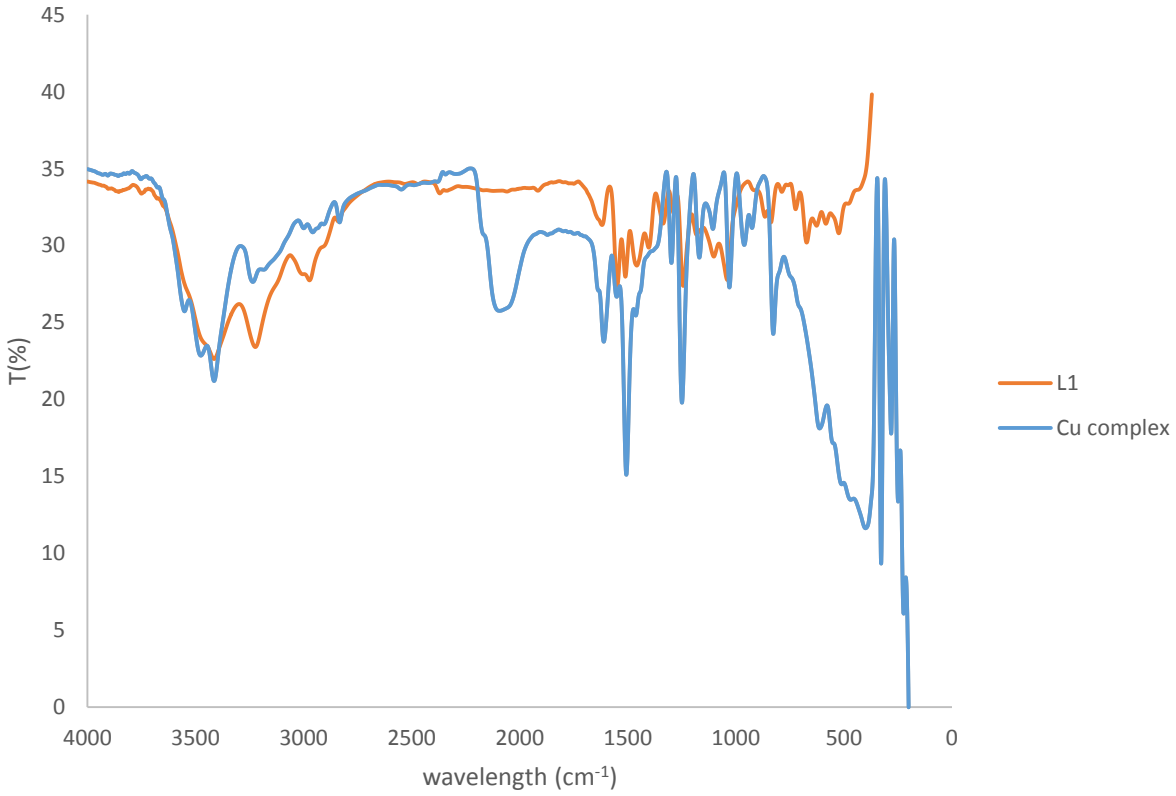

Figure 3.1: Overlay FTIR spectra of anisidine dithiocarbamate ligand and its copper(II) complex.

3.4.2. FTIR spectra of aniline dithiocarbamate (L2) and Copper(II) complex, $[Cu(L2)_2]$.

The ligand showed a band at 1476 cm^{-1} corresponding to ν(C-N) stretching vibration. In the complex, this band shifted to 1485 cm^{-1}, the shift is ascribed to the coordination of the Cu(II) ion to the sulfur atoms of the aniline dithiocarbamate ligands. This lead to a change of the C-N single bond to partial double bond formation. Two peaks in the range 950–1070 cm^{-1} were assigned to the symmetrical and asymmetrical vibrations of C-S at 994 cm^{-1} and 1137 cm^{-1} respectively. The complex showed a sharp single band at 1109 cm^{-1}. The band corresponding to the metal sulfur bond appeared at 328 cm^{-1}. As observed from Figure 3.2.

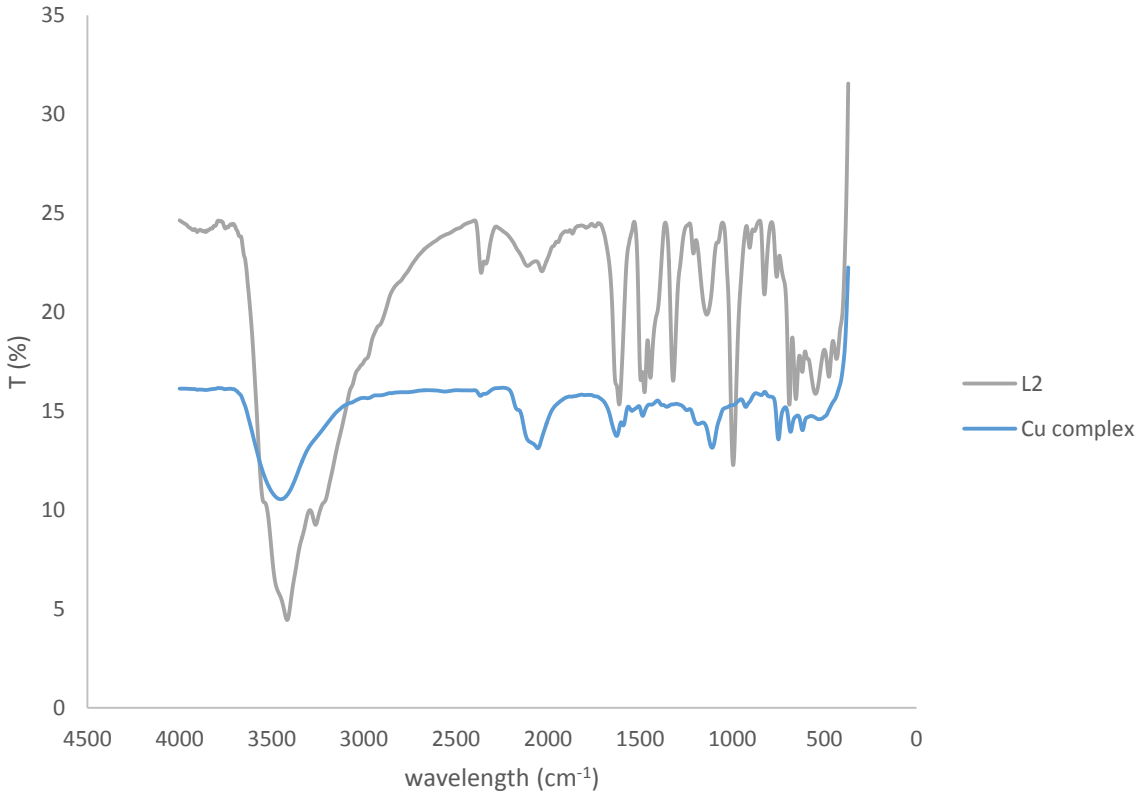

Figure 3.2: Overlay FTIR spectra of aniline dithiocarbamate ligand and its copper(II) complex.

3.4.3. FTIR spectra of ethyl aniline dithiocarbamate (L3) and Copper(II) complex, $[Cu(L3)_2]$.

In the free ligand, the peaks at 2976 cm^{-1} and 1623 cm^{-1} are due to the C-H stretching vibration of the ethyl group and ν(C=C) bond from the ring, respectively. Comparing the spectra of the ligand and that of the complex (Figure 3.3), the ν(C-N) stretching vibration was observed at 1448 cm^{-1} in the ligand and this band shifted in the complex to 1472 cm^{-1} and this shift is ascribed to the coordination of the metal ion to the ligand [3]. The C-S symmetrical and asymmetrical stretching vibrations were observed in the ligand at 990 cm^{-1} and 1055 cm^{-1} respectively. In the complex only one peak was observed at 1067 cm^{-1} which shows that the ligand is bidentately bonded to the copper(II) [3]. The ν(M-S) stretching vibration occurred at 329 cm^{-1} and this confirms the formation of the complex.

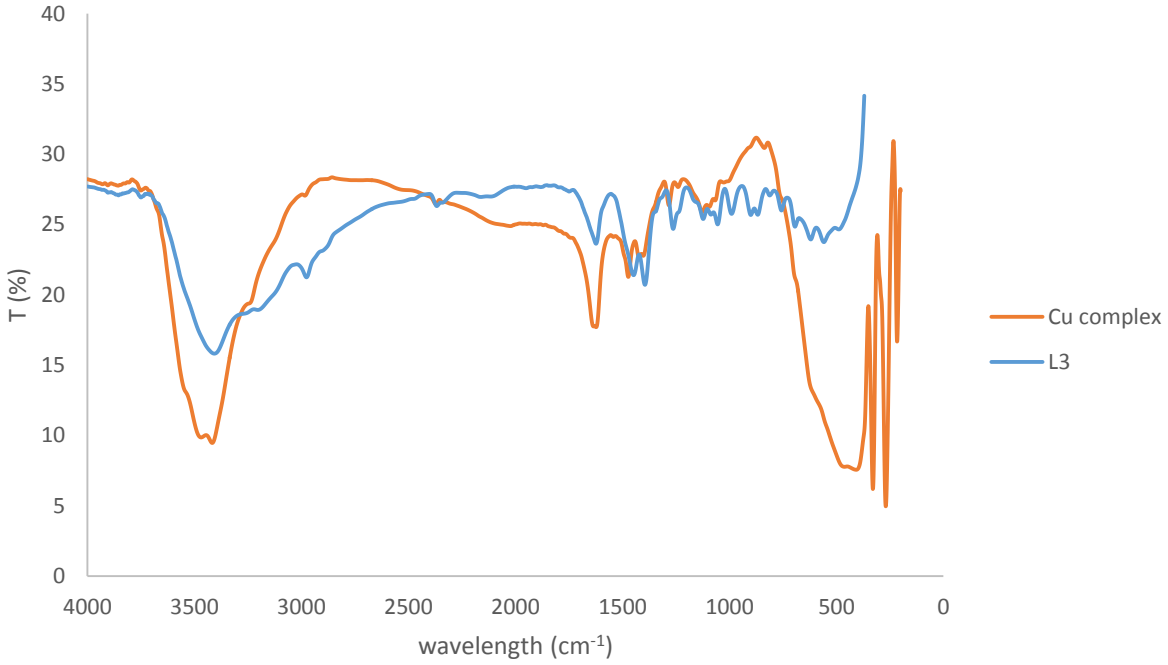

Figure 3.3: Overlay FTIR spectra of ethyl aniline dithiocarbamate ligand and its copper(II) complex.

3.4.4 FTIR spectra of butyl amine dithiocarbamate (L4) and Copper(II) complex, $[Cu(L4)_2]$.

The ligand showed a band at 1464 cm^{-1} corresponding to ν(C-N) stretching vibration. In the complex this band shifted to 1507 cm^{-1}, the shift is due to the coordination of the ligand to the copper(II) ion. The two peaks observed in the range 950–1070 cm^{-1} were assigned to the symmetrical and asymmetrical vibrations of C-S at 995 cm^{-1} and 1065 cm^{-1} respectively. The complex showed a single sharp band at 916 cm^{-1} which confirms the bidentate coordination of the ligand to the copper(II) ion. The band corresponding to the metal sulfur bond appeared at 327 cm^{-1}. Figure 3.4 shows the spectra of the ligand and the complex.

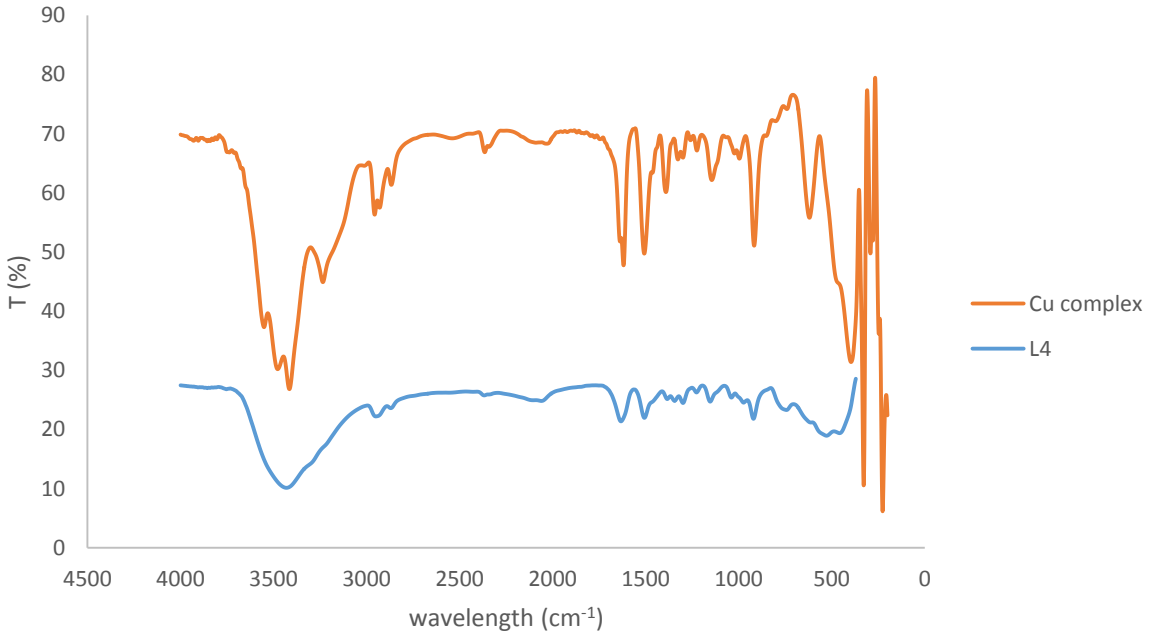

Figure 3.4: Overlay FTIR spectra of butyl amine dithiocarbamate ligand and its copper(II) complex.

3.4.5. FTIR spectra of piperidine dithiocarbamate (L5) and Copper(II) complex, $[Cu(L5)_2]$

The ν(C-N) vibration from NCSS moiety of the ligand was observed at 1468 cm^{-1}. In the complex, this band shifted to 1506 cm^{-1} and it correspond to the formation of partial double bond character of the C-N bond in the complex [14]. A single band of strong intensity was observed at 994 cm^{-1} which may be attributed to ν(C-S) vibration. A shift in comparison to the corresponding two bands at 965 cm^{-1} and 1006 cm^{-1} in the free ligand indicates the bidentate coordination of the dithiocarbamate ligand [14]. The band at 327 cm^{-1} in the complex is assigned to the metal sulfur stretching vibration. The FTIR spectra are shown in Figure 3.5.

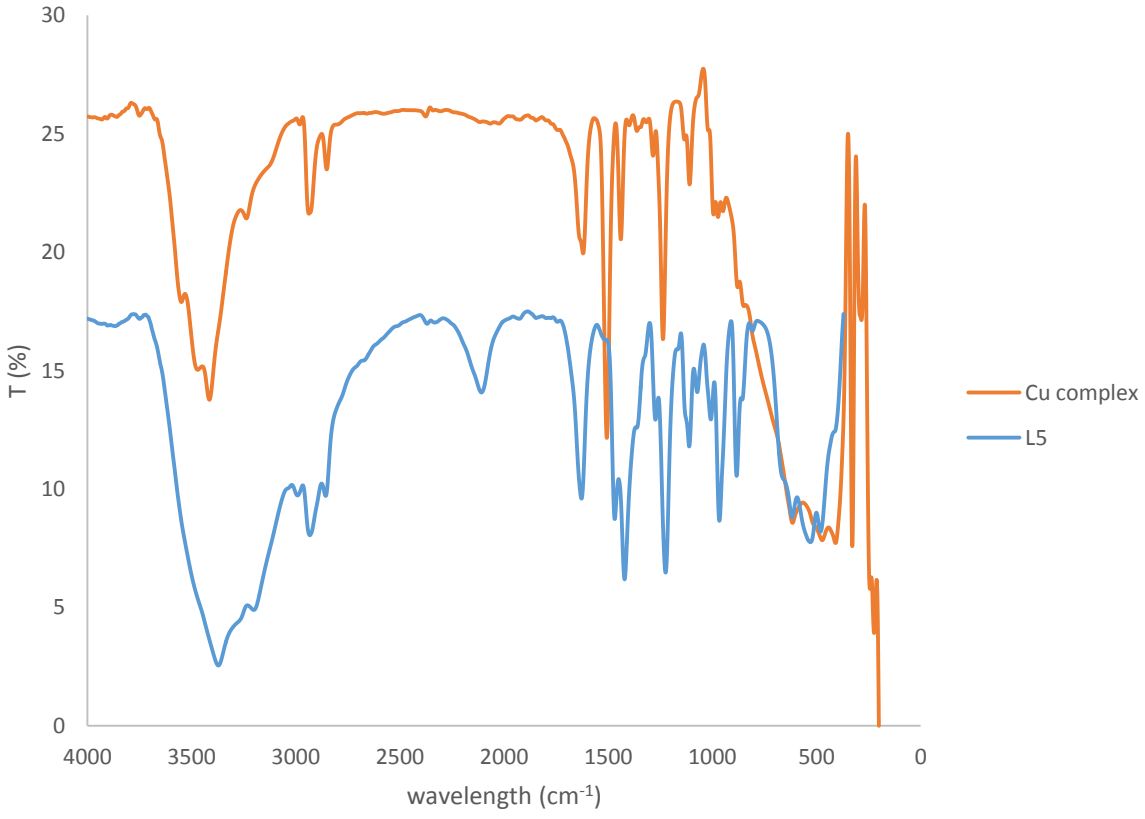

Figure 3.5: Overlay FTIR spectra of piperidine dithiocarbamate ligand and its copper(II) complex.

3.4.6 FTIR spectra of morpholine dithiocarbamate (L6) and copper(II) complex, $[Cu(L6)_2]$

In the free ligand, the ν(C-N) vibration appeared at 1461 cm^{-1} and shifted to 1484 cm^{-1} in the complex [13]. The ν(C-S) stretching vibration in the complex appeared at 1016 cm^{-1} as a single sharp band while there were two ν(C-S) vibrations in the ligand at 980 cm^{-1} and 1021 cm^{-1}, due to the symmetric and asymmetric ν(C-S) vibrations respectively, indicating that the ligand act as bidentate chelating ligand [15]. The metal sulfur, ν(M-S) stretching vibration was observed at 327 cm^{-1} confirming the formation of the complex.

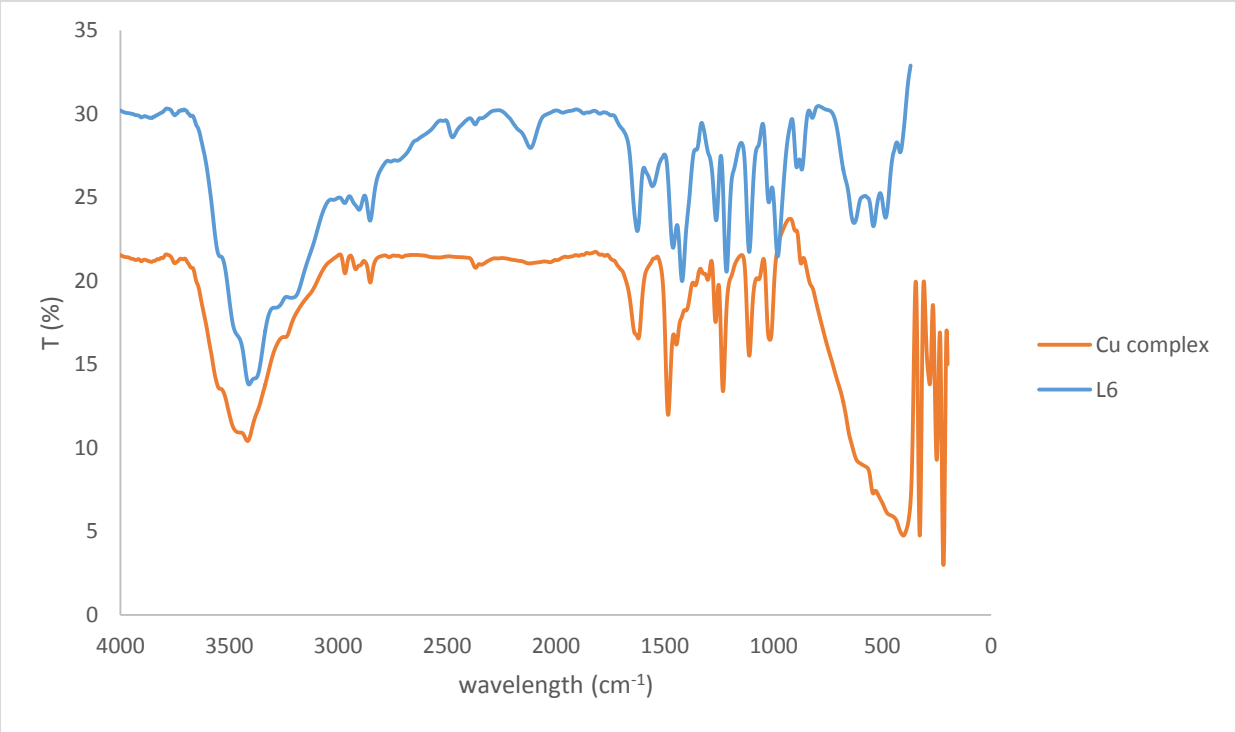

Figure 3.6: Overlay FTIR spectra of morpholine dithiocarbamate ligand and its copper(II) complex.

3.5. Electronic spectra of the ligands and their copper(II) complexes

The electronic spectra measurements were used to assign the stereochemistry of the metal ions in the complexes based on the observed d-d transitions [16]. Tetrahedral compounds of copper(II) are not very common, but they usually have a single broad band in the visible region [17]. Copper dithiocarbamate complexes are known to show an intense ligand-to-metal charge transfer (LMCT) band at around 430 nm, as well as a large absorption around 640 nm based on the d–d transition due to delocalized d–orbitals in the sulfur atoms of the dithiocarbamate ligands [18]. In the complexes, bands below 300 nm are attributed to the intraligand transitions [19]. There are three absorption bands expected in the electronic spectra of dithiocarbamate ligands, the first one is the intraligand $\pi \rightarrow \pi^*$ electronic transitions for the N-C=S and S-C=S group [3], and $n \rightarrow \pi^*$ occurring in the sulfur atoms. The other two expected transitions are metal ligand charge transfer transitions (LMCT) and the d-d transitions [2].

Detailed interpretations of the spectra of copper(II) ion are complicated because of the relatively low symmetry of the environments in which they are characteristically formed [20-22]. Almost all copper(II) compounds are blue or green due to an absorption band in the region 600-900 nm and these bands are usually unsymmetrical and arises from several overlapping transitions due to Jahn Teller distortion. Their definitive resolution into the different number of sub-bands is extremely difficult and almost impossible. Exceptions are due to charge transfer transitions that could make the compounds to appear red or brown [20].

In octahedral copper(II) complexes, a single absorption band is expected in the visible region [23]. These bands are due to several overlapping bands [20, 24]. A regular tetrahedral copper(II) complexes will show a single broad band located near the IR region while the copper(II) complexes in square planar environment show two bands in the visible region.

3.5.1. Electronic spectra of anisidine dithiocarbamate (L1) and copper(II) complex, $[Cu(L1)_2]$

The electronic spectra of the ligands and Cu(II) complex are shown in Figure 3.7. The complex showed two broad bands at 389 nm and 570 nm that maybe d-d transitions for a Cu(II) ion in a square planar crystal field. These transitions are assigned to $^2B_{1g} \rightarrow {}^2A_{1g}$ and $^2B_{1g} \rightarrow E_g$ transitions [20]. Transitions in the 370-396 nm are assigned to metal to ligand charge transfer transition. The other bands observed were due to intraligand transfer which are due to N-C=S and S-C=S groups of the dithiocarbamate ligands.

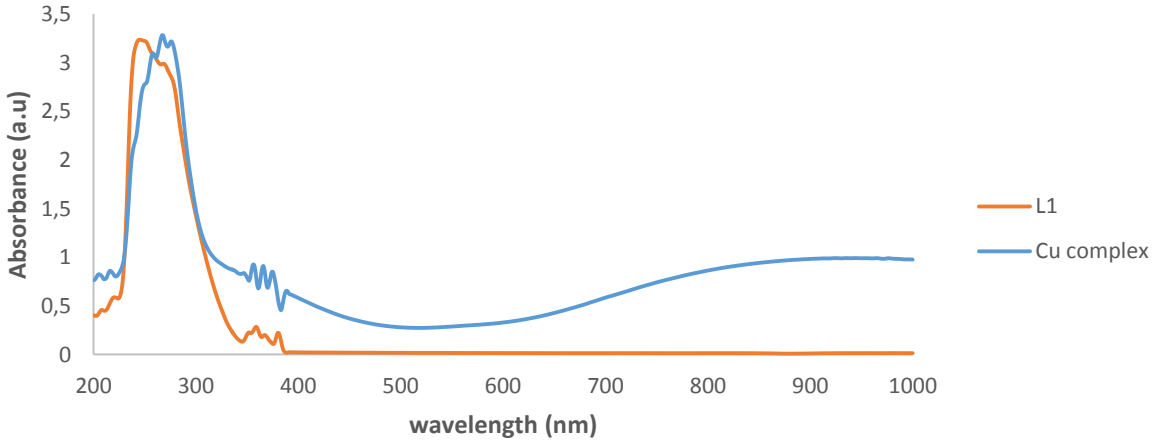

Figure 3.7: UV-Vis spectra of anisidine dithiocarbamate ligand and its copper(II) complex

3.5.2. Electronic spectra of aniline dithiocarbamate (L2) and copper(II) complex, $[Cu(L2)_2]$.

The ligand showed three bands that are assigned to π→π* attributed to N-C=S group, π→π* which is due to S-C=S group and n→π* transition which is due to the lone pairs of electrons on the sulfur atoms. The complex showed a band at 393 nm which was assigned to ligand to metal charge transfer transitions. The d-d transition was observed above 500 nm. All the bands below 300 nm were associated with the intra ligand charge transfer transition.

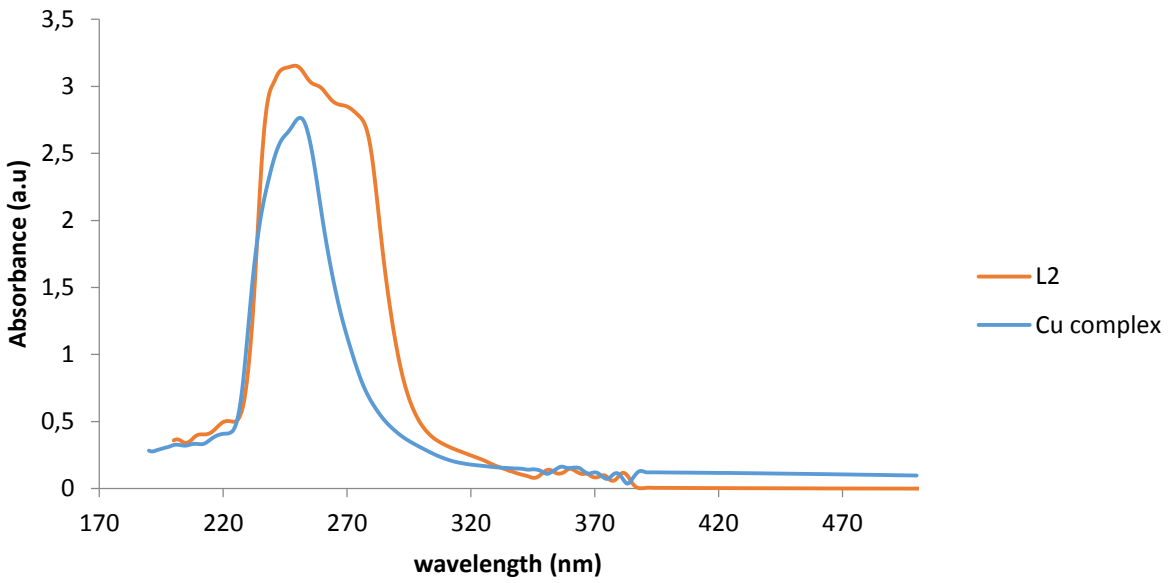

Figure 3.8: UV-Vis spectra of aniline dithiocarbamate ligand and its copper(II) complex

3.5.3. Electronic spectra of ethyl aniline dithiocarbamate (L3) and copper(II) complex, $[Cu(L3)_2]$.

The bands in the UV region at 241 nm and at 254-268 nm could be assigned to intra ligand charge transfer transitions. The complex exhibit two bands 405 nm and 571 nm which is due to d-d transition for Cu(II) ion in a square planar environment (Fig. 3.9B). The electronic spectrum of the complex also showed prominent MLCT in the region 300-400 nm (Fig. 3.9 A&B). The transitions due to the ligand π-π* and n-π* are more enhanced in the ligand spectrum than that of the metal as shown in Figure 3.9A.

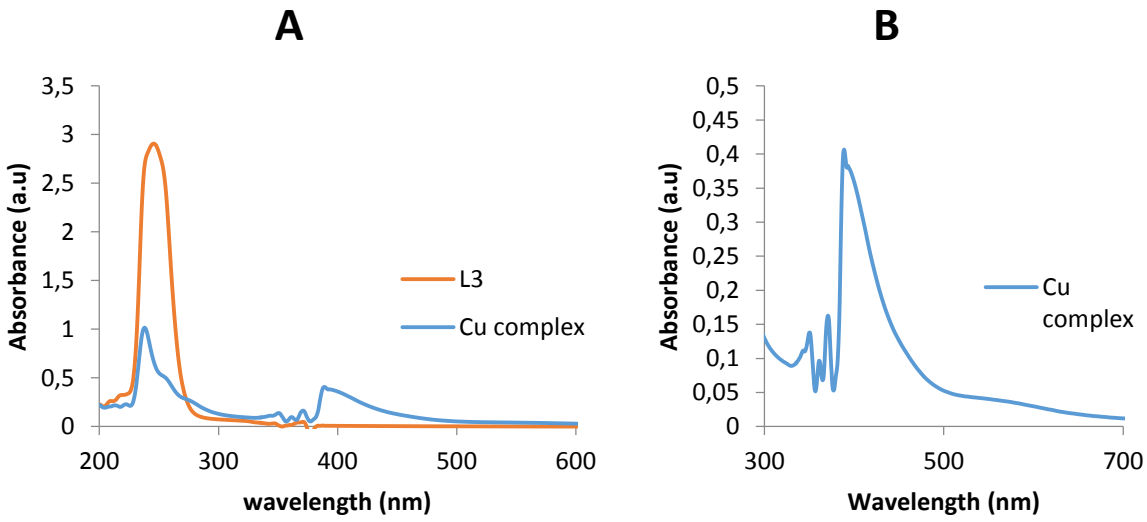

Figure 3.9: UV-Vis spectra of ethyl aniline dithiocarbamate ligand and its copper(II) complex

3.5.4 Electron spectra of butyl amine dithiocarbamate (L4) and copper(II) complex, $[Cu(L4)_2]$.

The electronic spectrum of the complex show two bands in the visible region at 446 and 651 nm (Fig 3.10B) that could be assigned to the d-d transition of a square planar Cu(II) complex. The band at 350 nm which is assigned to metal to ligand charge transfer. The other bands observed were due to intra ligand charge transfer transitions ascribed to N-C=S and S-C=S groups (Fig. 3.10A).

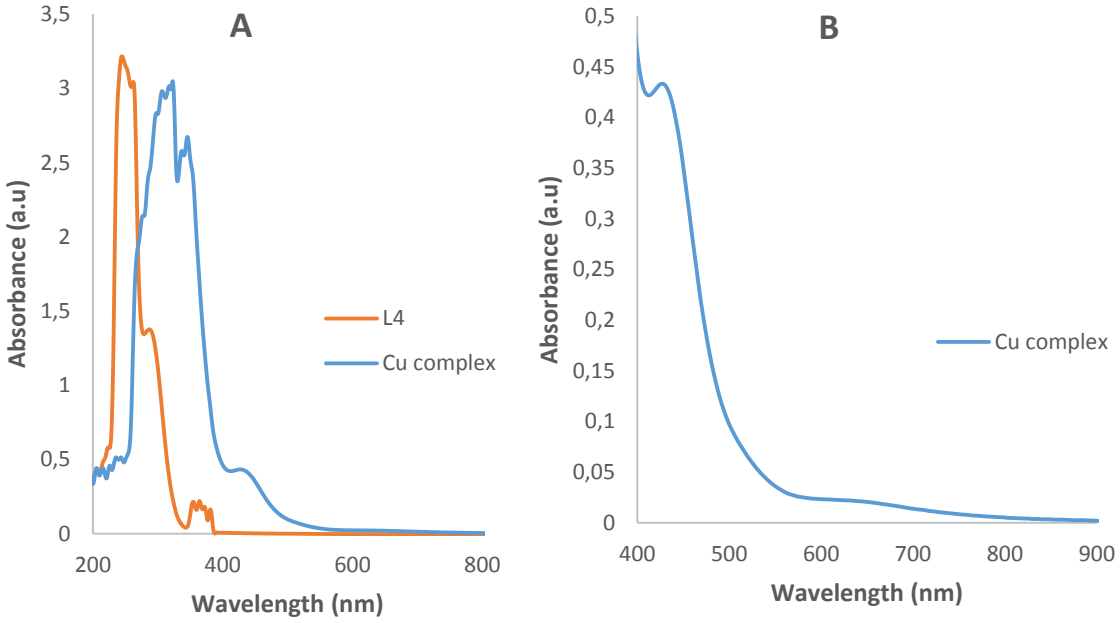

Figure 3.10: UV-Vis spectra of butyl amine dithiocarbamate ligand and its copper(II) complex.

3.5.5 Electronic spectra of piperidine dithiocarbamate (L5) and copper(II) complex, $[Cu(L5)_2]$

The electronic spectrum of the complex (Fig. 3.11) showed two broad bands at 414 and 579 nm assigned to the d-d transitions. This confirms the proposed square planar geometry for the complex. There is also shoulder at 348 nm which is assigned to metal to ligand charge transfer. The other bands observed were due to intra ligand charge transfer transitions from π→π* and n-π* from the N-C=S and S-C=S groups.

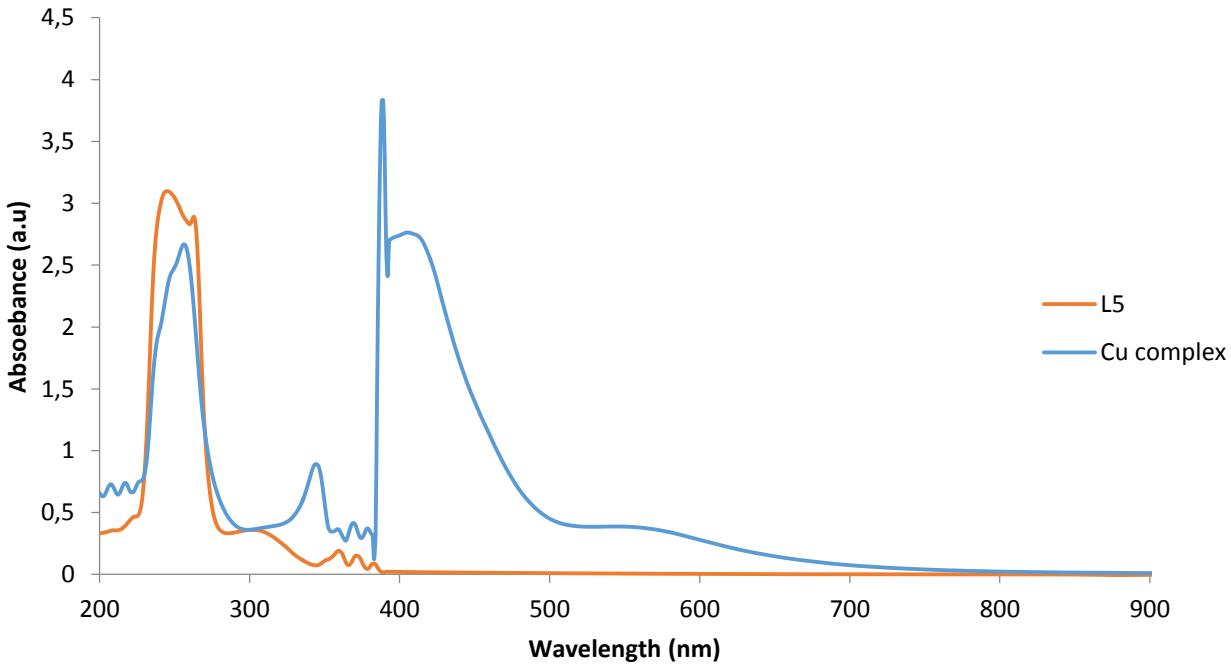

Figure 3.11: UV-Vis spectra of piperidine dithiocarbamate ligand and its copper(II) complex.

3.5.6 Electronic spectra of morpholine dithiocarbamate (L6) and copper(II) complex, $[Cu(L6)_2]$

The electronic spectra of the compounds are shown in Figure 3.12. The complex showed two bands at 414 nm and 562 nm in the visible region assignable to the d-d transitions of Cu(II) ion in a square planar geometry. The complex showed another band at 397 nm which is assigned to metal to ligand charge transfer. The other bands observed below 300 nm were due to intra ligand charge transfer transitions which are assigned to π→π* due to N-C=S and S-C=S groups.

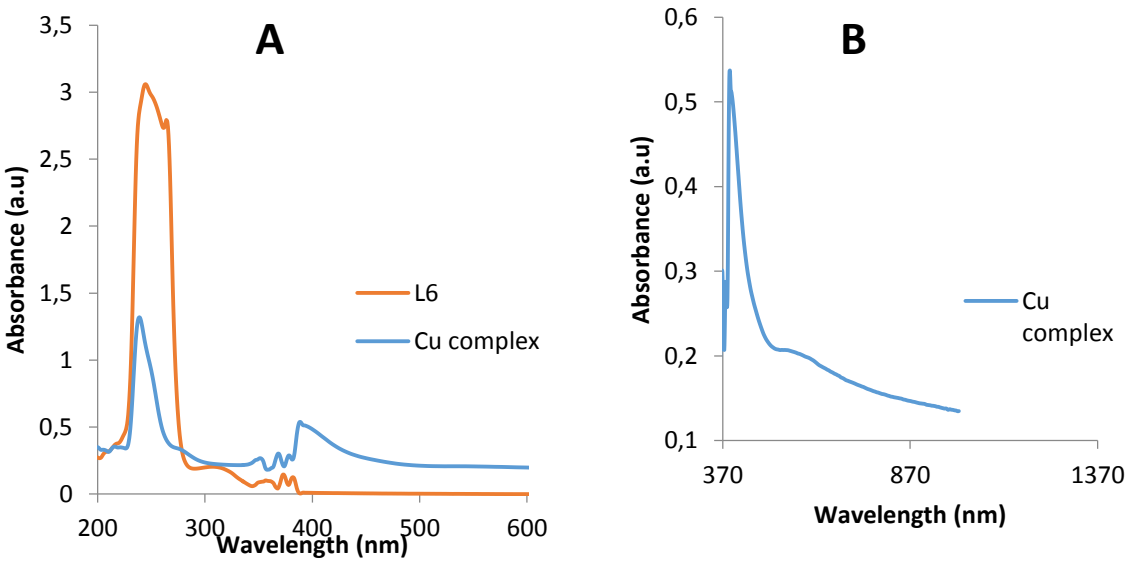

Figure 3.12: UV-Vis spectra of morpholine dithiocarbamate ligand and its copper(II) complex.

3.6. ^{13}C NMR and ^{1}H NMR spectra of dithiocarbamate ligands.

NMR experiment was used to characterize the dithiocarbamate ligands. In the NMR spectra of the ligands (Appendix A) all the chemical shifts were found in the expected regions. The ^{13}C NMR for all ligands showed all the expected chemical shifts for the ligands. Anisidine dithiocarbamate ligand (L1) ^{13}C NMR spectrum showed the resonance at 181.05 ppm which was assigned to $\delta(N^{13}CS_2)$ of NCS_2 moiety. The signals observed at 114.77 ppm and 127.52 ppm were assigned to the C=C bond in the aromatic ring. The spectrum also showed signals for C-N bond from CNH group in the ligand and the C-O bond from the OCH_3 group of the ligand at 55.52 and 77.22 respectively. There was only one extra peak at 158 ppm which is assumed to be due to the impurities of the ligand. The ^{1}H NMR spectrum for this ligand showed the CH_3 from O-CH_3 as a singlet at 1.28 ppm, while =CH from the aromatic ring appeared as a doublet around 6.95-6.94 ppm. There is also an extra quartet that might be due to the impurities.

For aniline dithiocarbamate ligand (L2), the ^{13}C NMR showed all the expected signals, the signals for C-N was observed around 39.5-40.5 ppm and the three different C=C due to their different environments showed signals around 127-128 ppm. The ^{1}H NMR of this ligand showed two triplets for the CH in the aromatic ring around 7.15-7.12 ppm and around 6.86-6.84 ppm. It also showed the doublet due to the =CH-N bond from the aromatic ring around 7.67-7.66 ppm. The first signal that appeared on the ^{13}C NMR spectrum of ethyl aniline dithiocarbamate ligand (L3) was the resonance at 215.74 ppm that was assigned to the $\delta(N^{13}CS_2)$ of the NCS_2 moiety. And the signal at 13.36 ppm was assigned to the CH_3 from the ethyl group.

The three different signals observed around 129.00-125.43 ppm were assigned to the C=C bonds in the aromatic ring. And it also showed the signal for the C-N at 51.31 ppm. The ^{1}H NMR spectrum of this ligand showed the CH_3 and CH_2 from the ethyl group as triplet around 1.07-1.04 ppm and quartet around 4.33-4.29 ppm respectively. For the CH in the aromatic ring doublet and two triplets around 7.06-7.05 ppm, around 7.12-7.09 ppm and around 7.28-7.26 ppm respectively.

The butyl amine dithiocarbamate ligand (L4) ^{13}C NMR spectrum showed the $\delta(N^{13}CS_2)$ resonance at 214.50 ppm. The spectrum also exhibits the signals around 13.54-14.30 ppm that are due to the CH_3 group. The signals around 19.65-20.24 ppm were assigned to the two CH_2 groups. While the signal that appeared around 40.17 ppm was assigned to the C-N bond.

^{13}C NMR spectrum of piperidine dithiocarbamate ligand (L5) exhibited the $\delta(N^{13}CS_2)$ resonance at 212.87 ppm. The signal that was due to the C-N bond from the ring appeared at 50.78 ppm. The two different CH_2 showed their signals around 24.81-26.20 ppm and 39.51-40.34 ppm. The morpholine dithiocarbamate ligand (L6) spectrum showed the two expected CH_2, N-CH_2 and O-CH_2 at 50.21 ppm and 66.59 ppm. The two expected peaks in the ^{1}H NMR spectrum of this ligand were observed as triplets around 4.30-4.28 ppm and around 3.51-3.48 ppm. The second triplet might not be seen clearly because of the solvent peak that made it a quartet. There were also singlets observed that might be due to some impurities.

References

[1] Kanchi, S.; Singh, P.; Bisetty, K. Dithiocarbamates as hazardous remediation agent: A critical review on progress in environmental chemistry for inorganic species studies of 20th century. *Arabian J. Chem*. **2014**, 7, 11–25.

[2] Mamba, S. M. Synthesis, characterization and applications of dithiocarbamate transition metal complexes. M. Sc. Thesis, University of Johannesburg, 2009. https://ujdigispace.uj.ac.za/bitstream/handle/10210/3629/Mamba.pdf?sequence=1&isAllowed=y

[3] Ahamad, M. M.; Rao, R. M.; Kumar, E. V. S.; Jayaraju, A.; Begum, T. N.; Sreeramulu, J. Synthesis, characterization and biological evaluation of novel dithiocarbamate metal complexes. *J. Chem. Pharmaceut. Res*. **2012**, 4(3), 1601-1605.

[4] Ajibade, P. A.; Onwudiwe, D. C. Synthesis and characterization of group 12 complexes of *N*,*N*-methyl phenyl-*N*,*N*-butyl phenyl dithiocarbamate. *J. Coord. Chem*. **2011**, 17(10), 2963-2973.

[5] Ajibade, P. A.; Ejelonu, B. C. Group 12 dithiocarbamate complexes: Synthesis, spectral studies and their uses as precursors for metal sulfides nanoparticles and nanocomposites. *Spectrochim. Acta*. *Part A*, **2013**, 113, 408-414.

[6] Awang, N.; Baba, I.; Yamin, B. M.; Halim, A. A. Preparation, characterization and antimicrobial assay of 1,10-phenanthroline and 2,2‘-bipyridyl adducts of cadmium(II) *N*-sec-butyl-*N*-propyldithiocarbamate: Crystal structure of $Cd[S_2CN(i\text{-}C_4H_9)(C_3H_7)]_2$ (2,2‘-bipyridyl). *World Appl. Sci. J.* **2011**, 12 (9), 1568-1574.

[7] Singh, N.; Kumar, A.; Prasad, R.; Molloy, K. C.; Mahon, M. F. Synthesis, crystal, photoluminescence and electrochemical investigation of some new phenylmercury(II) dithiocarbamate complexes involving ferrocene. *Dalton Trans*, 2010, 39, 2667-2675.

[8] Refat, M. S.; El-Deen, I. M.; Zein, M. A.; Adam, A. M. A.; Kobeasy, M. I. Spectroscopic, structural and electrical conductivity studies of Co(II), Ni(II) and Cu(II) complexes derived from 4-acetylpyridine with thiosemicarbazide. *Int. J. Electrochem. Sci*. **2013**, 8, 9894 – 9917.

[9] Salman, M. Infrared spectroscopic investigations on the reaction products resulted from the interaction between silver(I) salts with urea at 90 ^{o}C. *Int. J. Life Sci. Pharma. Res*. **2012**, 2(2), 128-138.

[10] Gopal, K. V.; Jyothi, P. S.; Raju, P. A. G.; Rameshbabu, K.; Sreeramulu, J. Synthesis and characterization of 2-amino pyridine dithiocarbamate ligand and it's Cu(II), Co(II) metal complexes. *J. Chem. Pharmaceut. Res*. **2013**, 5(6), 50-59.

[11] Onwudiwe, D. C.; Ajibade, P. A. Synthesis, characterization and thermal studies of Zn(II), Cd(II) and Hg(II) complexes of N-methyl-N-phenyldithiocarbamate: The single crystal structure of $[(C_6H_5)(CH_3)NCS_2]_4Hg_2$. *Int. J. Mol. Sci.* **2011**, 12, 1964-1978.

[12] Macias, B.; Villa, M. V.; Chicote, E.; Martin-Velasco, S.; Eiras, A. C.; Borras, J. Copper complexes with dithiocarbamates derived from natural occurring amino acids. Crystal and molecular structure of $[Cu(en)(EtOH)(H_2O)_3][Cu(dtc\text{-}pro)_2]$. *Polyhedron*, **2002**, 1899-1904.

[13] Pam, S.; Wang, Y. Crystal structure and spectroscopic studies of bis(morpholine dithiocarbamate) Ni(II) complex, $Ni(C_4H_8ONCS_2)_2$. *Chi. J. Chem*. **2010**, 19(9), 856-859.

[14] Sharma, M.; Sharma, A.; Sachar, R. Synthesis and characterization of the adducts of morpholinedithioccarbamate complexes of oxovanadium(IV), nickel(II), and copper(II) with piperidine and morpholine. *E-J. Chem*. **2012**, 9(4), 1929-1940.

[15] Onwudiwe, D.C; Ajibade, P. A. Synthesis and characterization of metal complexes of N-alkyl-N-phenyl dithiocarbamates. *Polyhedron*, **2010**, 29, 1431–1436.

[16] Gudasi, K. B.; Patil, S. I.; Vadavi, R. S.; Shenoy, R. V.; Patil, M. S. Synthesis and spectral studies of Cu(II), Ni(II), Co(II), Mn(II), Zn(II) and Cd(II) complexes of a new macroacyclic ligand N,N'-bis(2-benzothiazolyl)-2,6-pyridinedicarboxamide. *J. Serb. Chem. Soc.* **2006**, 71(5), 529–542.

[17] Osowole, A. A. Studies on some Vo(IV), Ni(II) and Cu(II) complexes of non-symmetrical tetradentate Schiff-bases. *Bull. Chem. Soc. Ethiop*. **2008**, 22(2), 219-224.

[18] Keniley, L. K. Tetrathiafulvalene-annulated phenanthroline and its complexes with transition metals. PhD Dissertation, The Florida State University College of arts and sciences, 2013. Electronic Theses, Treatises and its Dissertations. Paper 7447. http://diginole.lib.fsu.edu/etd/7447/

[19] Thankachi, M. S. D.; Suthakumari, S. Synthesis and characterization of Schiff base complexes of Cu(II) and Co(II). *J. Chem. Pharmaceut Res.* **2013**, 5(12), 1467-1473.

[20] Ajibade, P. A.; Zulu, N. H. Synthesis, characterization, and antibacterial activity of metal complexes of phenylthiourea: The X-ray single crystal structure of $[Zn(SC(NH_2)NHC_6H_5)_2(OOCCH_3)_2]\cdot C_2H_5OH$. *J. Coord. Chem*. **2010**, 63(18), 3229-3239.

[21] Greenwood, N. N.; Earnshaw, A. Chemistry of the elements, 1st Edn, Pergamon Press, New York, 1985, pp 1368.

[22] Cotton, F. A.; Wilkinson, G. Advanced Inorganic chemistry, 5th Edn, Wiley Inter-Science, New York, 1984, pp. 768.

[23] Lever, A. B. P. Inorganic electronic spectroscopy, 2nd Edn, Elsevier Science, New York, 1984.

[24] Hathway, B. J.; Billing, D. E. The electronic properties and stereochemistry of mono-nuclear complexes of the copper(II) ion. *Coord. Chem. Rev*. **1970**, 5, 143-207.

CHAPTER FOUR

4.0. SYNTHESIS AND CHARACTERIZATION OF HEXADECYLAMINE-CAPPED COPPER SULFIDE NANOPARTICLES

4.1. Introduction

The development of nano-materials with size and shape controlled morphologies opens new opportunities in exploring the chemical and physical properties of materials [1]. Copper sulfide nanoparticles has recently attracted considerable scientific and technological interest as promising material for applications in solar cells, optical filters, nanoswitches, thermoelectric and photoelectric transformers, and gas sensors [2-10]. Copper sulfide nanoparticles are a good prospective optoelectronic material, which is often used for ammonia gas sensing at room temperature. The gas sensitive parameters have been found to be dependent upon chemical composition and the morphology of the Cu_xS nanocrystals [11].

Copper sulfides are particularly interesting class of metal sulfides due to their ability to form with various stoichiometry. The Cu–S binary system consists of the stoichiometric end members Cu_2S (chalcocite) and CuS (covellite) with several stable and metastable phases of varying stoichiometry between those two compositions [12]. At room temperature, copper sulfide (Cu_xS) forms five stable phases: Covellite (CuS), anilite ($Cu_{1.75}S$), digenite ($Cu_{1.8}S$), djurleite ($Cu_{1.95}S$) and chalcocite (Cu_2S) [13]. They have different shapes, anilite has an orthorhombic shape, chalcocite (Cu_2S), roxbyite Cu_7S_4 ($Cu_{1.75}S$) and djurleite $Cu_{31}S_{16}$ ($Cu_{1.95}S$) are monoclinic in shape, digenite Cu_9S_5 ($Cu_{1.8}S$) cubic in shape, and hexagonal shaped covellite (CuS) [14].

Different kinds of CuS nanocrystals have been synthesized recently and exist in various forms such as nanoparticles, nanodisks [15], nanotubes [16], nanorods [17], and nanowires [18]. Several methods are being used for the preparation of copper sulfide nanocrystals, this include polyol method, wet chemistry, precipitation technique, sonochemical method, microwave assisted solvothermal route and single source precursor method [19].

In this study, copper(II) dithiocarbamate complexes were used as single source precursors to synthesize hexadecylamine (HDA)-capped copper sulfide nanoparticles. The preparation of semiconductor nanoparticles using the single source precursor method have been used to prepare different metal sulfide nanoparticles [20-30]. In this method, the molecular precursor contains both the metal ion bonded directly to the chalcogen. This method hasbeen successfully used to synthesize nanoparticles with narrow size distributions. The use of HDA as capping agent decreases the growth rate and usually improves the photoluminescence quantum efficiency by effectively passivating any surface defects of the nanoparticles [31-32].

The optical properties of the nanoparticles were studied with UV-Vis and photo luminescence spectroscopy. The structural morphology, composition and size of the copper sulfide nanoparticles were studied by powder X-ray diffraction (XRD) analysis, scanning electron microscopy (SEM), energy dispersive X-ray (EDX) spectroscopy and transmission electron microscopy (TEM) measurements. The six dithiocarbamate complexes were thermolyzed at 180 ^{o}C and three of them were further thermolyzed at 120 ^{o}C and compared to those thermolyzed at 180 ^{o}C to study the effect of temperature on the shapes and size of the corresponding nanoparticles.

4.2. Experimental

4.2.1. Materials

Hexadecylamine (HDA), trioctylphosphine (TOP), toluene and methanol were obtained from Sigma-Aldrich and used as obtained. Copper(II) aniline dithiocarbamate, copper(II) anisidine dithiocarbamate, copper(II) ethyl aniline dithiocarbamate, copper(II) butyl amine dithiocarbamate, copper(II) morpholine dithiocarbamate and copper(II) piperidine dithiocarbamate complexes prepared, the details are presented in section 2.4.

4.2.2. Physical Measurements

4.2.2.1. UV-Visible spectroscopy

The absorption spectra of the nanoparticles in solution were recorded using Perkin-Elmer Lambda 25 UV-Vis spectrometer. The samples were placed in quartz cuvettes of 1 cm path length. All nanoparticles were soluble in toluene, therefore toluene was used to dissolve the nanoparticles for optical studies measurements.

4.2.2.2. Photoluminescence spectroscopy

The emission spectra of the nanoparticles were measured using Perkin Elmer LS 45 fluorimeter. The samples were dissolved in toluene and placed in quartz cuvettes of 1 cm path length.

4.2.2.3. X-Ray Diffraction

A Bruker-D8 powder X-Ray diffractometer instrument at voltage of 40 kV with current of 30 mA and Cu kα radiation was used to carry the XRD spectra of the nanoparticles. The XRD samples were made by drop coating the samples on a glass plate. XRD was used to determine crystalline phase and the size of nanoparticles.

4.2.2.4. Scanning Electron Microscopy

To obtain the SEM images, Joel JSM 6390 LV at an accelerating voltage between 15-20 kV was used. The images were taken at different magnifications. The samples were coated with gold before their images were taken. It was used to study the morphology of the copper sulfide nanoparticles.

4.2.2.5. Energy Dispersive X-ray analysis

The composition of the elements in the nanoparticles were determined using the EDX. The energy dispersive spectra were obtained using dispersive X-ray analysis (EDX) attached to the Joel JSM 6390 LV used for SEM.

4.2.2.6. Transmission Electron Microscopy

The ZEISS Libra 120 electron microscope at 120 kV was used to obtain the TEM images. Toluene was used as a solvent to dissolve all the samples. The samples were prepared by placing drops of the sample solution on a carbon coated copper grid. Then they were allowed to dry completely over night at room temperature

4.2.3. Synthesis of CuS nanoparticles

The copper sulfide nanoparticles were prepared from the copper(II) dithiocarbamate complexes by adopting a reported literature procedure [19]. Each of the respective copper complex (0.20 g) was dissolved in TOP (4 mL) and injected into hot HDA (3 g) at 180 ^{o}C/120 ^{o}C. The solution was stabilized and the reaction was continued for 1 hour at 180 ^{o}C/120 ^{o}C. After completion, the reaction mixture was allowed to cool to 70 ^{o}C and cold methanol was added to precipitate the nanoparticles. The resulting solid was separated by centrifugation and washed three times with cold methanol. The resulting solid precipitates of HDA-capped CuS nanoparticles was dried for several weeks at room temperature before further analysis.

4.3. RESULTS AND DISCUSSION

4.3.1. Characterization of CuS nanoparticles from copper(II) aniline (C2), copper(II) ethyl aniline (C3) and copper(II) morpholine (C6) dithiocarbamate complexes.

4.3.1.1 Optical properties of CuS2, CuS3 and CuS6 nanoparticles

The optical properties of metal nanoparticles are strongly influenced by their size, shape, and chemical environment [33]. The absorption and emission spectra of the copper sulfide nanoparticles dispersed in toluene obtained from C2, C3 and C6 complexes represented as CuS2, CuS3 and CuS6 respectively are shown in Figures 4.1 and 4.2.

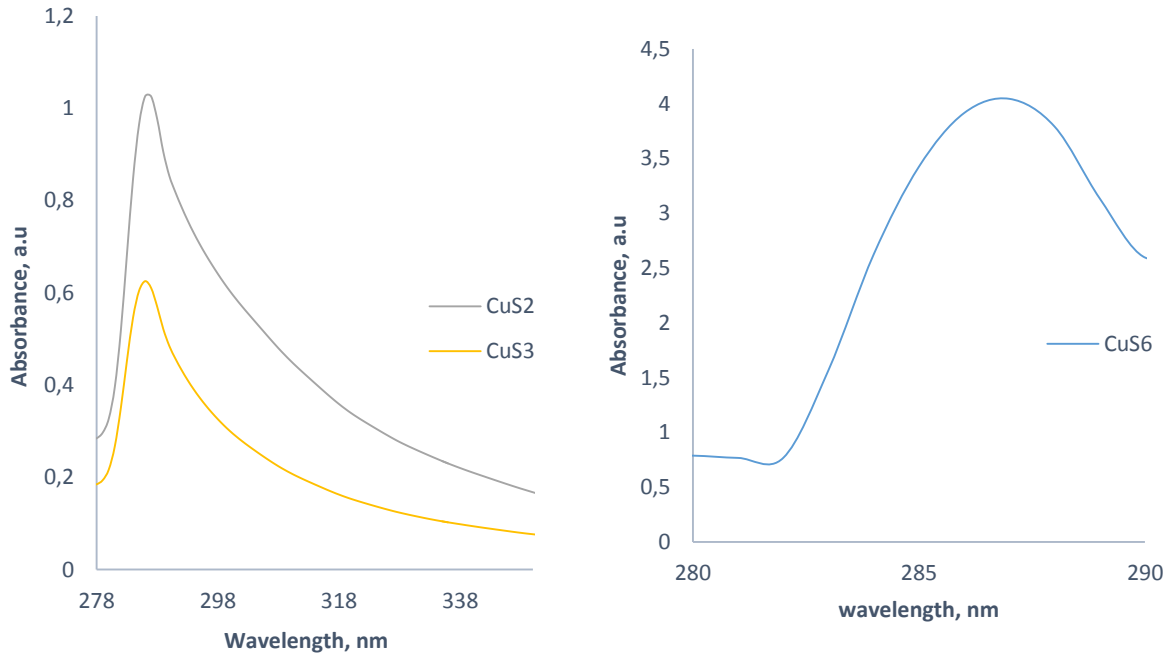

Figure 4.1: Absorption spectra of CuS2, CuS3 and CuS6 nanoparticles.

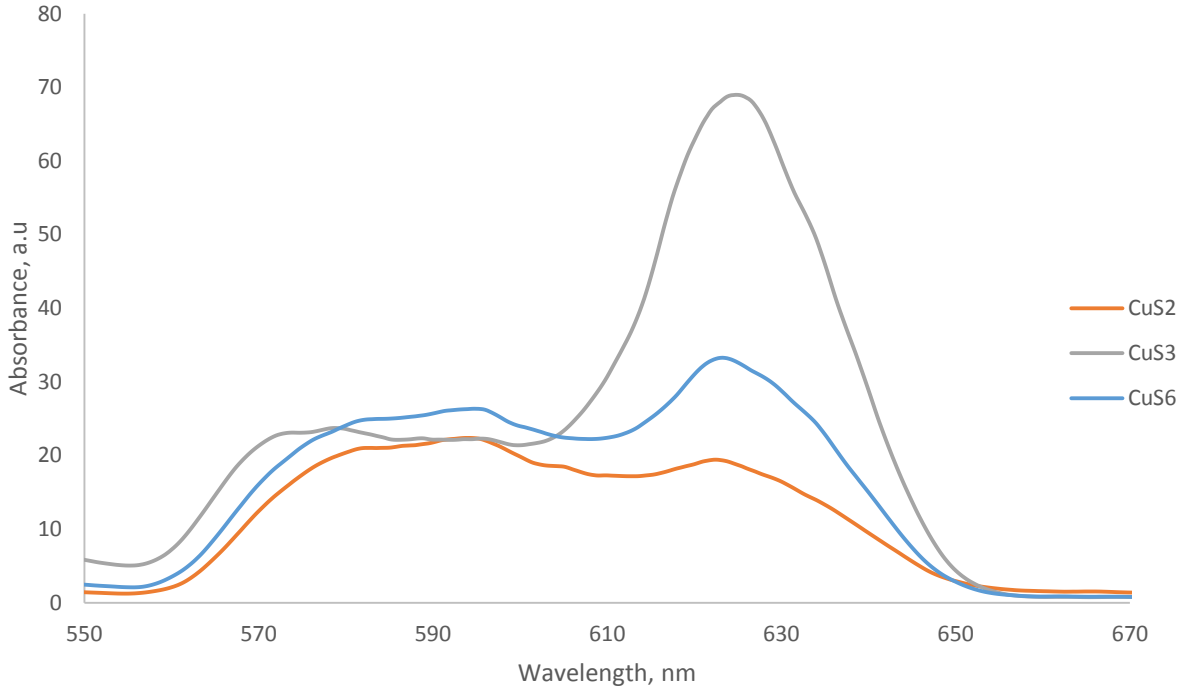

Figure 4.2: Emission spectra of CuS2, CuS3 and CuS6 nanoparticles.

Fig. 4.1 showed that the absorption peaks of CuS2 and CuS3 are similar and are in the range 278-338 nm with absorption maxima at 287 nm. The absorption spectra of CuS6 differs in shape from those of CuS2 and CuS3 and is in the range 282-290 nm and the difference might be because CuS6 is of the different phase. The absorption edges of each nanoparticle were used to calculate the energy band gap of the nanoparticles using equation 4.1 [34].

Band Gap Energy (E) = h*C/λ……4.1

Where: h = Planks constant = 6.626 x 10^{-34} Joules sec, C = Speed of light = 3.0 x 10^{8} meter/sec and λ = is the wavelength at which, absorption peak is obtained.

The calculated band gap energy for CuS2 and CuS3 is 4.33 eV. This value is greater than that of the bulk CuS which is 1.2 eV [14]. This indicates that the as prepared CuS2 and CuS3 nanoparticles exhibit strong quantum confinement effects [35], and their absorption spectra are blue shifted. CuS6 with absorption band edge at 286 nm have the band gap energy of 4.3 eV, which is also blue shifted and thus show quantum confinement.

The photoluminescence spectra (Fig. 4.2) showed broad emission curves with the emissions at 625, 624.5 and 623 nm, for CuS2, CuS3 and CuS6 nanoparticles respectively. The reduced broadness of the emission curves can be attributed to the narrow size distributions of the CuS nanoparticles. Although the absorption spectrum of CuS6 is slightly different from those of CuS2 and CuS3, its emission spectrum is similar to those of CuS2 and CuS3.

4.3.1.2. X-Ray diffraction studies of CuS2, CuS3 and CuS6 nanoparticles.

The powder XRD patterns of CuS2, CuS3 and CuS6 are shown in Figure 4.3. The average crystal size were estimated using Scherrer equation [36]:

$$d = k\lambda/\beta \cos\theta \quad \text{.....4.2}$$

Where d is the average crystallite size, k is the Scherrer constant (0.94), λ (0.15406 nm for CuKα) is the X-ray wavelength, β is the angular line width of the half maximum intensity of the diffraction peaks in radians unit. And θ is the Bragg angle corresponding to the maximum of diffraction peak in degrees unit.

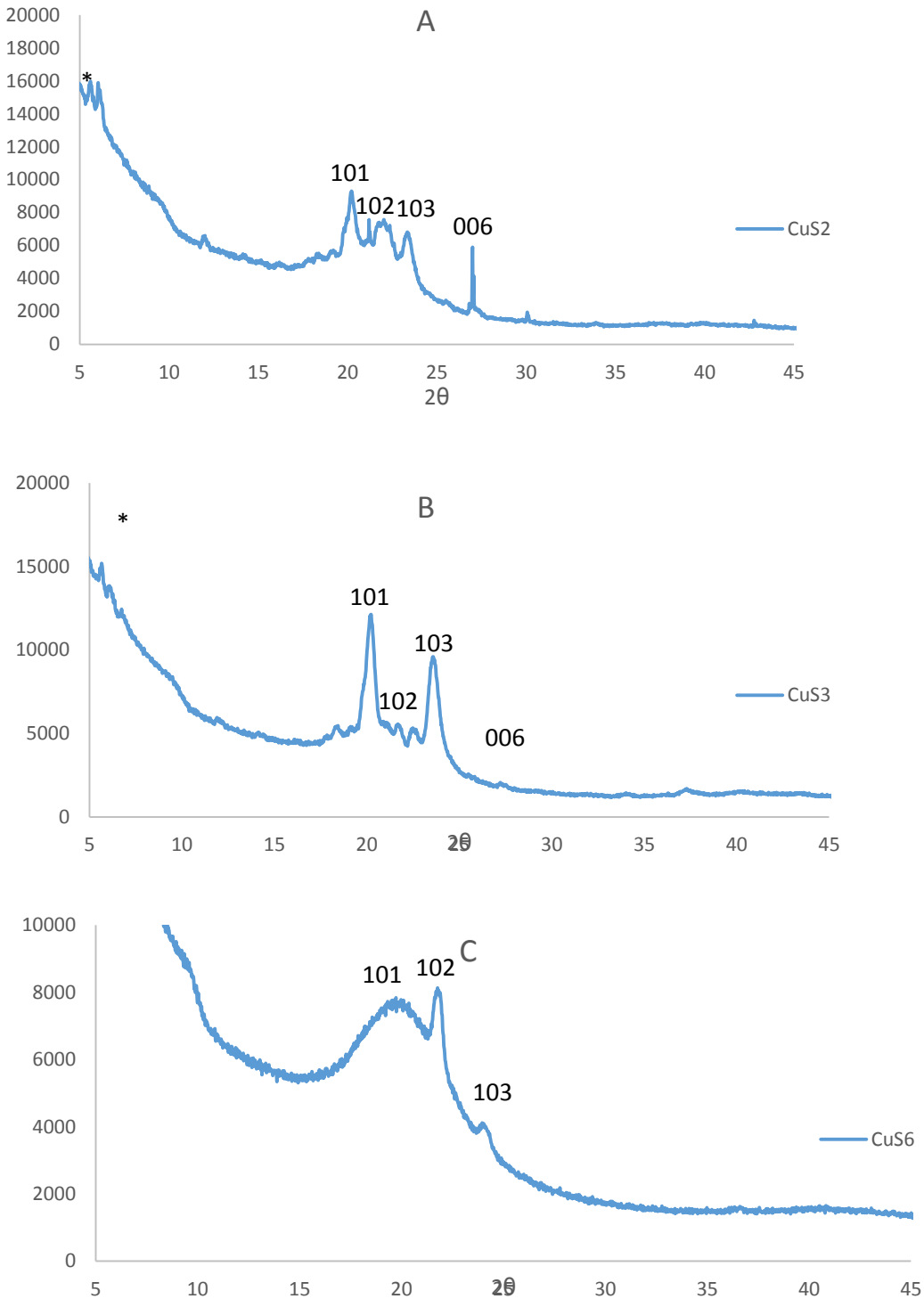

Figure 4.3: Powder XRD patterns of CuS2 (A), CuS3 (B) and CuS6 (C) nanoparticles.

* due to HDA

The estimated average crystallite sizes of the as-prepared CuS nanoparticles are 18.09 nm for CuS2, 17.3 nm for CuS3 and 18.6 nm for CuS6. The CuS nanoparticles XRD diffraction patterns show four important peaks corresponding to (101), (102), (103) and (006) crystal planes. These peaks correspond with hexagonal covellite phase of CuS nanocrystals (JCPDS file. no: 06-0464). The observed peaks broadening could be ascribed to the nanocrystalline nature of the nanoparticles and traces of HDA were also detected.

4.3.1.3. TEM of CuS2, CuS3 and CuS6 nanoparticles

The TEM images of the HDA-capped copper sulfide nanoparticles are shown in Fig.4.4 and all the nanoparticles have narrow size distributions. The TEM image of CuS2 shows copper sulfide nanoparticles with crystalline size in the range 5.10-9.80 nm. CuS2 nanoparticles appeared to be a mixture of rod like and some cubic shaped nanoparticles. The nanoparticles are not uniformly distributed as shown in the TEM images. The TEM image of CuS3 (Fig 4.4) showed CuS nanoparticles are spherical in shape and uniformly distributed. The average crystallite size of the CuS3 nanoparticles are 3.06-4.35 nm. The CuS3 nanoparticles although uniformly distributed contained some that agglomerated to secondary particles. The TEM image of CuS6 showed small spherically shaped nanoparticles with some aggregation with crystallite sizes in the range 3.02-4.32 nm.

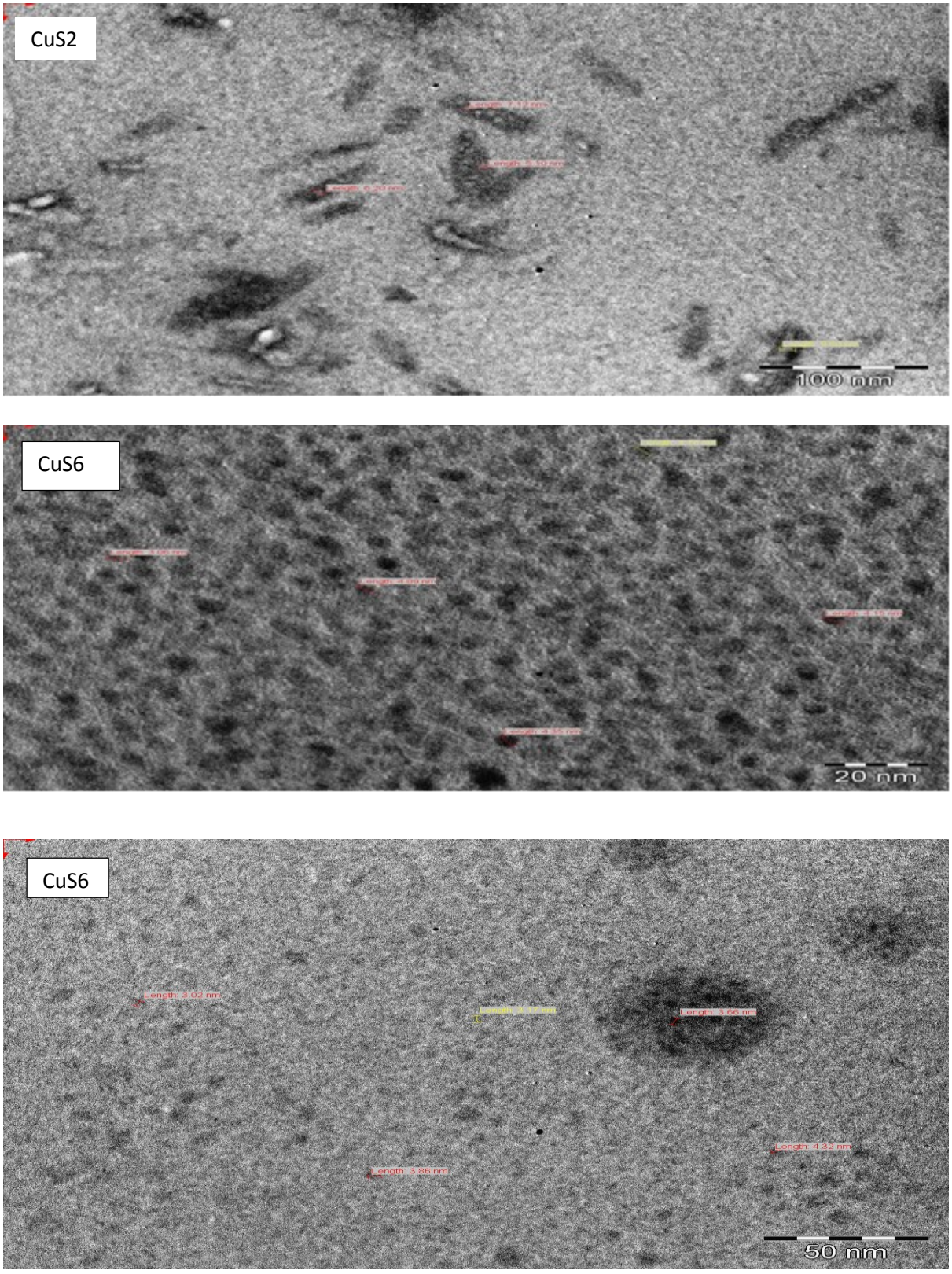

Figure 4.4: TEM images of CuS2, CuS3 and CuS6 nanoparticles.

4.3.1.4. SEM and EDX analysis of CuS2, CuS3 and CuS6 nanoparticles

The morphology of the as-prepared CuS2, CuS3 and CuS6 nanoparticles obtained from scanning electron microscopy (SEM) and their elemental composition as confirmed by energy dispersive X-ray (EDX) analysis are shown in Figure 4.5. The morphologies shows partly smooth surfaces except CuS6 which appears charred and contained small almost spherical particles. The charring of CuS6 can be ascribed to the sample not properly dried when the SEM/EDX analysis was carried out.

The EDX patterns show copper and sulfur confirming the formation of CuS nanoparticles except for CuS6 which was burned due to wetness of the sample when the analysis was done. Other peaks that are common in all EDX spectra are carbon, phosphorus, nitrogen and oxygen which are due to TOP used for dispersing the precursor and the HDA that was used as a capping agent.

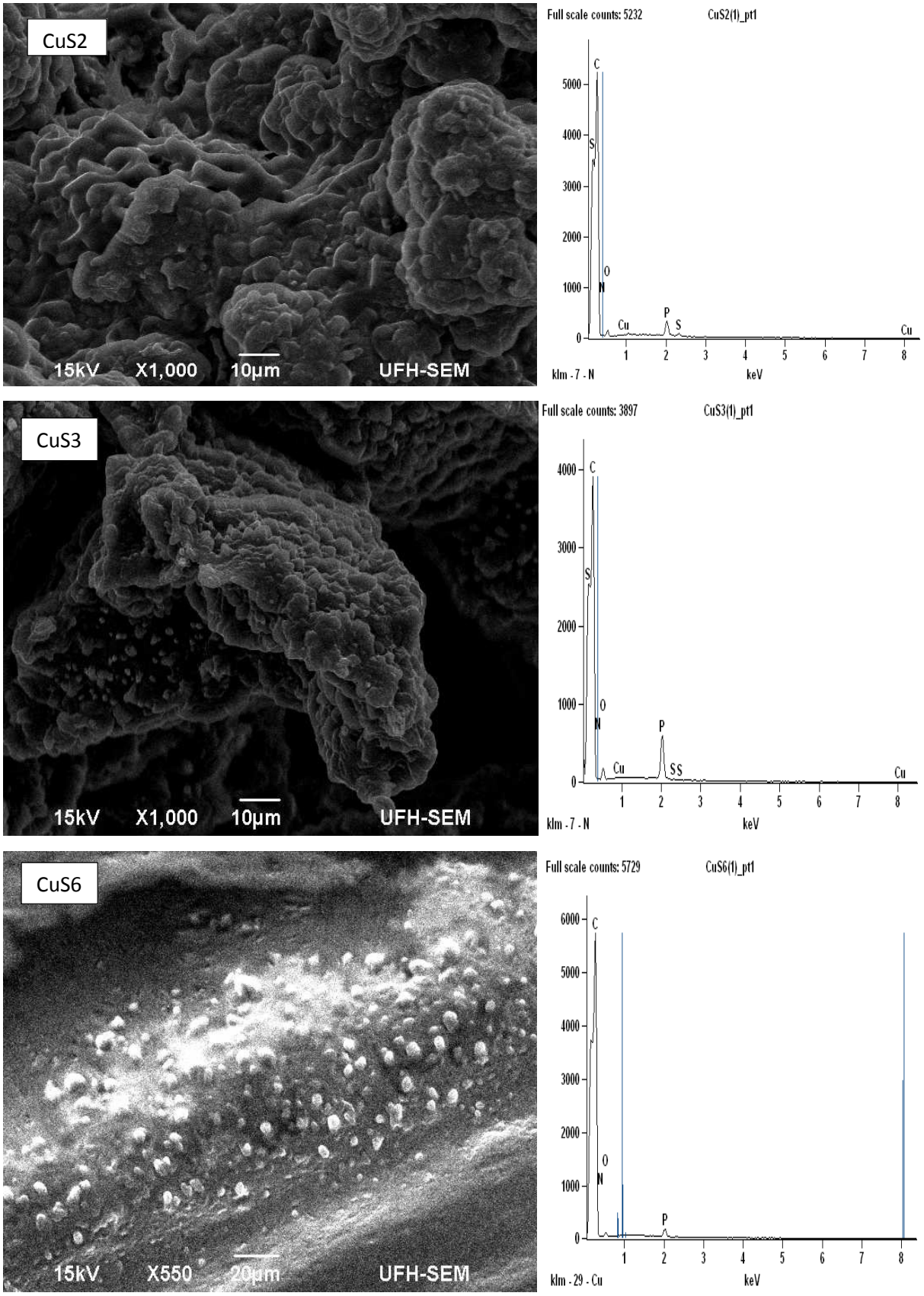

Figure 4.5: SEM images and and EDX spectra of CuS2, CuS3 and CuS6 nanoparticles

4.3.2. Characterization of CuS nanoparticles from copper(II) anisidine (C1), copper(II) butyl amine (C4) and copper(II) piperidine (C5) dithiocarbamate complexes.

4.3.2.1. Optical properties of CuS1, CuS4 and CuS5 nanoparticles.

Figure 4.6 and 4.7 shows the absorption spectra and emission spectra of the CuS1, CuS4 and CuS5 nanoparticles respectively. CuS1, CuS4 and CuS5 showed absorption band edges at 288, 287 and 287 nm respectively (Figure 4.6). The band gap energies of the nanoparticles were also determined using Equation 4.1. The calculated band gap energy for CuS1 is 4.31 eV, which is greater than that of the bulk CuS (1.2 eV) [14]. The CuS4 and CuS5 have the same absorption maxima that occurred at 287 nm and the calculated band gap energy is 4.33 eV. This value is greater than that of the bulk which is 1.2 eV [14]. Thus, the nanoparticles are blue shifted and this indicates that the nanoparticles exhibit strong quantum confinement [35].

The photoluminescence spectra of the nanoparticles (Fig. 4.7) shows two narrow emission curves at 621 and 623 nm, for CuS1 and CuS5 respectively. The reduced broadness of the emission curves is ascribed to the narrow size distributions of the CuS nanoparticles. The emission spectrum of CuS4 is different from those of CuS1 and CuS5, the wavelength of the emission peak is not different but the intensity is very low.

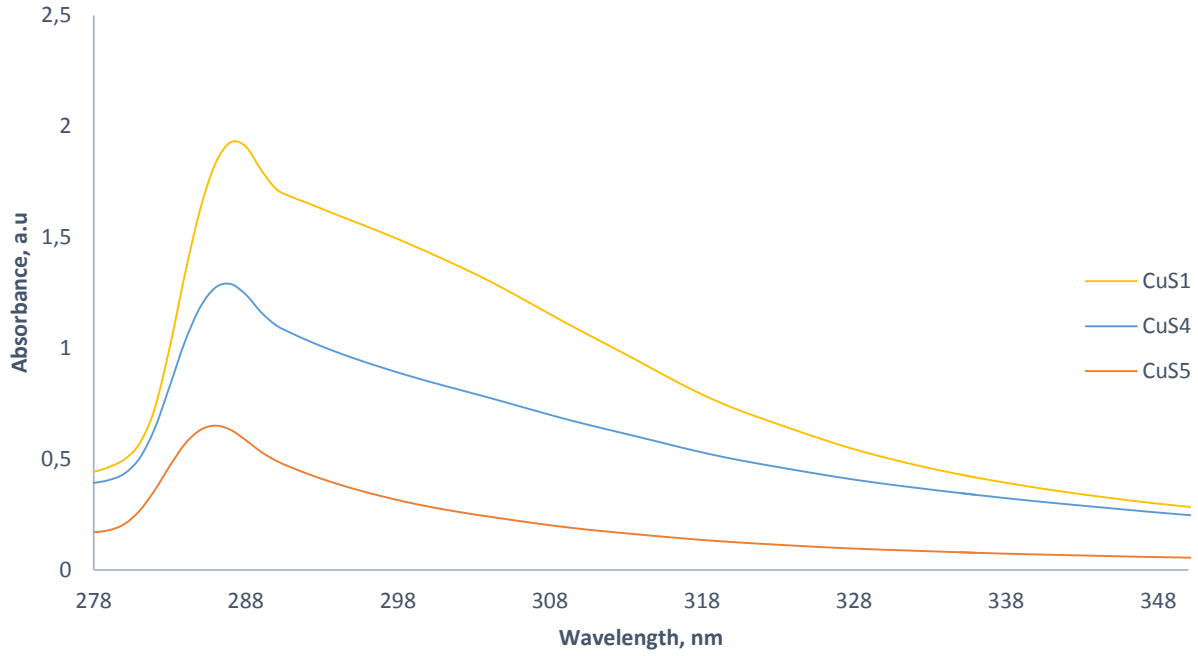

Figure 4.6: Absorption spectra of CuS1, CuS4 and CuS5 nanoparticles.

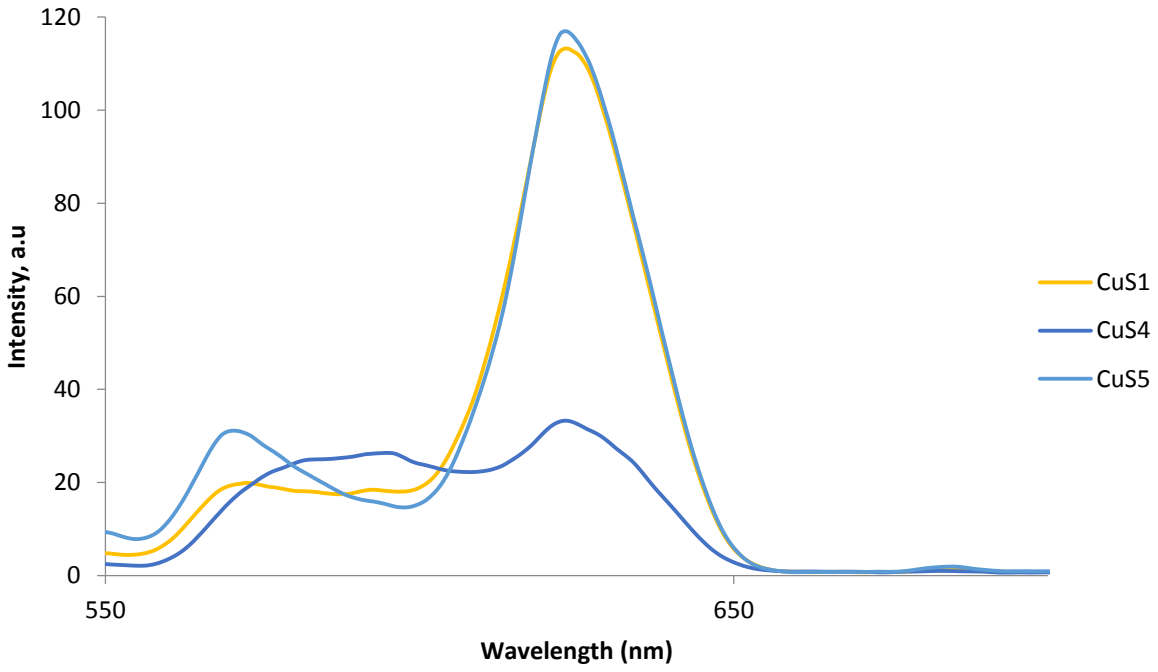

Figure 4.7: Emission spectra of CuS1, CuS4 and CuS5 nanoparticles

4.3.2.2. X-ray diffraction studies of CuS1, CuS2 and CuS5 nanoparticles.

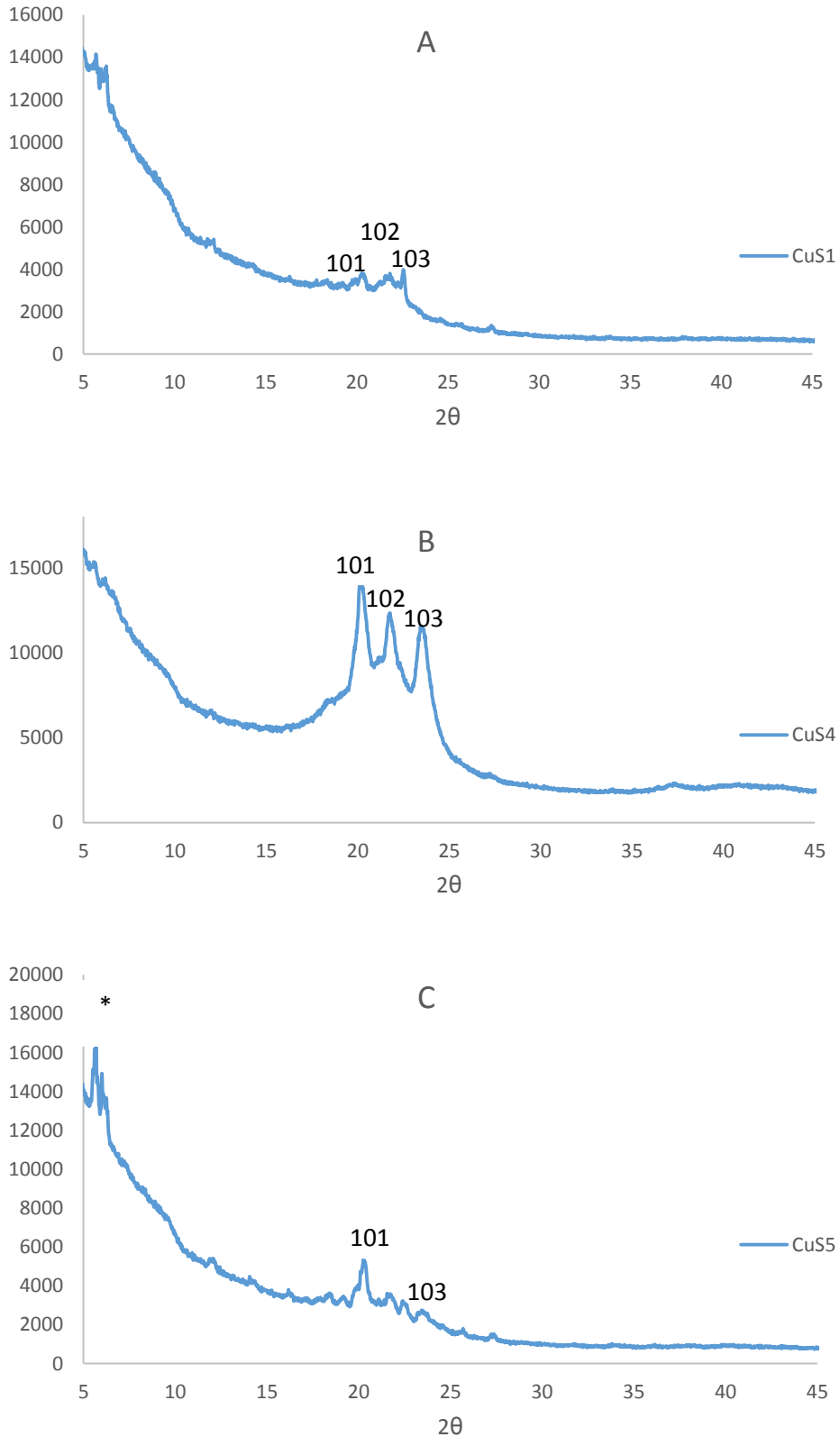

Figure 4.8: XRD patterns of CuS1, CuS4 and CuS5 nanoparticles. * due to HDA

The powder XRD patterns of CuS1, CuS4 and CuS5 are shown in Figure 4.8. Their average crystal sizes were estimated using Scherrer equation (Eq. 4.2) [36]. The estimated average crystallite size of the as prepared CuS nanoparticles are 40.31 nm for CuS1, 15.8 nm for CuS4 and 23.24 nm for CuS5. All the major diffraction peaks can be indexed to the standard diffraction data corresponding to the hexagonal phase of CuS (JCPDS 06-0464) and some HDA peaks are also observed

4.3.2.3. TEM of CuS1, CuS4 and CuS5 nanoparticles

Figure 4.9 shows the TEM images of as-synthesized CuS1, CuS4 and CuS5 nanoparticles. The TEM image of CuS1 shows particles that are semi spherical in shape with the size in the range 18.76-31.76 nm. The image did not show any agglomeration. The TEM image of CuS4 nanoparticles shows particles with the size in the range of 14.59-26.67 nm that are almost spherical in shape with agglomeration. The TEM image of CuS5 nanoparticles shows nanoparticles with diameters in the range 67.46-98.94 nm with considerable agglomeration. The nanoparticles have rod like shapes and their crystallite sizes are large in comparison to all the other nanoparticles. These three nanoparticles were further thermolysed at a different temperature (120 ^{o}C) to study the effects of temperature on the size and shape of the nanoparticles. Some changes were observed and described in section 4.3.3.

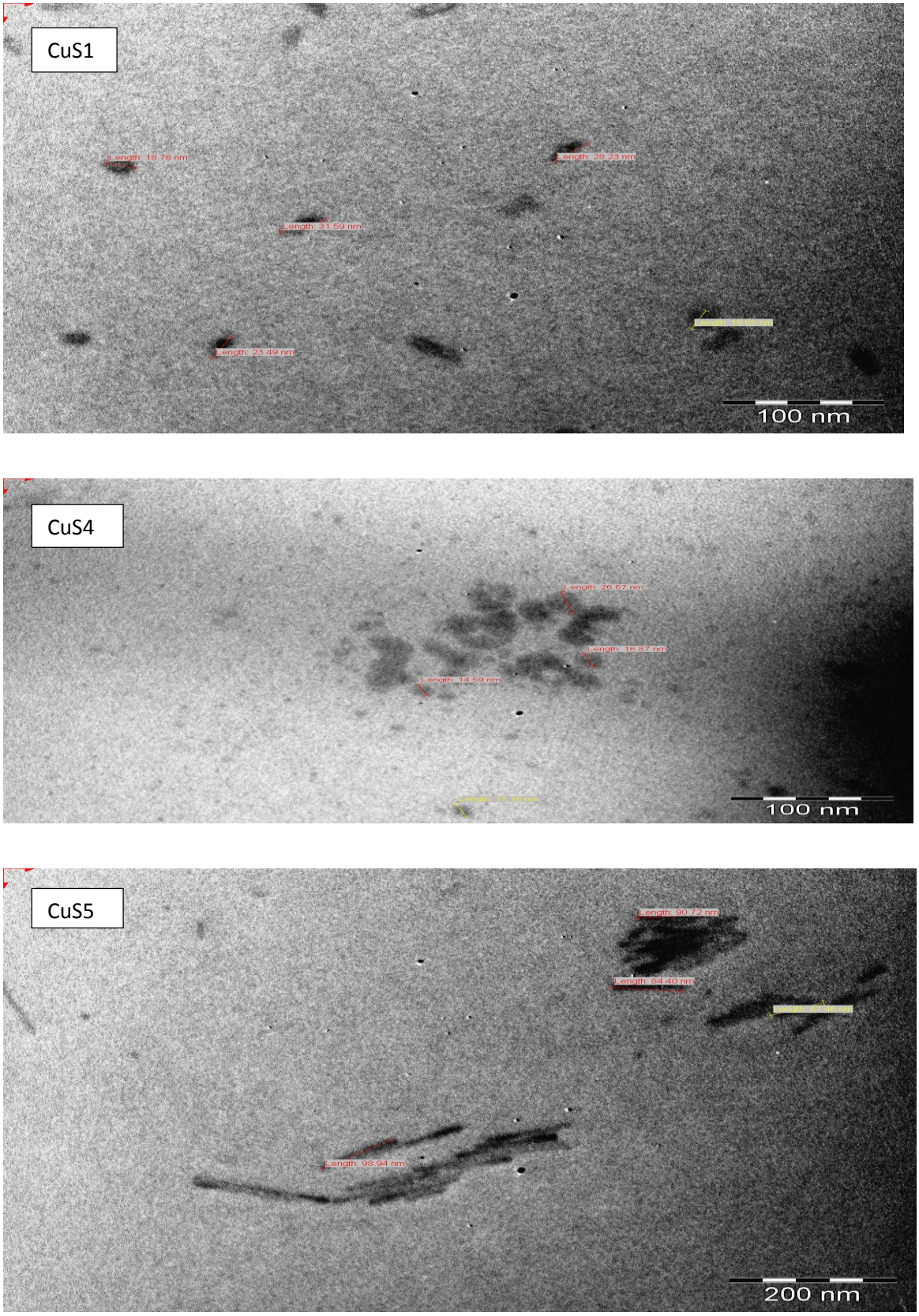

Figure 4.9: TEM images of CuS1, CuS4 and CuS5 nanoparticles.

4.3.2.4. SEM and EDX of CuS1, CuS4 and CuS5 nanoparticles.

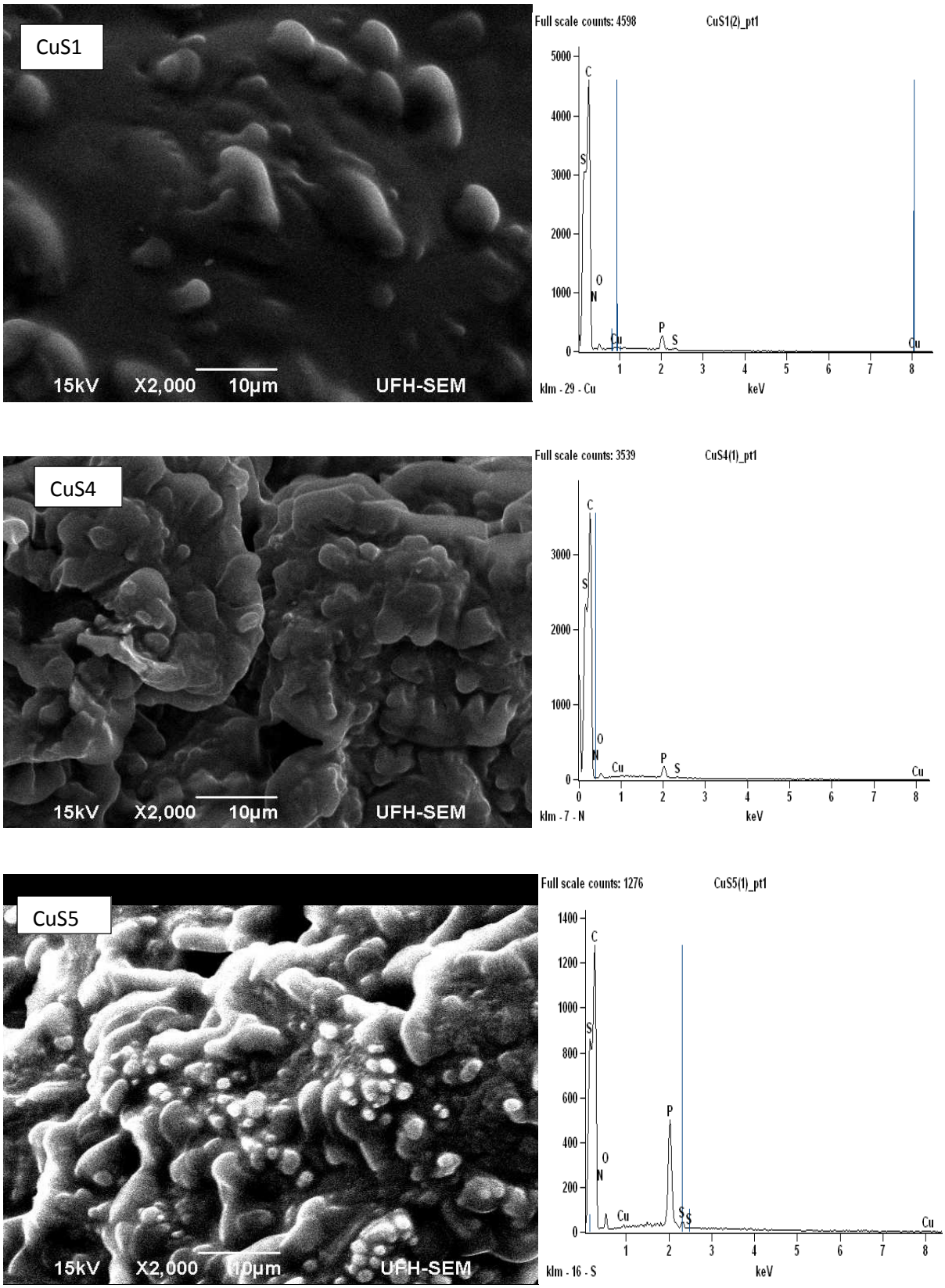

Figure 4.10: SEM images and EDX spectra of CuS1, CuS4 and CuS5 nanoparticles.

The morphology of the as-prepared CuS nanoparticles obtained from scanning electron microscopy (SEM) and their elemental composition as confirmed by energy dispersive X-ray (EDX) analysis are shown in Figure 4.10. The morphologies shows smooth surfaces except CuS5 which appears to be entirely smooth. The morphologies of the nanoparticles are not uniform in all the images, with some that appear to be composed of surfaces with mixture of rough and smooth edges. The EDX patterns show copper and sulfur confirming the formation of CuS nanoparticles. Other peaks that are observed in all the EDX spectra are C, P, N and O due to TOP used for dispersing the precursors and the HDA that was used as capping agent.

4.3.3. Characterization of CuS nanoparticles from copper(II) anisidine (C1), copper(II) butyl amine (C4) and copper(II) piperidine (C5) dithiocarbamate complexes thermolysed at 120 ^{o}C.

The resulting nanoparticles from complexes C1, C4, and C5 thermolysed at 120 ^{o}C are represented as CuS1a, CuS4a and CuS5a respectively.

4.3.3.1. Absorption spectra studies of CuS1a, CuS4a and CuS5a nanoparticles.

Fig. 4.11. Shows the absorption spectra of CuS1a, CuS4a and CuS5a nanoparticles that appear to be almost similar with little or no difference. CuS4a and CuS1a have the same absorption band edge at 312 nm while CuS5a absorption maxima occurred at 310 nm. When these wavelengths are compared with CuS1, CuS4 and CuS5 nanoparticles from the same precursors but thermolysed at different temperatures, they are larger and that shows that these nanoparticles when they are prepared at 180 ^{o}C their band gap energies are wider than when the thermolysis is done at 120 ^{o}C.

The band gap energies for CuS1a, CuS4a and CuS5a were also determined using Equation 4.1. The band gap energy of 3.98 eV was obtained for CuS1a and CuS4a which is greater than that of the bulk CuS and show quantum confinement of the nanoparticles. This band gap energy is less than the 4.31 eV for CuS1 and 4.33 eV for CuS4. The CuS5a nanoparticle have the absorption maxima at 310 nm with 4.00 eV band gap which is less than 4.33 eV obtained for CuS5. Since the band gap is greater than that of the bulk which is 1.2 eV [14]. The nanoparticles are blue shifted and this indicates that the nanoparticles exhibit strong quantum confinement [36]. It can thus be concluded that the temperature at which the thermolysis was done did affect the size of the nanoparticles as shown by the difference in their optical absorption properties.

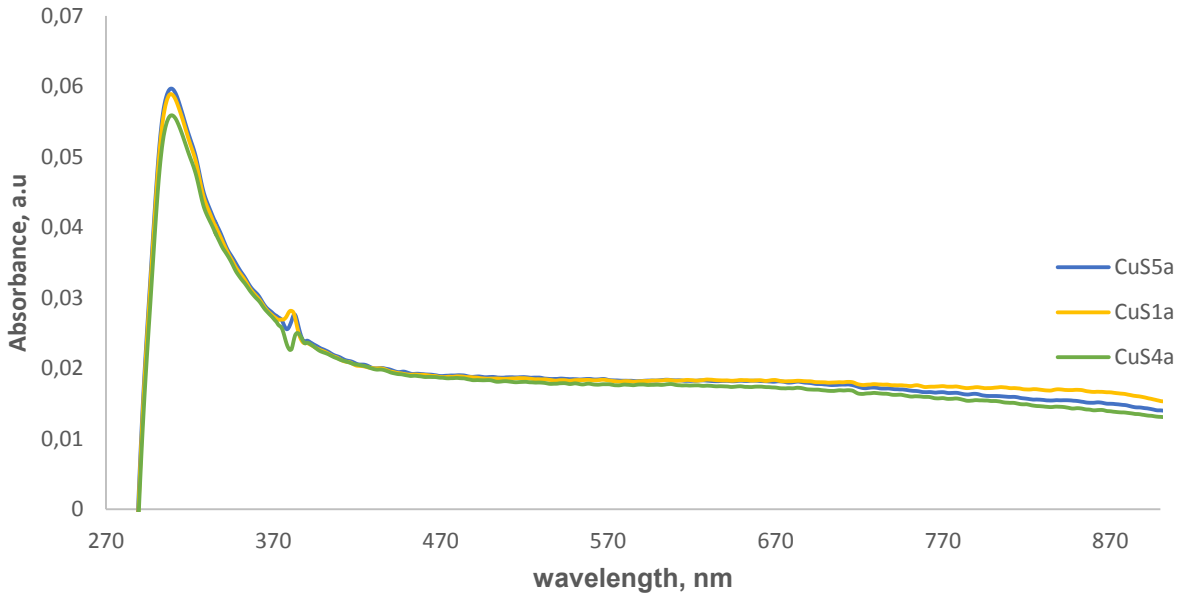

Figure 4.11: Absorption spectra of CuS1a, CuS4a and CuS5a nanoparticles.

Table: 4.1 Comparison of the absorption band, band gap and average crystal size of CuS nanoparticles thermolyzed at 180 ^{0}C and 120 ^{0}C

compounds	Absorption band (nm)	Band gap (eV)	Average crystal size (nm)
CuS1	288	4.31	40.31
CuS1a	312	3.98	23.05
CuS4	287	4.33	15.8
CuS4a	312	3.98	19.06
CuS5	287	4.33	23.24
CuS5a	310	4.00	22.8

.

4.3.3.2 X-ray diffraction patterns of CuS1a, CuS4a and CuS5a nanoparticles

The powder XRD patterns of CuS1a, CuS4a and CuS5a are shown in Figure 4.12. The average crystal size were estimated using Scherrer equation (Eq. 4.2.) [36]. The estimated average crystallite size of the as prepared CuS nanoparticles are 23.05 nm for CuS1a, 19.06 nm for CuS4a which is not that different from 15.8 nm of CuS4 thermolysed at a different temperature and 22.8 nm for CuS5a which seems to be approximately the same with the average crystal size when thermolysed at 180 ^{o}C which is 23.24 nm. The XRD patterns as illustrated in Figure 4.12 shows the crystal phase of CuS1a, CuS4a and CuS5a to correspond well to the hexagonal phase covellite CuS nanoparticles which can be indexed to the JCPDS 06-0464.

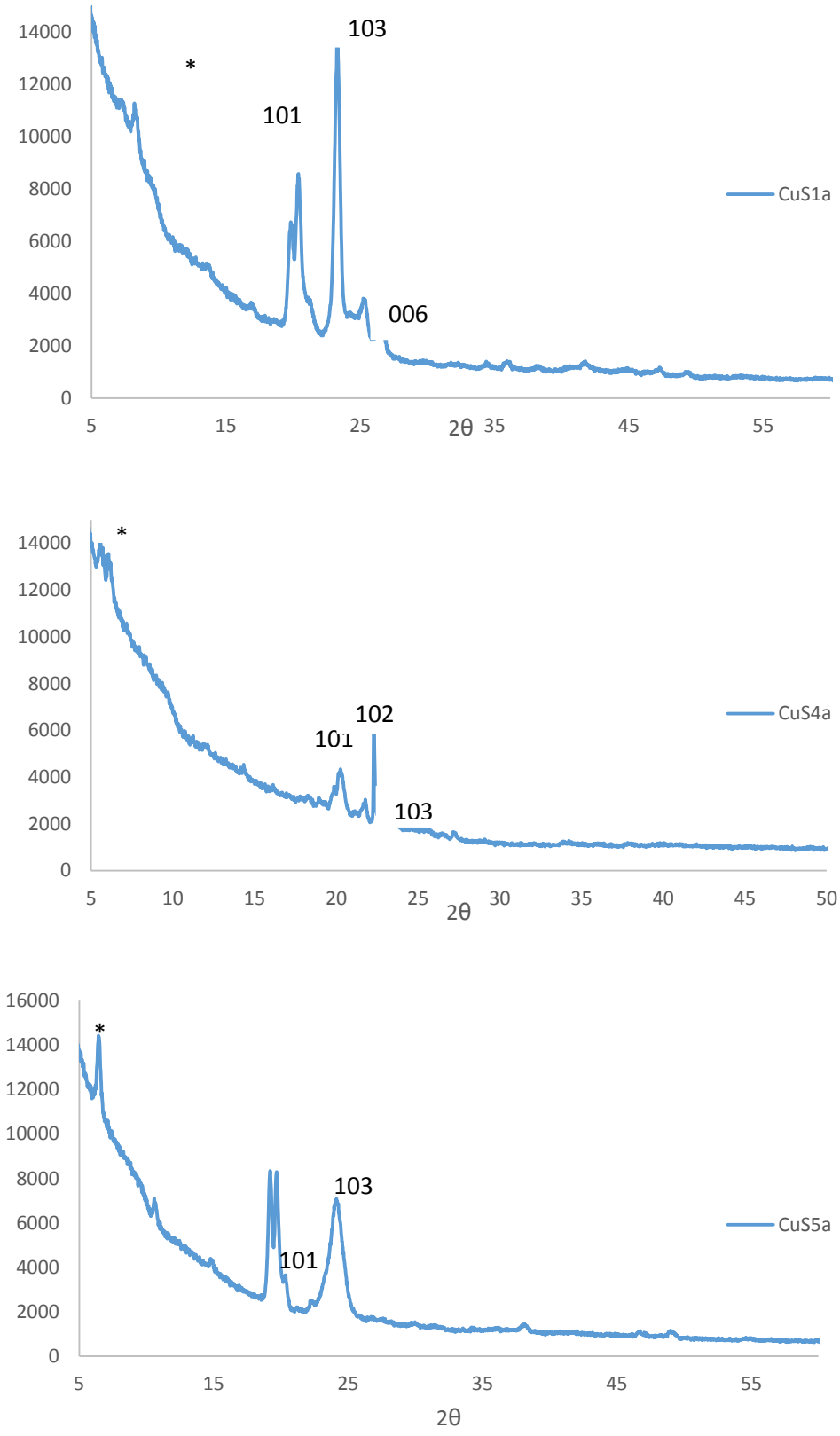

Figure 4.12: XRD of CuS1a, CuS4a and CuS5a nanoparticles. * Due to HDA

4.3.3.3. TEM of CuS1a, CuS4a and CuS5a nanoparticles

Figure 4.13 shows the TEM images of CuS1a, CuS4a and CuS5a nanoparticles. The first image which is for CuS1a shows mixed particles that have spherical and semi spherical shapes. The size of the CuS1a nanoparticles are in the range 14.94-28.99 nm. The image also showed prominent agglomeration of the nanoparticles. The average crystallite size of CuS1a is slightly smaller than that of CuS1 obtained at 180 ^{o}C that ranges between 18.76-31.59 nm and also the shape is not different. The TEM image shows that CuS4a nanoparticles with particle size in the range of 3.34-7.47 nm and they seem to be the smallest particles, this average crystallite size is totally different from the CuS4 nanoparticles that were synthesized at a different temperature (180 ^{o}C) and this confirms that the temperature at which the thermolysis was carried out does affect the nanoparticle size.

The TEM image of CuS5a nanoparticles shows the nanoparticles which ranges between 23.06-45.92 nm in size and this size is also totally different from those nanoparticles synthesized at 180 ^{o}C from the same precursor which ranged between 84.40-98.94 nm and the shape also changed from rod like for nanoparticles synthesized at 180 ^{o}C to semi spherical for those prepared at 120 ^{o}C. This shows that the temperature at which the nanoparticles were thermolysed have an effect on the size and shape of the nanoparticles.

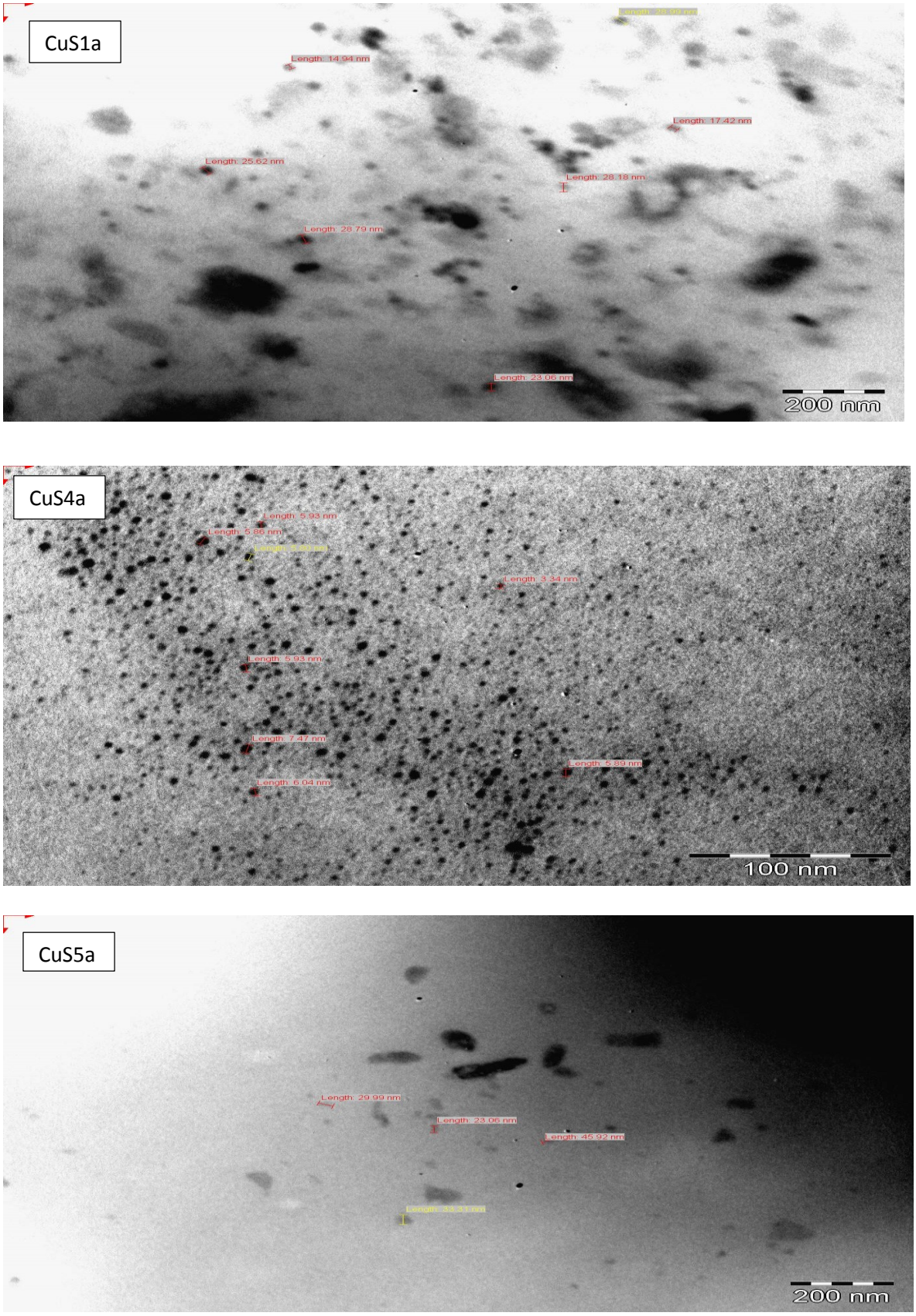

Figure 4.13: TEM images of CuS1a, CuS4a and CuS5a nanoparticles.

4.3.3.4. SEM and EDX analysis of CuS1a, CuS4a and CuS5a nanoparticles

The morphology of the CuS nanoparticles were determined using the scanning electron microscopy (SEM). The possible elemental composition was determined using the energy dispersive X-ray (EDX). Fig. 4.14 shows the SEM images at 1000 magnification and the EDX spectra of CuS1a, CuS4a and CuS5a nanoparticles thermolysed at 120 ^{o}C. The SEM images of CuS1a and CuS5a shows flowery surface and the SEM image of CuS5a shows that the morphology of the nanoparticles are not uniform. The morphology of CuS4a is totally different from CuS1a and CuS5a, its image shows a smooth morphology with some charred surfaces. The EDX spectra of the nanoparticles confirmed the presence of copper and sulfur along with C, O, P and N peaks from the HDA capping agent and TOP used to dissolve the complex so it can be injected into the hot HDA.

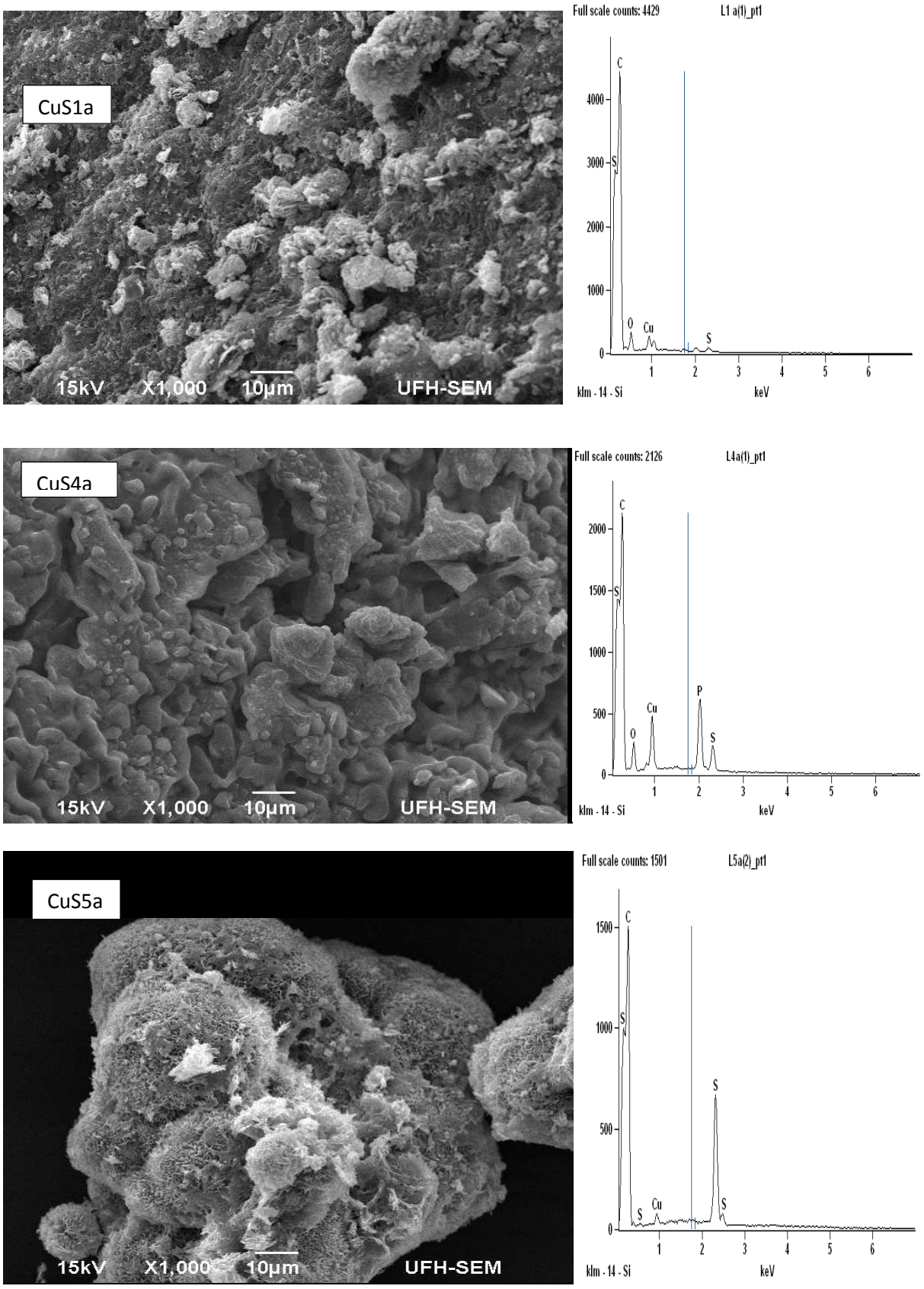

Figure 4.14: SEM images and EDX spectra of CuS1a, CuS4a and CuS5a nanoparticles.

References

[1] Lia, Y.; Zhanga, L.; Yua, J. C.; Shu-Hong Y. Facet effect of copper(I) sulfide nanocrystals on photoelectrochemical properties. *Mater. Int.* **2012**, 22(6), 585–591.

[2] Kundu, M.; Hasegawa, T.; Terabe, K.; Yamamoto, K.; Aono, M. Structural studies of copper sulfide films: Effect of ambient atmosphere. *Sci. Technol. Adv. Mater.* **2008**, 9, 1-6.

[3] Tan, Z. G.; Zhu, Q.; Guo, X. Z.; Zhang, J. F.; Wu, W. Y.; Liu, A. P. Synthesis of flower-shaped CuS microsphere superstructures by a solvothermal route and its photocatalytic properties. *Acta*. *Chim*. *Sin*. **2011**, 69**,** 2812-2820.

[4] Sagade, A. A.; Sharma, R. Copper sulphide (Cu_xS) as an ammonia gas sensor working at room temperature. *Sensor Actuat B- Chem*. **2008**, 133**,**135-143.

[5] Reijnen, L.; Meester, B.; Goossens, A.; Schoonman, J. Atomic layer deposition of Cu_xS for solar energy conversion. *Chem. Vapor*. *Depos*. **2003**, 9, 15-20.

[6] Chung, J. S.; Sohn, H. J. Electrochemical behaviors of CuS as a cathode material for lithium secondary batteries. *J. Power Sources.* **2002,** 108, 226-231.

[7] Singh, K. V.; Martinez-Morales, A. A.; Bozhilov, K. N.; Ozkan, M. A simple way of synthesizing single-crystalline semiconducting copper sulfide nanorods by using ultrasonication during template-assisted electrodeposition. *Chem. Mater*. **2007**, 19, 2446-2454.

[8] Zhu, T.; Xia, B.; Zhou, L.; Wen Lou X. Arrays of ultrafine CuS nanoneedles supported on a CNT backbone for application in supercapacitors. *J*. *Mater*. *Chem*. **2012**, 22**,** 7851-7855.

[9] Athanassiou, E. K.; Grass, R. N.; Stark, W. J. Large-scale production of carbon-coated copper nanoparticles for sensor applications. *Nanotechnology*, **2006**, 17(6), 1668–1673.

[10] Chen, J.; Deng, S.; She, J.; Xu, N.; Zhang, W.; Wen, X.; Yang, S**.** Effect of structural parameter on field emission properties of semiconducting copper sulphide nanowire films. *J. Appl. Phys*. **2003**, 93**,** 1774-1777.

[11] Gorai, S.; Ganguli, D.; Chaudhuri, S. Synthesis of copper sulfides of varying morphologies and stoichiometries controlled by chelating and nonchelating solvents in a solvothermal process. *Cryst. Growth Des*. **2005**, 5(3), 875-877.

[12] Ancutiene, I.; Janickis, V. Formation and characterization of Cu_xS layers on polyethylene film using the solutions of sulfur in carbon disulfide. *Cent. Eur. J. Chem.* **2010**, 8(6), 1281-1287.

[13] Pathana, H. M.; Desaib, J. D.; Lokhande, C. D. Modified chemical deposition and physico-chemical properties of copper sulphide (Cu_2S) thin films. *Appl. Surface Sc.* **2002**, 202, 47–56.

[14] Tsofnat, S.; Jurgen, J.; Yuval, G. A comparative study of the structure and optical properties of copper sulfide thin films chemically deposited on various substrates. *RSC Adv.* **2013**, 3, 23066–23074.

[15] Zhang, P.; Gao, L. Copper sulfide flakes and nanodisks. *J. Mater. Chem.* **2003**, 13, 2007–2010.

[16] Tan, C.; Zhu, Y.; Lu, R.; Xue, P.; Bao, C.; Liu, X.; Fei, Z.; Zhao, Y. Synthesis of copper sulfide nanotube in the hydrogel system. *Mater. Chem. Phys.* **2005**, 91, 44–47.

[17] Zhang, W.; Wen, X.; Yang, S. Synthesis and characterization of uniform arrays of copper sulfide nanorods coated with nanolayers of polypyrrole. *Langmuir.* **2003**, *19,* 4420-4426.

[18] Ghahremaninezhad, A.; Asselin, E.; Dixon, D. G. Electrodeposition and growth mechanism of copper sulfide nanowires. *J. Phys. Chem*. **2011**, 115, 9320–9334.

[19] Ajibade, P. A.; Onwudiwe, D. C.; Moloto, M. J. Synthesis of hexadecylamine capped nanoparticles using group 12 complexes of N-alkyl-N-phenyl dithiocarbamate as single-source precursors. *Polyhedron*. **2011**, 30, 246-252.

[20] Nair, P. S.; Radhakrishnan, T.; Revaprasadu, N.; Kolawole, G. A.; O'Brien, P. The synthesis of HgS nanoparticles in polystyrene matrix. *J. Mater. Chem*. **2004**, 14, 581-584.

[21] Moloto, N.; Coville, N. J.; Ray, S. S.; Moloto, M. J. Morphological and optical properties of MnS/polyvinylcarbazole hybrid composites. *Physica B*, **2009,** 404 4461–4465.

[22] Sohrabnezhad, S. H.; Pourahmad, A. CdS semiconductor nanoparticles embedded in AlMCM-41 by solid-state reaction. *J*. *Alloys Compd.* **2010,** 505, 324–327.

[23] Pourahmad, S. H.; Sohrabnezhad, M. S. Sadjadi, Zare, K. Preparation and characterization of host (mesoporous aluminosilicate material)–guest (semiconductor nanoparticles) nanocomposite materials. *Mater*. *Lett*. **2008**, 62, 655–658.

[24] Radhakrishnan, T.; Georges, M. K.; Nair, P. S.; Luyt, A. S.; Djokovic, V. Composites comprising CdS nanoparticles and poly (ethylene oxide): Optical

properties and influence of the nanofiller content on the thermal behaviour of the host matrix. *Colloid*. *Polym*. *Sci*., **2008**, 286, 683–689.

[25] Zhang, Y. C.; Wang, G. Y.; Hu, X. Y. Solvothermal synthesis of hexagonal CdS nanostructures from a single-source molecular precursor. *J*. *Alloys Compd*. **2007**, 437, 47-52.

[26] Ajibade, P. A.; Benjamin, C. E. Group 12 dithiocarbamate complexes: Synthesis, spectral studies and their use as precursors for metal sulfides nanoparticles and nanocomposites. *Spectr*. *Acta Part A*: *Mol*. *Biomol*. *Spectro*. **2013**, 113, 408-414.

[27] Afzaal, M.; Malik, M. A.; O'Brien, P. Indium sulfide nanorods from single-source precursor. *Chem. Comm*. **2004**, 334-335.

[28] Kedarnath, G.; Kumbhare, L. B.; Jain, V. K.; Phadnis, P. P.; Nethaji, M. Group 12 metal monoselenocarboxylates: Synthesis, characterization, structure and their transformation to metal selenide (MSe; M = Zn, Cd, Hg) nanoparticles. *Dalton Trans*. **2006**, 2714-2718.

[29] Kedarnath, G.; Dey, S.; Jain, V. K.; Dey, G. K.; Varghese, B. 2-(N,N-dimethylamino)ethylselenolates of cadmium(II): Syntheses, structure of $[Cd_3(OAc)_2(SeCH_2CH_2NMe_2)_4]$ and their use as single source precursors for the preparation of CdSe nanoparticles. *Polyhedron*, **2006**, 25 2383-2391

[30] Jin, M.; Guannan, H.; Zhang, H.; Zeng, J.; Xie, Z.; Xia, Y. Shape-controlled synthesis of copper nanocrystals in an aqueous solution with glucose as a reducing agent and hexadecylamine as a capping agent. *Ang*. *Chem*. *Inter*. *Ed*. **2011**, 50, 10560-10564.

[31] Mthethwa, T.; Pullabhotla, V. S. R.; Mdluli, P. S., Wesley-Smith, J.; Revaprasadu *N.* Synthesis of hexadecylamine capped CdS nanoparticles using heterocyclic cadmium dithiocarbamates as single source precursors. *Polyhedron*, **2009**, 28, 2977-

2982.

[32] Park, J. Y.; Aliaga, C.; Renzas, R. J.; Lee, H.; Somorjai, G. The role of organic capping agents layers of platinum nanoparticles in catalytic activity of CO oxidation. *Catal*. *lett*. **2009**, 129, 1- 6.

[33] Kvitek, O.; Siegel, J.; Hnatowicz, V.; Svorlik, V. Noble metal nanostructures influence of structure and environment on their optical properties. *J. Nanomater*. **2003**, 1-15.

[34] Gupta, P.; Ramrakhiani, M. Influence of the particle size on the optical properties of CdSe nanoparticles.*TONANOJ,* **2009**, 3, 15-19.

[35] Chandran, A.; Francis, N.; Jose, T.; George, K. C. Synthesis, structural characterization and optical bandgap determination of ZnS nanoparticles. *SB Academ. Rev.* **2010**, 17-21.

[36] Mercy, A.; Selvaraj, R. S.; Boaz, B. M.; Anandhi, A.; Kanagadurai, R. Synthesis, structural and optical characterization of cadmium sulfide nanoparticles. *Indian J. Pure Appl. Phys.* **2013,** 51, 448-452.

CHAPTER FIVE

5.0. ANTIMICROBIAL STUDIES OF SOME OF THE COMPOUNDS

5.1. Introduction

In vitro susceptibility testing plays an increasingly important role in guiding therapeutic decision and it is an aid in drug development studies [1]. Methods used for susceptibility testing include disc diffusion, agar dilution and broth dilution procedures [2]. The most commonly used methods to screen antifungal susceptibility of fungal crop pathogens is *in vitro*, it involves direct-plating of isolates in media amended with various concentrations of fungicide and determining inhibition of growth and/or spore germination [5]. Numerous *in vitro* factors such as media, buffer, inoculum, incubation and end point criteria can affect results significantly. Most methods are therefore reported to provide at best an estimation of the Minimum inhibitory concentration (MIC) value within two-fold dilution steps [3].

The standardization of antifungal susceptibility testing methods is crucial for the evaluation and development of antifungal drugs. It is through these methods that existing and new therapies can be compared. Although these methods have been standardized for a long time for bacteria, they only recently have been adopted for fungal pathogens. Although many clinical microbiology laboratories are comfortable with handling antibacterial specimens and implementing long-approved testing methods, the same level of comfort does not yet exist for fungi [4]. In this study the antimicrobial and antifungal properties of three copper complexes soluble in DMSO were determined against four fungi strains and four bacterial strains. The activities of the other compounds and the nanoparticles could not be studied due to solvent

miscibility issues. The nanoparticles were soluble in toluene but the solvent is not suitable for growing the microorganisms.

5.2. Experimental

5.2.1. Materials and Methods

Compounds C1, C4 and C5

20 mg each was dissolved in 5 mL of dimethyl sulfoxide (DMSO) to obtain final concentration of 2 mg/mL for the compounds.

5.2.2. Test Microorganisms

Candida rugosa, Candida neoformans, Candida albocans and Trychophyton mucoides were used to investigate the antibacterial activity of the compounds. These organisms were obtained from the Department of Biochemistry and Microbiology, University of Fort Hare, South Africa, and were maintained on nutrient broth (Oxoid LTD, Basingstoke, Hampshire, England) for 24 hours before being used.

5.2.3. Antimicrobial activity

The MIC values for the compound against bacteria were determined by using two-fold serial microdilution method as described by Eloff [6]. Organisms were maintained on the nutrient agar at 4 °C in the refrigerator and were revived for bioassay by sub-culturing in fresh nutrient broth (Oxoid Ltd, Basingstoke, Hampshire and England) prepared in 20% DMSO for 24 hours before use. Briefly, organisms were cultured

overnight (24 h) in an autoclaved nutrient Broth (Oxoid LTD, Basingstoke, Hampshire, England) and was adjusted to a final density of 10^6 ufl. This was used to inoculate 96-well microtitre plates containing serial two fold dilutions of the extracts (0.5 - 0.0039 mg/mL) under aseptic condition.

The plates were incubated under aerobic conditions at 37 °C and examined after 24 h. Controls were prepared from compound free microtitre plates. 40 µl of 0.2 mg/mL p-iodonitrotetrazolium (97% purity, Sigma, South Africa) solution was added to each well as an indicator of microbial growth and incubated for 30 min at 37 °C. Tetrazolium salt was reduced to coloured (red) product which is an indication of organism growth. Therefore, red coloured wells indicated presence of organisms, while clear wells indicated inhibition of organisms. Each treatment was performed in duplicate.

5.3. Results and discussion

The search for antimicrobials from natural sources has received much attention and efforts have been put in to identifying compounds that can act as suitable antimicrobials agent to replace synthetic ones [8]. Copper(II) anisidine dithiocarbamate (C1), copper(II) butyl amine dithiocarbamate (C4) and copper(II) piperidine dithiocarbamate (C5) complexes were screened each against four organisms for antifungal activity. The minimum inhibitory concentration (MIC) of the compounds against each of the three organisms is shown in Tables 5.1 and 5.2. MIC is defined as the lowest concentration able to inhibit any visible bacterial growth on the culture plates [7].

Table 5.1: Antifungal activity of compounds C1, C4 and C5

Organism	Compound (mg/mL)		
	C1	**C4**	**C5**
Candida rugose	0.125	0.125	0.500
Candida neoformans	0.063	0.063	0.500
Candida albicans	0.031	0.063	0.500
Trychophyton mucoides	0.031	0.063	0.500

The antifungal activity of each compound was measured *in vitro* against *Candida rugosa, Candida neoformans, Candida albocans and Trychophyton mucoides* microorganisms. All compounds were active against the organisms. C5 was more active than the other two compounds (C1 and C4) against the four organisms. It gave the MIC's of 0.500 for all the four organisms. C1 and C4 gave equal MIC's against *Candida rugosa* and *Candida neoformans* which are 0.125 and 0.063 mg/mL respectively. C4 gave the same MIC for *Candida albicans* and *Trychophyton mucoides* which is 0.031 mg/mL. And also C4 gave the MIC of 0.063 mg/mL for both *Candida albicans* and *Trychophyton mucoide* organisms. C1 is observed to be the less active compound against all the screened organism.

The compounds were further then screened against four bacteria isolates *Escherichia coli (ATCC 8739), Staphylococcus aureus (ATCC 6538), Salmonella typhi* and *Salmonella typhimurium*. The compounds showed promising antibacterial activities. C5 is still the most active compound in comparison to the other two complexes against

the bacterial species organisms. C1 again is the less active compound as compared to the others.

Table 5.2: Antibacterial activity of compounds C1, C4 and C5

Organism	Compound (mg/mL)		
	C1	**C4**	**C5**
Escherichia coli ATCC 8739	0.063	0.250	0.500
Staphylococcus aureus ATCC6538	0.031	0.125	0.250
Salmonella typhi	0.031	0.063	0.250
Salmonella typhimurium	0.063	0.125	0.500

References

[1] Kanafani, Z. A.; Perfect, J. R. Antimicrobial resistance: Resistance to antifungal agents, mechanisms and clinical impact. *Clin Infect Dis*. **2008**, 46(1), 1-120.

[2] Kumar, R.; Shrivastava, S. K.; Chakraborti, A. Comparison of broth dilution and disc diffusion method for the antifungal susceptibility testing of *Aspergillus flavus. Am. J. Biomed. Sci*. **2010**, 2(3), 202-208.

[3] Cabanas, R.; Abarca, M. L.; Bragulat, M. R.; Cabanes, F. J. *In vitro* activity of imazalil against *Penicillium expansum*: Comparison of the CLSI M38-A broth microdilution method with traditional techniques. *Int. J. Food Microbiol*. **2009**, 129(1), 26-35.

[4] Lozano-chiu, M.; Arikan, S.; Paetznick, L. V.; Anaissie, E. J.; Rex, J. H. Optimizing voriconazole susceptibility testing of candida: Effects of incubation time, endpoint rule, species of candida, and level of fluconazole susceptibility. *J. Clin. Microbiol*. **1999**, 37(9), 2755–2759.

[5] Alvarez-Barrientos, A.; Arroyo, J.; Canton, R.; Nombela, C.; Sanchez-Perez, M. Applications of flow cytometry to clinical microbiology. *Clin. Microbiol. Rev*. **2000**. 13(2), 167-195.

[6] Eloff, J. N. A sensitive and quick microplate method to determine the minimal inhibitory concentration of plant extracts for bacteria. *Planta Med*. **1998**, 64(8), 711–714

[7] Sen, A.; Batra, A. Evaluation of antimicrobial activity of different solvent extracts of medicinal plant: *Melia azedarach l*. *Int. J Curr. Pharm. Res*. **2012**, 4(2), 67-73.

[8] Hashempour, N.; Zali, M. H. S.; Yousefi, S.; Hashempour, A. Compared antibacterial and antiyeast effect of *Citrus sinensis* and *Musa sapientum* with the antibiotic penicillin on two pathogenic agent. *Sch. J. App. Med. Sci*. **2014**, 2(4E), 1458-1461.

CHAPTER SIX

6.0. CONCLUSIONS AND FUTURE PROSPECTS

6.1. Conclusions

Six dithiocarbamate ligands were synthesized from anisidine, aniline, ethyl aniline, butyl amine, piperidine and morpholine. Copper(II) dithiocarbamate complexes were synthesized from these ligands. The ligands and complexes were all characterized by conductivity measurements, melting point/decomposition temperature, FTIR, UV-Vis and ligands were further characterized by NMR. The results showed that the complexes and ligands were successfully synthesized. The electronic spectra of the ligands showed $\pi \rightarrow \pi^*$ transitions that are due to N-C=S and S-C=S groups of the dithiocarbamate moiety.

The formation of the complexes from the ligands were confirmed with new absorbance peaks including the MLCT and d-d transitions for each complex were observed. The electronic spectra measurements also confirmed the proposed stereochemistry of the complexes as four coordinate square planar. The FTIR spectra showed all the functional groups that were expected from the dithiocarbamate compounds which are C-S, C=S, N-CS, N-H and M-S vibrations. The FTIR also confirmed that the dithiocarbamate ligands are bidentately coordinated to the Cu ions.

Nine nanoparticles were prepared from the six copper(II) dithiocarbamate complexes synthesized. All the complexes were thermolysed at 180 ^{o}C, and three of them were further thermolysed at 120 ^{o}C to study the effects of temperature on size and shape

of the resulting nanoparticles. The optical properties of the copper sulfide nanoparticles were studied with UV-Vis and photoluminescence spectroscopy. The absorption peak maxima were used to calculate the band gap energies. The obtained band gap energies were greater than the band gap energy of bulk copper sulfide which is 1.2 eV. This confirmed that the as-prepared CuS nanoparticles are blue shifted and are quantum confined due to their sizes being in the nanometer range.

The absorption spectra of the nanoparticles thermolysed at 120 ^{o}C shifted to higher wavelengths when compared to those obtained at 180 ^{o}C and that shows that the band gap energies of those obtained at 120 ^{o}C are wider. Therefore, temperature had an effect on the optical properties of the nanoparticles. The XRD was used to estimate the particle sizes. For all the particles, the crystallite sizes were estimated to be in the range 15.8-23.24 nm which is totally different from the sizes obtained from the TEM analysis which is 3.02-98.94 nm. The XRD patterns of the nanoparticles were indexed to the hexagonal CuS crystalline phase.

The TEM images showed that the copper sulfide nanoparticles prepared have different shapes and varies from spherical, semi spherical, cubic to rodlike. SEM images showed different morphologies for the nanoparticles with their surfaces varying from smooth to rough. The EDX confirmed the formation of copper sulfide nanoparticles by showing the peaks of Cu and S except for sample CuS6 which was not dry when the analysis was done. The metal complexes are therefore efficient single source precursors for the preparation of CuS sulfide nanoparticles.

6.2. Future prospects

The nanoparticles prepared were not screened against fungi organisms due to solubility problem. All the nanoparticles could only dissolve in toluene which is not miscible with water, and also the nanoparticles did not dissolve in water that is because of the capping agent that is not water soluble. So it is recommended that the HDA capping agent be replaced with water soluble capping agent such as polyvinyl alcohol, thioglycolic acid or other water soluble polymers. This will enhance their solubility in water and make it easy to study their biological activities.

The functionalization of the dithiocarbamate ligands should also be explored by replacing some of the alkyl or hydrogen on the ligands with hydrophilic groups to enhance their solubility and thus their biological studies. The complexes were synthesized using two molecules of each dithiocarbamate ligand to synthesize four coordinate square planar copper(II) complexes. It is necessary to synthesize six coordinate octahedral copper(II) complexes using a 1:3 scale ratio of copper salt to the dithiocarbamate ligand. These compounds might be able to give insight about structure-activity relationship of the metal complexes. Thermolysis of the six coordinate complexes might also be interesting to see whether one might be able to get other crystalline phases of CuS nanocrystals such as the sulfur rich roxbyite and anilite. It is also necessary to study the effects of different capping agents on the shapes, sizes and morphologies of the copper sulfide nanoparticles and explore their potentials anticancer agents.

Appendix A

Appendix A1: ^{1}H NMR of anisidine dithiocarbamate

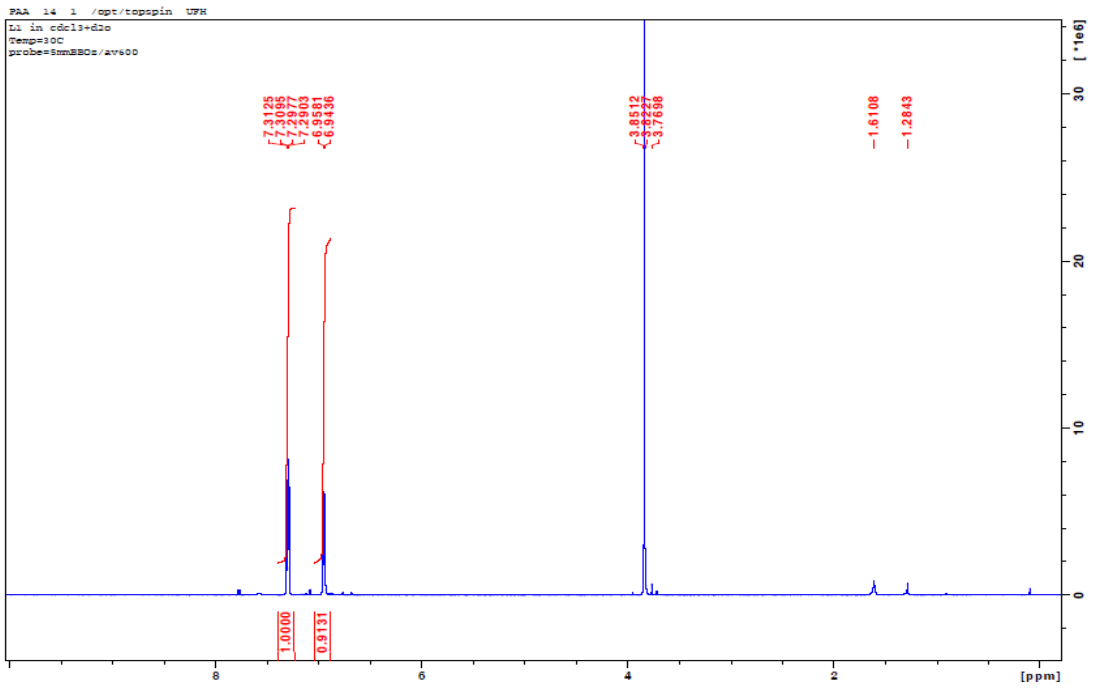

Appendix A2: ^{13}C NMR of anisidine dithiocarbamate

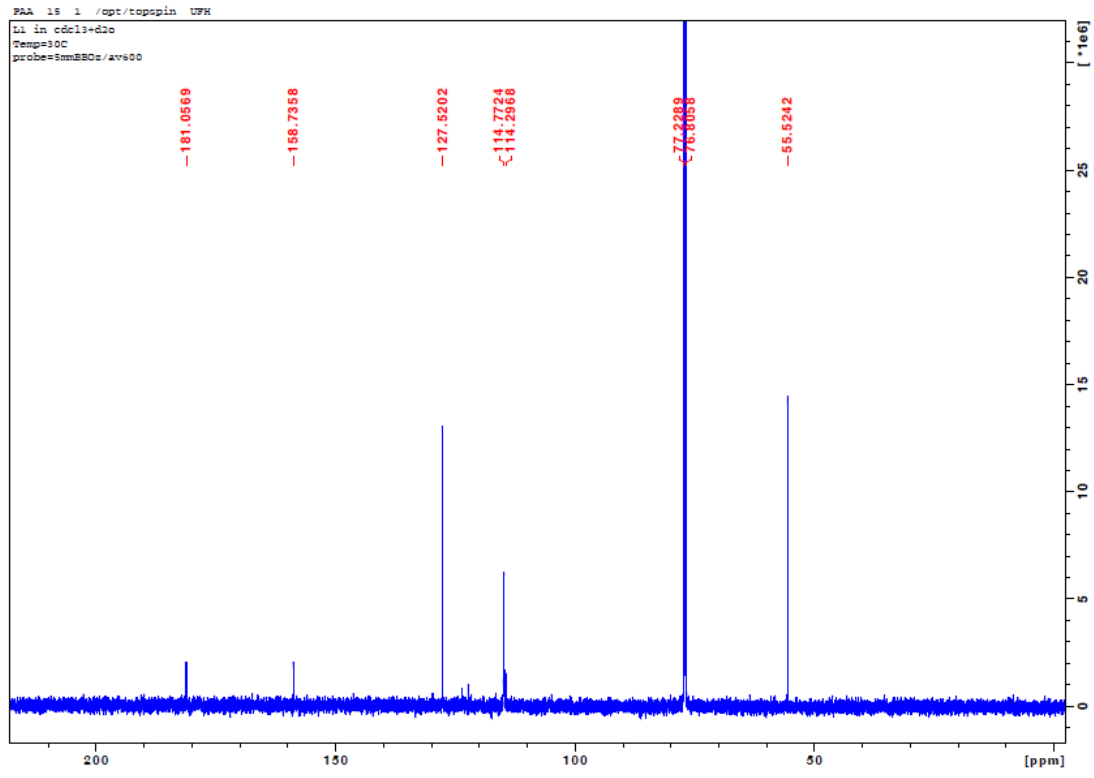

Appendix A3: ^{1}H NMR of aniline dithiocarbamate

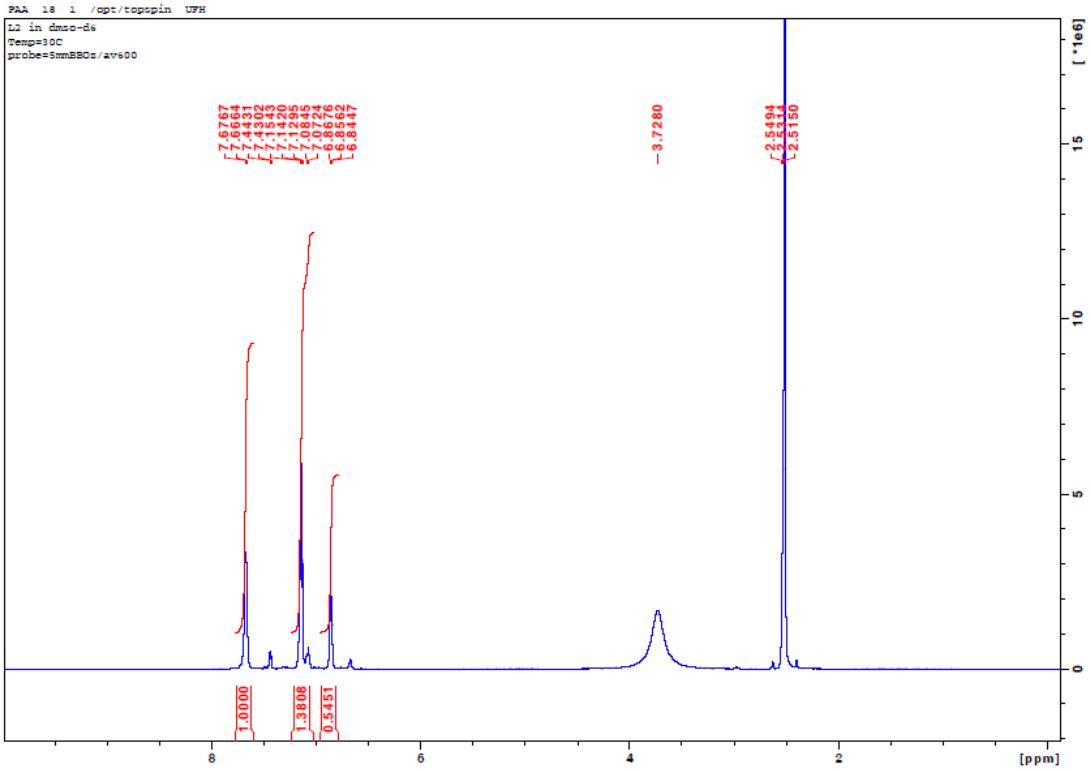

Appendix A4: ^{13}C NMR of aniline dithiocarbamate

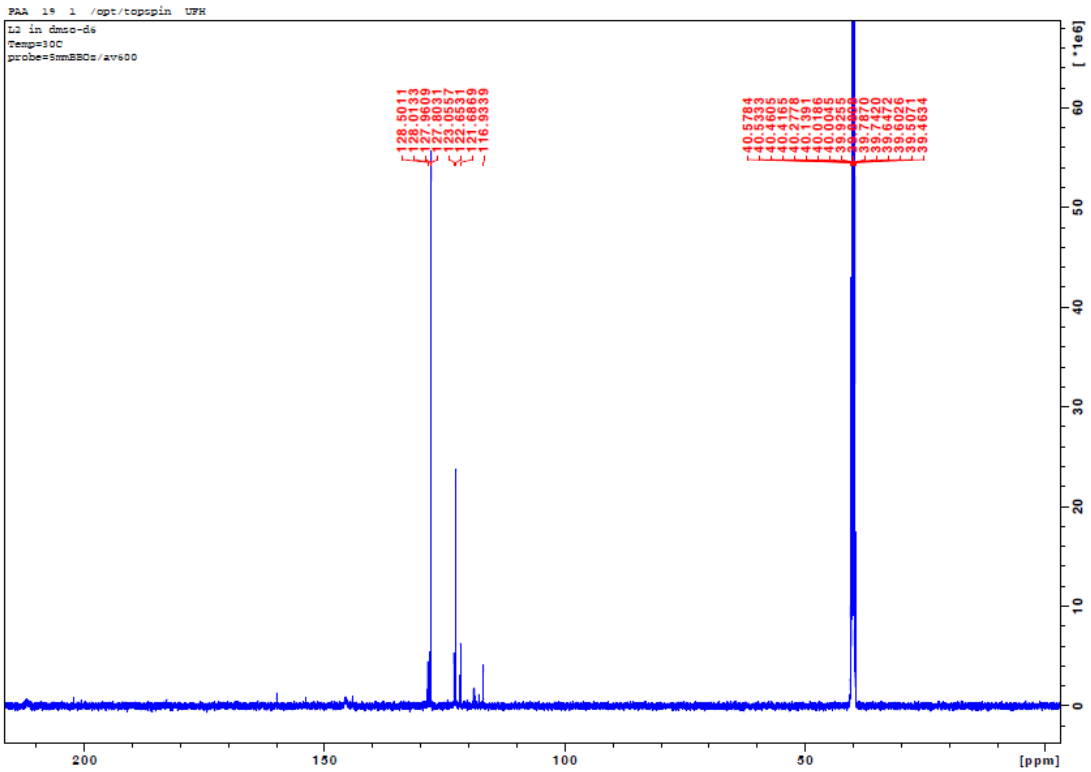

Appendix A5: ^{1}H NMR of ethyl aniline dithiocarbamate

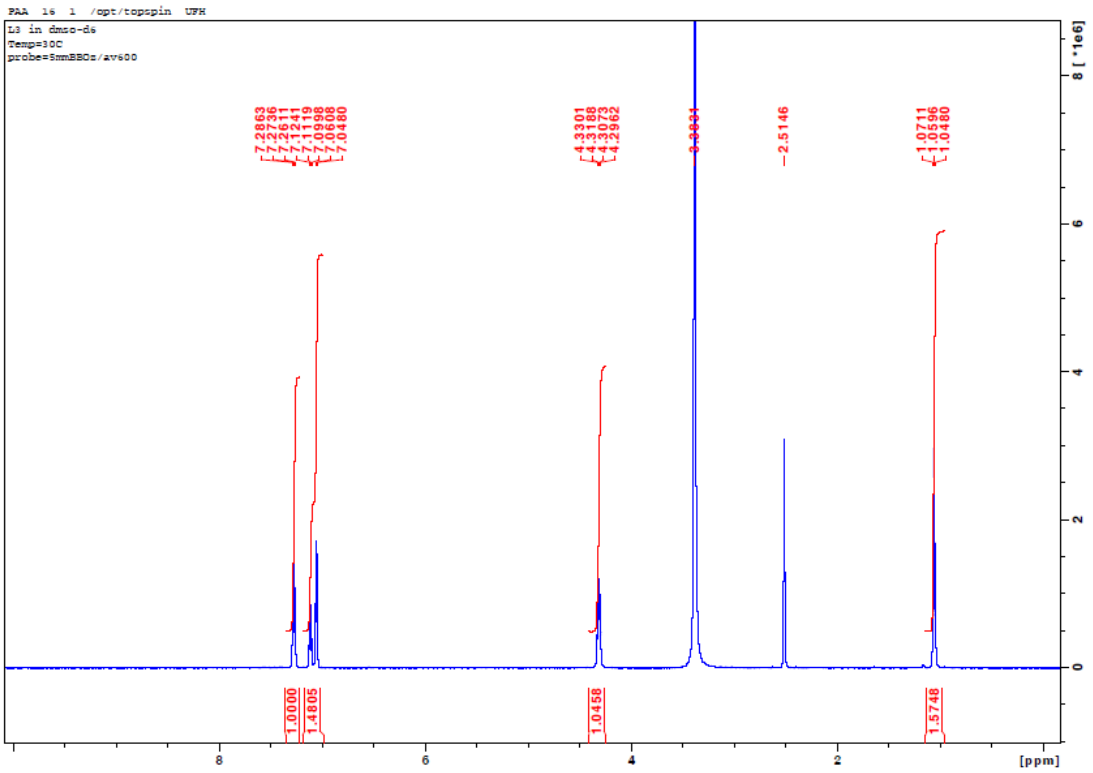

Appendix A6: ^{13}C NMR of ethyl aniline dithiocarbamate

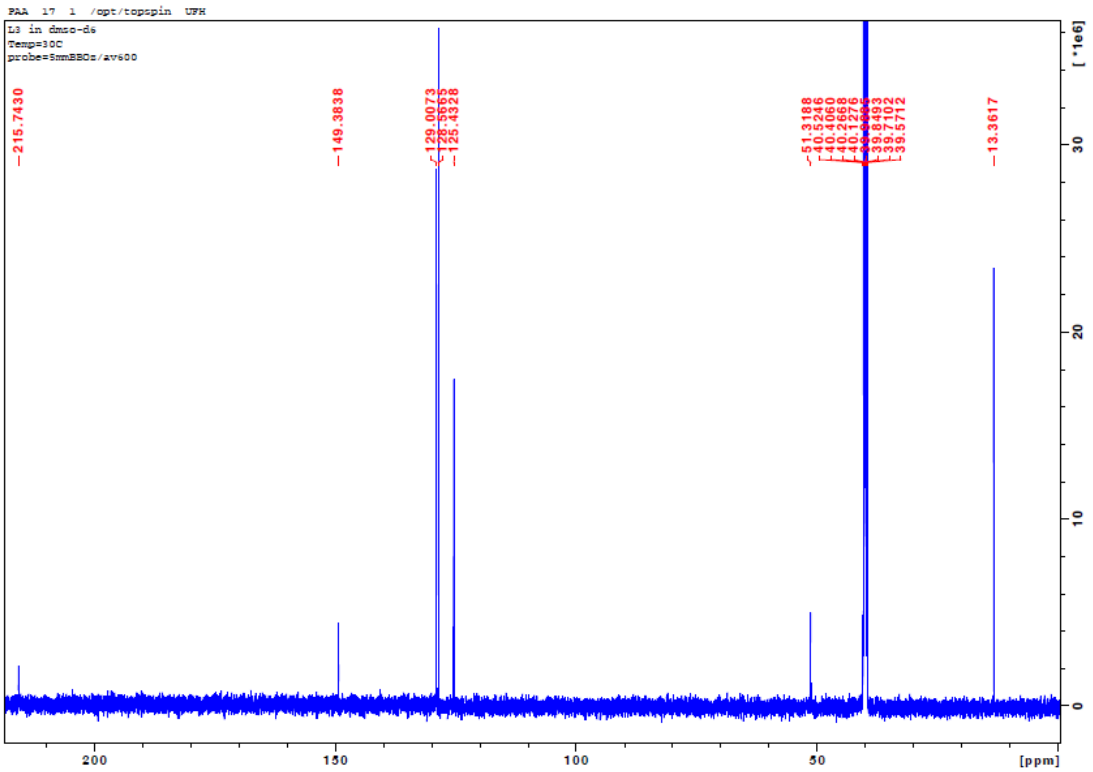

Appendix A7: ^{1}H NMR of butylamine dithiocarbamate

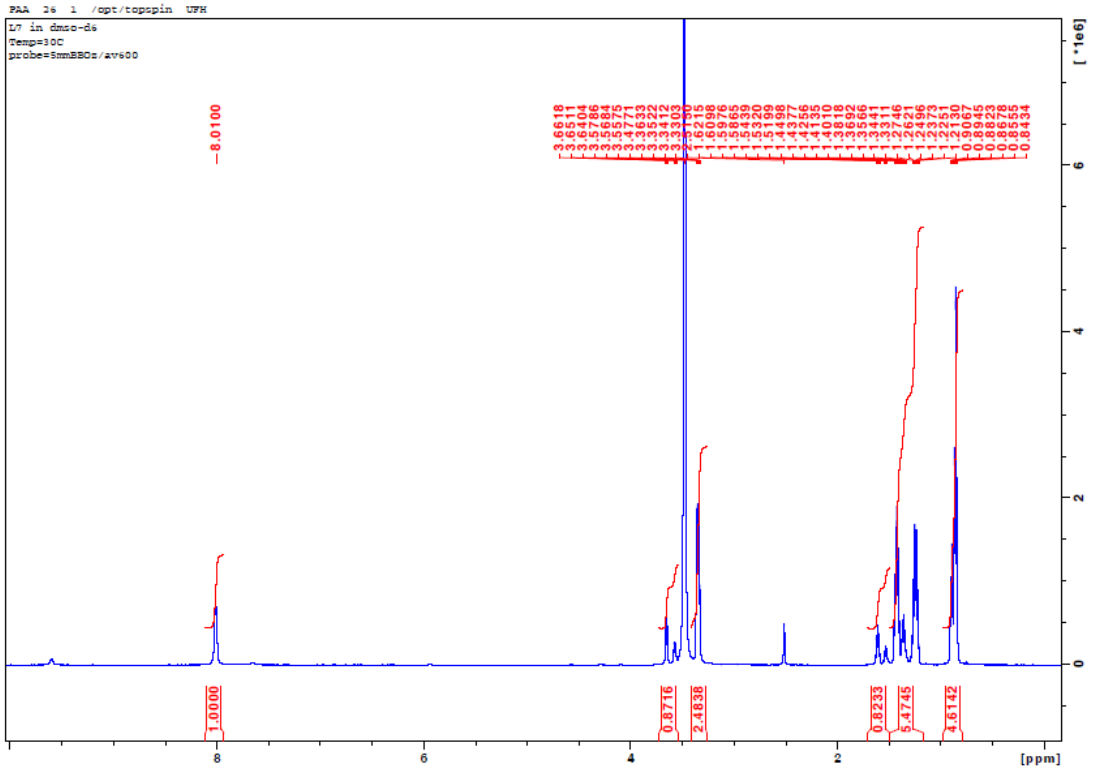

Appendix A8: ^{13}C NMR of butylamine dithiocarbamate

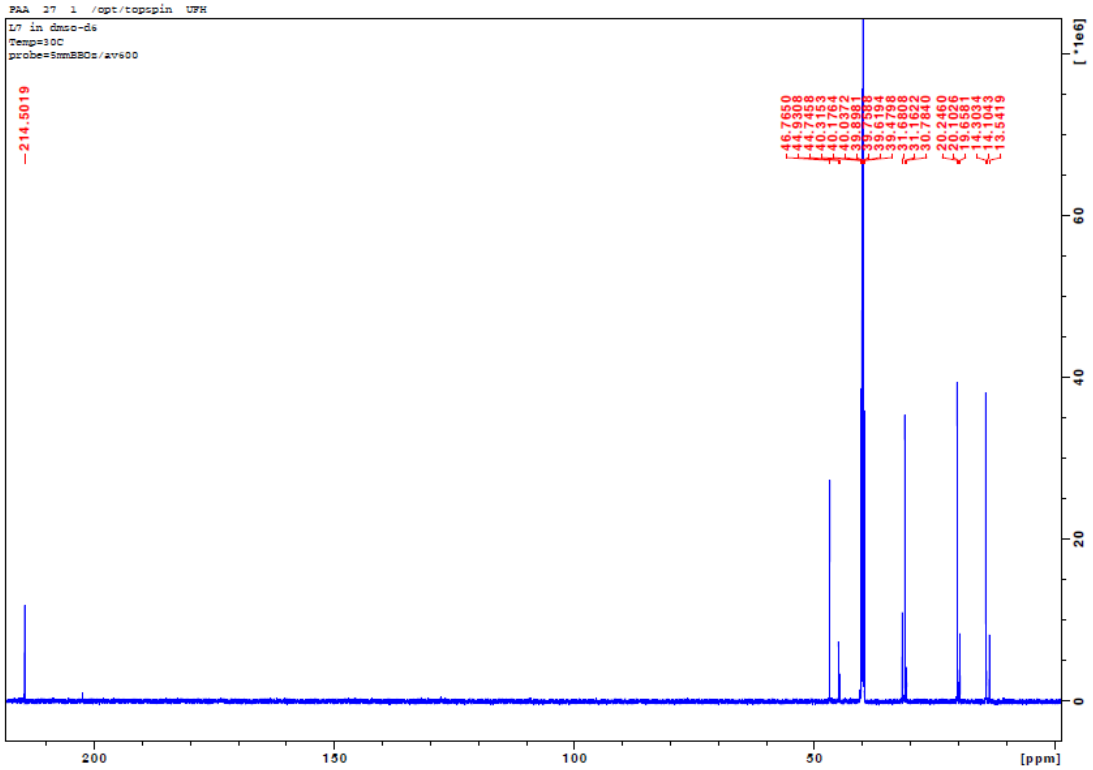

Appendix A9: ^{1}H NMR of piperidine dithiocarbamate

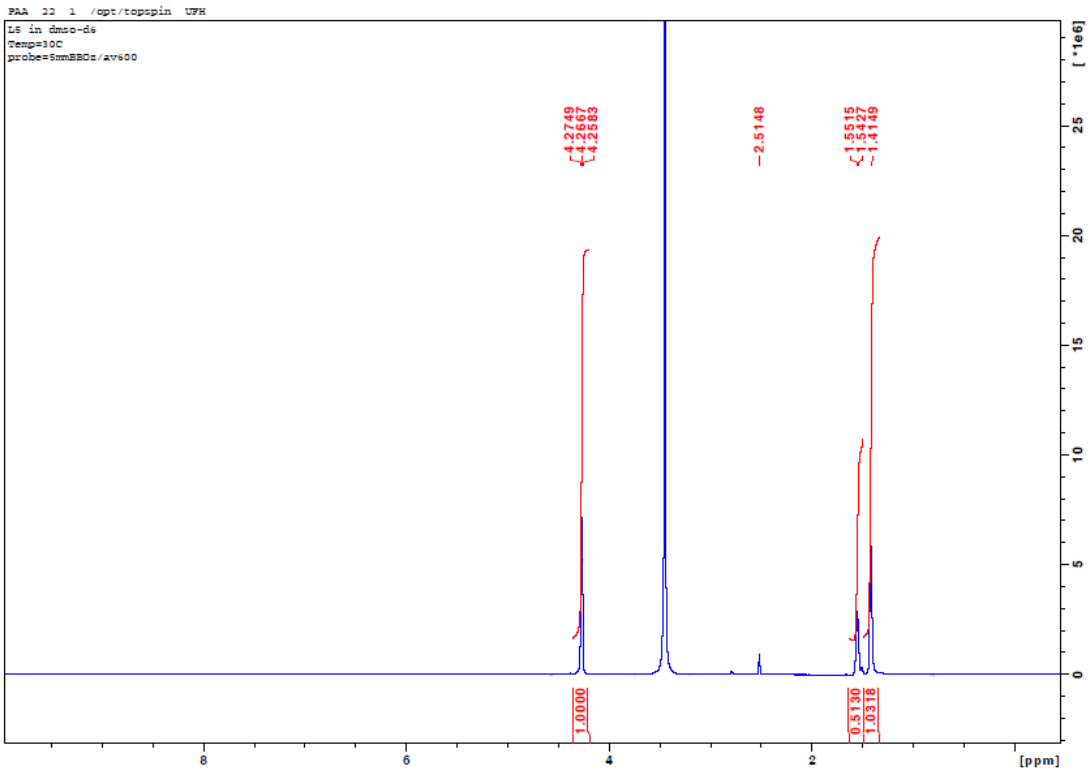

Appendix A10: ^{13}C NMR of piperidine dithiocarbamate

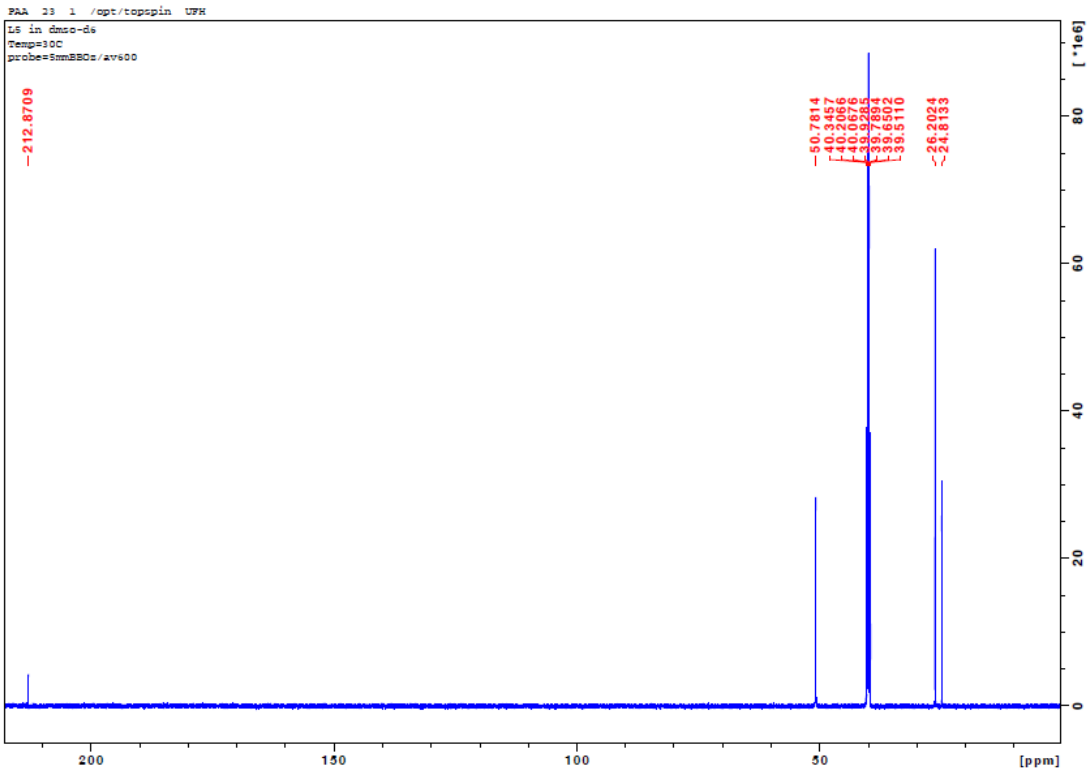

Appendix A11: ^{1}H NMR of morpholine dithiocarbamate

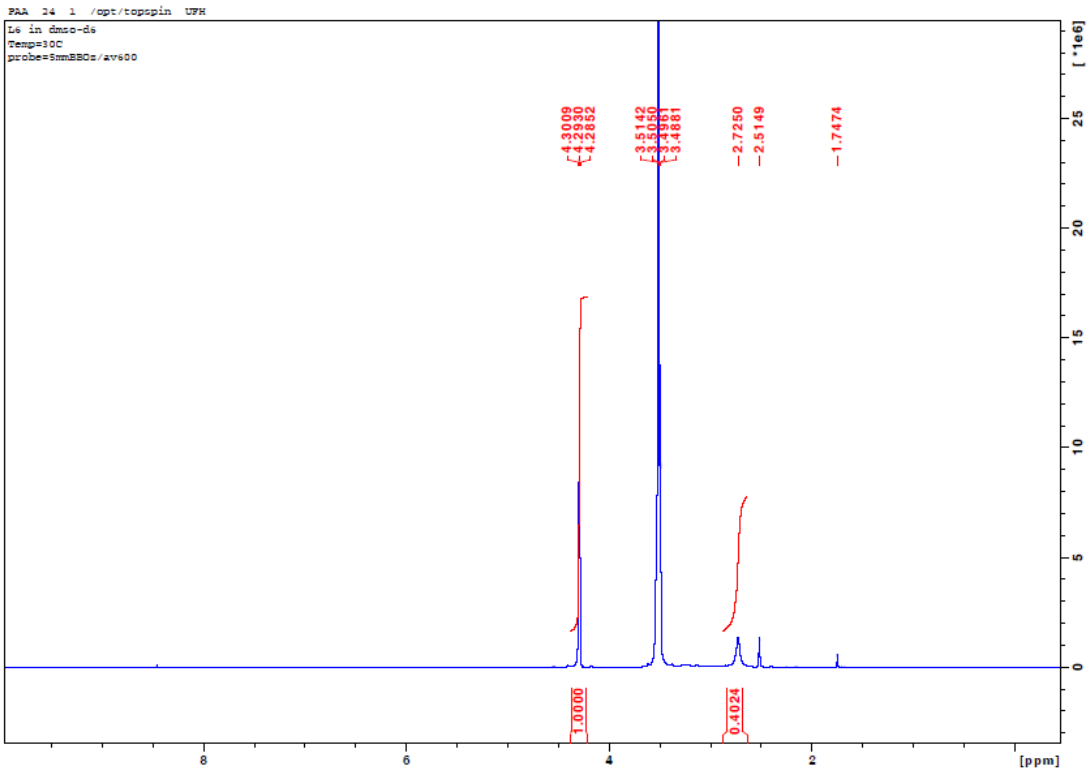

Appendix A12: ^{13}C NMR of morpholine dithiocarbamate